AN EXPERIMENTAL STUDY OF AMMONIA RESISTOJETS

A Thesis

presented for the Degree of

DOCTOR OF PHILOSOPHY

of the

UNIVERSITY OF SOUTHAMPTON

in the

Faculty of Engineering and Applied Science

by

R. LEWIN

ABSTRACT

FACULTY OF ENGINEERING AND APPLIED SCIENCE

AERONAUTICS AND ASTRONAUTICS

Doctor of Philosophy

AN EXPERIMENTAL STUDY OF AMMONIA RESISTOJETS

by Robert Lewin

The development of a mass sampling system is described which is used to measure the exhaust gas composition of ammonia resistojets. The design of a molecular beam sampling system of the Kantrowitz-Grey type and its application in sampling gas from the exhaust flow from an ammonia resistojet is described in detail. The underexpanded flow from the resistojet nozzle into a vacuum chamber is used as a source for a molecular beam type skimmer, the sampled flow is then analysed by a mass spectrometer.

Measurements made on three stainless steel resistojets in the temperature range 900 - 1075^{o}K shows ammonia dissociation to be time dependent and accompanied by formation of a surface nitride which ultimately lead to the blockage of one resistojet. A nickel resistojet operated in the same temperature range showed consistent behaviour with no time dependence. Performance predictions using the results of the nickel resistojet are used to show how the total mass of a pulsed thermal storage resistojet system depends critically on the temperature dependence of both the degree of dissociation and the heat losses.

CONTENTS

List of Figures

Acknowledgements

The author would like to thank the following people:

Dr. R. E. W. Jansson, who as project supervisor, has provided much help and encouragement during the course of the work and in the preparation of this thesis.

Professor K. N. C. Bray, for his help, interest and encouragement.

Mr. A. Earl of the Royal Aircraft Establishment, Farnborough whose continuing interest and encouragement made this work possible.

Introduction

A resistojet motor is a low thrust rocket, consisting of a heater and a convergent-divergent nozzle. It is essentially an energy conversion device in which the heater converts electric power to thermal energy by resistance heating, the heat subsequently being transferred to the gas stream, adding to the energy inherent in the propellant. Upon expansion through the nozzle the internal energy of the propellant is converted into kinetic energy.

A resistojet system consists basically of four parts; propellant storage, power source, control equipment, and the resistojet itself. Uses of resistojets fall into two broad categories, auxiliary propulsion and prime propulsion. Most spacecraft require some form of auxiliary propulsion for such functions as manoeuvring, station keeping and attitude control. Ammonia fuelled resistojets have been considered for attitude control of low orbit satellites and it is this type of resistojet which is considered in this work. Ammonia was chosen as a propellant because:

(1) It is easily stored for long periods as a saturated liquid in a simple thin walled pressure vessel.

(2) It is a low molecular weight fuel and if the heater temperature is high enough to dissociate the ammonia the products (hydrogen and nitrogen) have an even lower average molecular weight (low molecular weight fuels produce the highest specific impulse).

Analysis[19] of the nozzle flow from ammonia fuelled resistojets with thrust levels of the order of 0.05N has shown the performance to be considerably better than the cold flow gas jets presently used but the accurate prediction of thrust level depends critically on knowing the composition of the exhaust gases. It was with the intention of providing this information on composition that the present work was undertaken.

The equilibrium constants for ammonia indicate that under equilibrium conditions ammonia would begin to dissociate into hydrogen and nitrogen at temperatures above 300°K but in practice because of kinetic considerations significant dissociation does not occur until much higher temperatures. Dissociation of ammonia may be accomplished by two mechanisms, homogeneous gas phase reactions and hetrogeneous wall catalysed reactions. Sawyer[38] notes that temperatures in excess of 1500°K were necessary to produce measurable ammonia decomposition from the homogeneous reaction while Logan and Kemball[39] have measured the rate of wall catalysed reactions at temperatures as low as 700°K and found the rate to be dependent on both temperature and the wall material. The aim of this work is to measure the rate of dissociation of ammonia by the wall catalysed reaction for typical resistojet geometries and materials. The initial choice of materials limited the temperature range to below 1100°K.

The contents of this thesis are arranged as follows. Chapter 1 describes the flow handling system for ammonia and the vacuum chamber necessary to provide the low pressure environment in which the resistojet operates. The design and construction of a mass sampling probe is described in Chapter 2. Chapter 3 details the instrumentation necessary to perform the experiments and to make the required measurements. Resistojet design is considered in Chapter 4 and Chapter 5 outlines the experimental method required for the various measurements. Results are presented and analysed in Chapter 6 whilst Chapter 7 is devoted to a discussion of the various parameters affecting the design of ammonia resistojets in particular and electrothermal thrusters in general.

Chapter 1

AMMONIA FLOW SYSTEM

1.1 Introduction

This chapter describes the parts of the apparatus which were involved with the ammonia flow except the resistojet itself, that is the ammonia supply system which controlled and measured the flow of gas from a storage cylinder to the resistojet, the vacuum pumping system which provided the low background pressure for the production of the free jet and the exhaust system which disposed of the gas from the vacuum pumps. The complete flow system will be described briefly here and then each part described in more detail later.

Ammonia is a toxic, corrosive gas having a very distinctive smell in small concentrations ($\approx$ 50ppm in air) and creating a health hazard in larger concentrations ($\approx$ 1000ppm). For these reasons it was necessary that the flow handling system should have a high system integrity to avoid an accidental escape of ammonia yet it should still be simple and straightforward to operate.

The ammonia was kept as a liquid in a storage cylinder at a pressure of approximately 8 Bars absolute, this pressure was reduced to give a supply of gas at a pressure of 1.3 Bars absolute. The regulated supply was admitted to a constant pressure gasometer for flow rate measurement and then via a manual needle valve to the resistojet. The filling of the gasometer and supply of gas to the resistojet was controlled by magnetic valves suitably interlocked with sensors to guard against an ammonia escape. The vacuum chamber containing the resistojet was evacuated by three vapour booster pumps each booster being backed by a separate rotary mechanical pump. The gas discharge from these pumps which could be

ammonia or an NH_3 - H_2 - N_2 mixture was piped to an exhaust duct. This duct had a stream of air passing up provided by a fan near the bottom of the duct to dilute the discharge gases such that they were always well below their respective flammability limits (NH_3 15.5 to 27.0% in air, H_2 4.0 to 74.2% in air). The diluted discharge gas was allowed to disperse into the atmosphere several feet above the roof of the building ($\approx$ 20 metres above ground level).

Each section of the flow handling system will now be described in more detail with reference to the criteria chosen for its operation.

1.2 Ammonia Supply System

The requirements for the resistojet programme were for ammonia flow rates up to 10^{-4}kg/sec at resistojet supply pressures up to 1 Bar absolute. The ammonia supply system was physically separated into two parts for convenience; the first section provided a supply at a constant pressure of 1.3 Bars absolute from the storage cylinder and the second section controlled the gas to the gasometer and the resistojet.

1.2.1 Pre-regular Section

Ammonia was stored as a liquid at a pressure of approximately 8 Bars absolute at 20°C in an Air Products type APL300 cylinder. The pressure was reduced to 1.3 Bar absolute with a Matheson Regulator type 71 which was followed by a Skinner solenoid valve (type V52OA 2100, V_2 in Figure 1) fitted with a butyl rubber seat insert (as were all the solenoid valves) for use with ammonia. To enable the section of pipe between the storage cylinder and the valve V_2 to be purged with ammonia a Hoke valve V_8 (type 7122 F4Y) was connected from the low pressure side of the regulator to the exhaust vent. A pressure relief valve (Stephen Wells type C20) set to 1.7 Bar absolute was connected to the regulator outlet to guard against

high system pressures which could have been caused by a failed or incorrectly set regulator. The vent port on the relief valve was also piped to the exhaust duct. The low pressure pipework for this section was constructed in 9.5mm outside diameter 0.9mm wall thickness type AISI 304 stainless steel tube and was connected together with Keelering fittings (Industrial Hydraulics) fitted with butyl rubber "O" rings. The high pressure connection between the storage cylinder and the regulator was heavy duty 6.35mm outside diameter mild steel tubing fitted with Betabite connectors.

This section of the flow system was mounted on the wall above the ammonia storage cylinder away from the vacuum chamber. The low pressure outlet from this section was taken via a 9.5mm outside diameter stainless steel tube to the main control unit and second section of the flow control system which was mounted in the frame underneath the vacuum chamber.

1.2.2 Control Section

The ammonia supply to this section (at 1.3 bars absolute) was admitted to the gasometer via magnetic valve V_3 (Skinner valve type V52DA3007). The gasometer was constructed in stainless steel and was sealed by a low vapour pressure oil which prior experiment had established was not affected by contact with ammonia. Flow from the gasometer was controlled by a needle valve V_5 (Hoke valve type 2315 F4Y) and a magnetic valve V_6 (Skinner type V52DA2100). The gasometer could be vented into the exhaust duct via magnetic valve V_4 (Skinner type V51DA2150). A second outlet was taken from the downstream side of the needle valve via a manual valve V_7 (Hoke valve type 7122 F4Y) to provide an auxiliary supply. A combination of 9.5mm outside diameter stainless steel and nylon tube connected

with Keelering fittings was used to construct this part of the flow system, nylon tube being used where some freedom of movement was required.

Magnetic valves V_2, V_3, V_4, V_6 were operated with push buttons from the control unit which were connected to a relay logic circuit designed to operate the valves in a safe manner. The logic circuit also obtained information from sensors which were

(1) Pirani vacuum gauge in the vacuum chamber sensing chamber pressure which operated a switch at pressures greater than 5 torr.

(2) A flow switch in the exhaust duct which gave an indication when there was insufficient air flow in the exhaust duct to safely dilute any discharge gases.

(3) A low level switch on the gasometer.

(4) A high level switch on the gasometer.

(5) Two additional level switches on the gasometer, one just below the high level switch and one just above the low level switch. (The gasometer level switches were cam operated microswitches).

Valves V_3, V_4, V_6 had push buttons for both open and close but V_2 had only an open button since this valve which would normally be open, would close for a fault condition or as a result of opening the gasometer vent valve. The flow diagram for the complete ammonia inlet system is shown in Figure 1 and the circuit diagram for the controller in Figures 2 and 3.

A brief description of the controller is given to illustrate its operation. V_3 the gasometer fill valve could be controlled manually or automatically, such that it would open when the higher of the low level limits was reached and close when the lower of the

upper limits was reached; this facility allowed automatic filling of the gasometer during the course of an experiment. To allow gas to flow to the resistojet V_2 and V_6 would normally be open and V_4 closed. Valve V_3 was opened automatically as demanded, when the gasometer needed filling.

The sequence of events for a particular fault will now be described briefly.

(1) Vacuum chamber overpressure; V_6 closes and stops closed until manually opened after overpressure was removed.

(2) Insufficient flow in exhaust duct; V_2 and V_6 close and stay closed until manually opened after the exhaust flow had been restored. If the gasholder was being vented at the time valve V_4 would also be closed. Closure of the three valves V_2, V_4, V_6 ensures that no ammonia could be discharged from the pumps when there was insufficient air flow in the duct.

(3) Low limit on gasholder reached; V_6 would close and stay closed until gasholder was refilled above lower limit when V_6 could be opened manually.

(4) High limit on gasometer reached. This could only happen when V_3 was being manually operated and then V_2 would close and V_4 open, to vent the gasometer until the upper limit for the automatic filling of the gasometer was reached, when V_4 would close. V_2 would have to be manually reopened.

When a fault condition occurred a lamp on the control panel lit to tell the operator of the particular fault, lamps were also used to show the state of valves V_2, V_4 and V_6. A large red button was also provided which when actuated performed a similar function to that of fault (2) above and essentially closed off the ammonia

system. Should two or more faults occur together the system would go to the safest condition which was consistent with the faults which had occurred. Disconnection of any of the sensors from the control system would effect the fault associated with the particular sensor, thus precluding the overiding of any sensor by its removal and allowing a potentially dangerous situation to occur.

The flow system performed reliably and without leakage for three years and satisfied the criteria of being simple to operate yet still providing a completely safe supply of ammonia.

1.3 Vacuum Chamber and Pumping Equipment

The vacuum chamber used for the present work had been used previously to provide a low background pressure for an arc-heated wind tunnel[1, 2]. The vacuum system then consisted of the chamber itself, 740mm internal diameter, 1.46 m long, and was pumped by two Edwards High Vacuum 18B3 vapour booster pumps separately backed by an Edwards 1SC 3000 and a Kinney GKD110 rotary vacuum pumps. In this form the vacuum system had several drawbacks, (i) The vapour booster pumps were connected to the chamber by 90° baffle valves which were designed to stop oil backstreaming from the vapour pumps into the vacuum chamber, however, they were not completely effective and the inside of the chamber become covered with a film of oil. (ii) The plasma jet experiment (now removed) had been mounted in the chamber itself the connections being made through ports in the cylindrical wall of the chamber, which proved inconvenient for removal of the experiment and for in situ adjustments. (iii) The pumping capacity of the vacuum pumps was not thought to be great enough for the projected series of experiments with ammonia.

Backstreaming of oil was stopped by installing cooled chevron baffles between the booster pumps and the baffle valves. These baffles were held at a temperature of -25°C by a small freon refrigerator, this temperature being sufficiently low to ensure that any oil droplets striking the cooled surfaces would be held there as a solid deposit which would drop back into the pump when the baffle was warmed up. These baffles completely stopped oil droplets from reaching the chamber itself.

The difficulties found in assembling the experiment within the chamber were overcome by mounting the new experiment on an aluminium subframe fixed to the door of the chamber. This necessitated the construction of a new door and a mobile stand on which it could be removed from the chamber (Fig. 26). Six apertures were provided in the door for lead-throughs such that all connections could be made through the door allowing easy removal of the experiment from the chamber.

The pumping capacity of the chamber was increased by the addition of an Edwards 9B3 vapour booster pump mounted on the end wall of the chamber. Oil backstreaming from this pump was stopped by a liquid nitrogen cold trap interposed between the pump and its right angle baffle valve. The liquid nitrogen trap not only stopped oil backstreaming but also acted as a very efficient cryopump for ammonia giving a considerable increase in pumping speed especially at higher chamber pressures. The 9B3 vapour booster pump was backed by an Edwards 1SC 450B rotary vacuum pump. The complete vacuum facility is shown in Figures 4 and 5 with and without the door in position.

1.4 Compatability of Materials Used in the Pumping System with Ammonia

The vacuum chamber, its associated pumps, valves and connecting pipes had not been chosen specifically to operate with ammonia but had

been designed for use with argon; it was therefore necessary to consider the compatability of the materials from which they were constructed with ammonia. The chamber itself was constructed of mild steel and was painted inside and out with an epoxy resin paint, both of these materials being compatible with ammonia. The epoxy resin paint had been applied to halt any further rusting which had occurred when the plasma jet was installed. (Due to water leaks inside the tank). The main vacuum pipes from the vapour booster pumps to the rotary pumps and from the rotary pumps to the chamber were of copper, which is a material commonly used for vacuum systems but is not recommended for use with ammonia. The presence of ammonia normally leads to severe corrosion of copper, however because of the low density of the ammonia in contact with the copper, the absence of water vapour and the relatively short exposure time it was thought that corrosion of the copper would not be a serious problem. After three years of running with ammonia the copper used in the vacuum system has shown no signs of deteriorating. The vacuum valves were made of either aluminium or steel with nitrile rubber diaphragms. Nitrile rubber is not normally used with ammonia but again because of the low densities involved no deterioration was observed. All the "O" rings in the vacuum system were of nitrile rubber.

The booster pumps, baffles, cold trap and rotary pumps were constructed in mild steel or stainless steel and were compatible with ammonia. All oils used in the booster and rotary pumps were suitable for use with ammonia but to prevent a slow deterioration in the pumping speed of the rotary pumps it was necessary to change the oil every six months (approximately 200 hours of running time).

1.5 Exhaust System

When previously used with argon the discharge gases from the rotary pumps had been piped outside the laboratory and allowed to disperse into the atmosphere at ground level. Ammonia being a very toxic gas it was necessary to dispose of the discharge gases such that they would not cause any harmful effects. Two methods were proposed;

(1) To pass the discharge gases through a scrubber to remove the ammonia and allow any nitrogen and hydrogen to disperse into the atmosphere.

(2) To dilute the discharge gases with air and discharge at a high point where they could disperse.

The first method only removed the ammonia and there was still the problem of safely dispersing any hydrogen present to avoid an explosion.

The second alternative was simpler to construct and it could be designed to dilute any hydrogen present below its detonation concentration. The ammonia would in this case be discharged into the atmosphere but because of the small quantities involved would not present a hazard or a major source of pollution. This method was the one chosen and will now be described in more detail.

Discharge gases from the rotary pumps were lead via two 35mm internal diameter steel pipes into the side of a 150mm internal diameter asbestos duct. The pipes were connected into the duct about 2 metres from the bottom end of the duct. To provide an air flow in the duct a 150mm diameter fume cupboard fan was installed 0.75metre below the point where the discharge pipes entered the duct. The duct discharged into the atmosphere 3 metres above the top of the building which was about 20 metres above ground level and away from other buildings. Air speed in the duct was approximately 2 metres/sec. The maximum concentration of ammonia in the duct was calculated to be 0.4% by volume for a mass flow of 10^{-4}kg/sec, the upper bound flowrate; and the maximum concentration of hydrogen assuming full dissociation of 10^{-4}kg/sec of ammonia, was 0.6% by volume.

These concentrations are well below both the detonation and flammability limits for both hydrogen and ammonia.

1.6 Skimmer Pumping Requirements

The skimmer which is described in detail in the next chapter required a separate pumping system having a pumping speed of approximately 20 litres/sec of air at the skimmer in the pressure range 5×10^{-3} torr to 10^{-6} torr. This was provided by an Edwards E02 water cooled oil diffusion pump backed by an Edwards 1SC 150 rotary vacuum pump. An E02 oil diffusion pump complete with water cooled baffle, to reduce oil backstreaming, and $\frac{1}{4}$ swing butterfly valve has a pumping speed of 50 litres/sec in the pressure range 5×10^{-3} torr to 10^{-6} torr. To ensure that a pumping speed of 20 litres/sec would be available at the skimmer the diffusion pump was mounted inside the vacuum chamber alongside the resistojet as close to the skimmer as possible, thus minimising the length of connecting pipe required. The skimmer chamber and the diffusion pump were connected by a length of 51mm internal diameter copper tube with two right angle bends which was calculated to give a pumping speed of 20 litres/sec at the skimmer.

Water required for cooling the pump and baffle was piped through a cover plate in the door of the vacuum chamber. The backing line for the diffusion pump also come through this cover plate and was connected to the rotary pump, which was mounted beneath the vacuum chamber. The $\frac{1}{4}$ swing butterfly valve was operated from outside the chamber via a rotary lead-through and a linkage.

To reduce the likelihood of arcing in the vacuum chamber the diffusion pump heater which was supplied to operate at 240V r.m.s. was changed for one operating at 110V r.m.s. To further reduce the voltage

between the heater and earth the heater was run from the centre tapped secondary of a 240V to 110V isolating transformer the centre tap being taken to earth, so that the maximum voltage with respect to ground was 55V r.m.s. The wiring diagram for the pump heater is shown in Figure 6 which also shows the connections to the thermal cut out mounted on the pump body which turned the heater off in the event of overheating.

The water supply to the diffusion pump was passed through two magnetic valves, one in the supply and the other in the waste connected to isolate the water pipes inside the vacuum chamber should a water leak develop, which if left unchecked would flood the chamber. These valves were controlled from the ammonia inlet control system and would shut when the vacuum chamber overpressure switch was actuated.

Chapter 2

PRODUCTION OF A FREE JET AND SKIMMER DESIGN

2.1 Introduction

The aim of the experimental work presented here was to measure the degree of ammonia dissociation during its passage through a heated resistojet. The chemical reaction leading to the dissociation of ammonia is predominantly a surface catalysed reaction at the temperatures envisaged for attitude control resistojet operation, the homogeneous gas phase reaction does not contribute significantly until the temperature is raised to approximately 1800°K.

To measure the degree of dissociation it is necessary to analyse a sample of the flow; in this case a mass-spectrometer was used as the analyser. It is possible to obtain a sample of gas in the plenum chamber of the resistojet, reduce its pressure and temperature and inject it into the mass-spectrometer. Unfortunately this method suffers from several disadvantages:

(1) The sampled flow had not passed through the nozzle where secondary reaction may alter the composition.

(2) The sampled gas would have to flow through an undefined length of hot sample tube which would have made an unknown contribution to the amount of dissociation.

(3) Reducing the sample pressure from plenum pressures (0.25 to 1 BAR) to mass-spectrometer pressures (10^{-6} to 10^{-8} torr) would cause unpredictable changes in gas composition. It was desirable for these reasons to obtain a sample after the flow had traversed the nozzle and with a sampling probe which would not change the degree of dissociation of the ammonia.

Since in this programme small area ratio nozzles were of interest (Area ratio 25:1) the gas expanding into the vacuum chamber was under-expanded in the nozzle and underwent further expansion in the vacuum chamber. This further expansion produced a radially expanding, low density, high Mach number flow. The problems involved in sampling from this type of flow are exactly those encountered in the formation of molecular beams from nozzle sources of the Kantrowitz-Grey[3] type. Generation of molecular beams from nozzle sources has been widely reported in the literature and considerable expertise has been demonstrated by some workers.

The design philosophy behind the Kantrowitz-Grey type of molecular beam generator can be summarized as follows:

(1) From continum flow through a nozzle produce a free expansion where Mach number increases and density and temperature fall.

(2) Insert in the expanding flowfield a conical skimmer probe to extract a small portion of the flow which is further expanded to a lower pressure to obtain free molecular flow conditions.

Free molecular flow within the skimmer can be made compatible with the flow required for the mass-spectrometer by choice of a suitable pressure reducing orifice.

The use of a Kantrowitz-Grey type molecular beam generator allows sampling from resistojet nozzle flows without physical connection between resistojet and sampling probe thus allowing the resistojet design and operation to be completely independent of the sampling system.

The remainder of this chapter describes the design of a skimmer type sampling system for resistojet nozzle flows.

2.2 Mach Disc

The expansion from an underexpanded nozzle into a region of finite pressure rather than a perfect vacuum produces a shock wave system as shown in Figure 7. Gas expanding within the barrel shock and mach disc is unaware of a finite background pressure P_1 until the shock wave structure bounding the flow is reached. For meaningful skimming the skimmer must always be within the shock structure and for a skimmer on the axis, upstream of the mach disc.

The position of the mach disc for a sonic orifice as shown in Figure 7 is given by

$$\frac{x_m}{D^*} = 0.67 \left(\frac{P_o}{P_1} \right)^{\frac{1}{2}}$$

which has been experimentally derived by Ashkenas and Sherman[4]. This expression has been found to be independent of the nature of the gas.

The background and plenum pressures are not independent variables, for a given nozzle the mass flowrate is a function of the plenum pressure and temperature and for the vacuum system the pumping speed, hence mass flowrate which can be pumped, is a function of chamber pressure. The mass flowrate of ammonia as a function of chamber pressure was measured for the vacuum chamber pumping system, with and without the cold trap filled with liquid nitrogen, the results are shown in Figure 8. When the cold trap was filled with liquid nitrogen it acted as a cryopump for ammonia and increased the pumping speed considerably in the range 10^{-2} - 10^{-1} gm/sec. which is the range of mass flowrates encountered in ammonia resistojets.

The nozzle used in the present experiments was of the convergent-divergent type with a 20° half angle divergent section, an area ratio of 25:1 and a throat diameter of 1mm. The mass flowrate through this nozzle

as a function of pressure and temperature has been calculated [5] for ammonia and is shown for three temperatures in Figure 9. For given resistojet plenum conditions there is a particular mass flowrate of ammonia and hence from Figure 8 a particular vacuum chamber pressure. Therefore, for given plenum conditions there is a unique position for the mach disc which is shown in Figure 10 where the mach disc position is shown as a function of plenum conditions.

In deriving Figure 10 it has been assumed that the mach disc position is the same for a convergent-divergent nozzle as for a sonic orifice under identical conditions. This assumption will be discussed later in this chapter.

On inspection of Figure 10 it can be seen that if a skimmer were placed 70 nozzle diameters (70D) downstream of the nozzle it would be forward of the mach disc for all realistic plenum conditions. The flow bounded by the barrel shock and mach disc is a freely expanding flow and within this region the flow may be treated as if it were expanding into a vacuum, the presence of a backpressure within the test chamber does not become apparent until the mach disc and barrel shock are reached.

2.3 Axial Mach Number

A description of the flow field of a nozzle exhausting into a vacuum may be obtained by a method-of-characteristics solution, but for the present application where extreme accuracy is not required and it is only the far field which is of interest it is sufficient to use one of the approximate methods to calculate the Mach number and density in the far field. A further simplification is that it is only the axial Mach number and density decay which is needed for a skimmer placed on the nozzle axis.

The Mach number as a function of axial distance from the nozzle exit plane has been derived by Greenwald[6],

$$Mo = \left[2/(\gamma - 1)\right]^{\frac{1}{2}} \left\{ \left[5(x/D^*)^2 (1 - \cos \theta m)\right]^{\gamma - 1} - 1 \right\}^{\frac{1}{2}}$$

where Mo = axial Mach number

x = axial distance from nozzle exit plane

θm = angle of limiting streamline

However in the far field

$$\left[5(x/D^*)^2 (1 - \cos \theta m)\right]^{\gamma - 1} \gg 1$$

Therefore:

$$\lim \left[Mo \right] = \left[2/(\gamma - 1)\right]^{\frac{1}{2}} \left[5(1 - \cos \theta m)\right]^{\left(\frac{\gamma - 1}{2}\right)} (x/D^*)^{\gamma - 1}$$

$\frac{x}{D^*} > 10$

The value of θm can be obtained from Sibulkin and Gallaher[7] where for

$$\frac{Ae}{A^*} = 25, \quad \gamma = 1.31 \quad (300^\circ K)$$

$$(\theta m)_{\theta e = 0} = 75^\circ$$

and for

$$\frac{Ae}{A^*} = 25, \quad \gamma = 1.18 \quad (1000^\circ K)$$

$$(\theta m)_{\theta e = 0} = 120^\circ$$

Now $\theta m = (\theta m)_{\theta e = 0} + \theta e$

where θe = angle of nozzle at exit plane

$= 20^\circ$ in present case.

$\therefore$ For $\gamma = 1.31$ $\quad \theta m = 95^\circ$

$\gamma = 1.18$ $\quad \theta m = 140^\circ$

The calculated values of Mo versus (x/D^*) for $(\frac{Ae}{A^*}) = 25$ $\theta e = 20^o$ and $\gamma = 1.18$ and 1.31 are plotted in Figure 11. The axial density decay is given by Sibulkin and Gallaher[7] in the form

$$(\rho/\rho_o) = B(x/D^*)^{-2}$$

where the parameter B is given as:

$$B = 0.4\pi / \left\{ 2\pi(1 - \cos \theta m) \right\}$$

the value of B has been evaluated for the values of θm above and the ratio (ρ/ρ_o) has been plotted against (x/D^*) in Figure 12. The above approximation for density decay shows good agreement with the approximation of Hill and Draper[8] especially for a nozzle with an area ratio of 25.

2.4.1 Skimmer Mass Flowrate

In the present investigation the skimmer is used to sample the expanded flow without the sampled gas experiencing a shock in which one would expect temperature and pressure recovery with the possibility of further chemical reaction. The expansion is used to quench the chemical reactions in the resistojet and the skimmer used to sample the "quenched" flow. The ability of a skimmer to extract a sample of the invicid flow with minimum disturbance to that sample increases as the nozzle-skimmer distance increases[9] until a point just inside the mach disc is reached. A large nozzle-skimmer distance is also consistent with a low skimmer mass flowrate which will decrases as the nozzle-skimmer distance is increased, for constant akimmer area. The mass spectrometer analyser requires low flow rates at low pressures ($\approx 10^{-7}$ torr) and these requirements can be best met by large nozzle-skimmer distances.

The flux through the skimmer is given by Parker[10] as a function of Mach number, γ and number density in front of the skimmer:-

$$N \approx n_1 a_o S_1 \frac{M}{\sqrt{\left\{1 + \left[(\gamma - 1)/2\right] M^2\right\}}} \quad \text{molecules/sec}$$

$M \geq 3$

where n_1 = molecules per cc in front of skimmer

a_o = velocity of sound at stagnation conditions

S_1 = area of skimmer entrance

M = local Mach number

which can be written as

$$N \approx n_o \left(\frac{\gamma K T_o}{m}\right)^{\frac{1}{2}} S_1 \frac{M}{\left\{1 + \frac{1}{2}(\gamma - 1)M^2\right\}^{(\gamma + 1)/2(\gamma - 1)}} \quad \text{molecules/sec}$$

$M \geq 3$

where n_o = stagnation number density

T_o = stagnation temperature

m = molecular ~~weight~~ *mass*

K = Boltzmann's constant

this is the expression given by Campargue[11] in terms of the stagnation conditions. This expression was evaluated for ammonia as a function of Mach number for four limiting stagnation conditions expected in the present investigation. The four limiting conditions were

(1)	P_o = 1 Bar	T_o = 300°K	γ = 1.31
(2)	P_o = 0.25 Bar	T_o = 300°K	
(3)	P_o = 1 Bar	T_o = 1000°K	γ = 1.18
(4)	P_o = 0.25 Bar	T_o = 1000°K	

The results are shown in Figure 13, the ordinate having been converted into mgm sec^{-1} per sq. mm of skimmer area. However Mach number is a function of nozzle-skimmer distance as shown in Figure 11, by combining this and Figure 13 one obtains the skimmer mass flowrate as a function of nozzle-skimmer distance. This is shown in Figure 14.

2.4.2 Skimmer Position and Size

It has been shown by previous workers [9, 12] in the production of molecular beams that interaction between the skimmer and the beam is reduced as the nozzle-skimmer distance is increased. Fenn and Decker [12] introducing the parameter $\frac{\text{skimmer Knudsen number}}{\text{Mach number}}$ $\left(\frac{Kn_\infty}{M}\right)$ showed that the intensity of the molecular beams they produced approached the theoretical intensity with increasing (Kn_∞/M) up to the value of 1. To maximise (Kn_∞/M) it is necessary to have large nozzle-skimmer distances because Kn increases quicker than Mach number for increasing nozzle-skimmer distance.

From Figure 10 it can be seen that for a nozzle-skimmer distance of 100 nozzle diameters or greater the skimmer would interact with the mach disc which could lead to the formation of a detached bow shock wave. A nozzle-skimmer distance of 70 nozzle diameters (70D) was chosen as a starting point to ascertain if a skimmer placed at this position could skim effectively over the range of nozzle stagnation conditions.

The skimmer chamber requires pumping to ensure the skimmer does not choke and to maintain a low background pressure such that molecular flow conditions are established. Molecular flow in the skimmer chamber reduces the scattering of the skimmed gas by the background gas and also the possibility of a shock being formed

inside the skimmer. It was hoped initially that the skimmer could be pumped by an Edwards High Vacuum E02 oil diffusion pump which could be mounted inside the main vacuum chamber to keep the vacuum line as short as possible. To obtain the maximum pumping speed the diffusion pump should have been located directly below the skimmer, but because of restricted height in the chamber this was not possible. With the diffusion pump mounted alongside the resistojet (Figure 16) the pumping speed available at the skimmer is reduced by the impedance of the connecting pipe.

The E02 diffusion pump complete with water-cooled baffle and valve had a pumping speed for air of 50 litres/sec in the pressure range 5×10^{-3} to 10^{-6} torr, however by the addition of the necessary connecting pipes this was reduced to approximately 20 litres/sec of air at the skimmer. The pumping speed for ammonia should be greater than 20 litres/sec (conductance of a tube is higher for a lighter molecule) but in the absence of any data on the performance of the diffusion pump with ammonia the value of 20 litres/sec was also used for ammonia in further calculations.

The static pressure in the skimmer chamber was evaluated for the stagnation conditions of Figure 14 for a skimmer having a 1 sq. mm (1.13mm diameter) hole placed 70D from the nozzle assuming a pumping speed of 20 litres/sec of ammonia, (The pumping speed of 20 litres/sec for ammonia was converted to a mass flowrate of ammonia at 295°K. This assumes molecular flow in which the skimmed gas molecules have attained a temperature of 295°K after collisions with the walls) and is shown in Table I.

TABLE I

Plenum Pressure BAR	Stagnation Temperature ^{o}K	Skimmer Mass Flowrate Kg/sec	Pressure torr	Mean Free Path mm
1	300	2.7×10^{-8}	1.46×10^{-3}	27
0.25	300	6.6×10^{-9}	3.56×10^{-4}	110
1	1000	4.8×10^{-9}	2.6×10^{-4}	151
0.25	1000	1.25×10^{-9}	6.7×10^{-5}	587

Also shown in Table I is the mean free path of ammonia at the corresponding pressure and a temperature of $295^{o}K$. From the above table, for a skimmer chamber typical dimension of 50mm one can expect molecular flow for the high temperature stagnation conditions. For the low temperature stagnation conditions the flow will be predominantly transitional in the skimmer chamber, these conditions are of no real interest for dissociation studies but are used here as a lower bound for the design study.

2.4.3 Mean Free Path in Isentropic Flow Outside Skimmer

The free stream mean free path of the gas molecules in the free jet as measured in gas fixed co-ordinates is given by (13)

$$\lambda_{\infty} = \lambda_{o} \left\{ 1 + \left[(\gamma - 1)/2 \right] M^{2} \right\}^{1/\gamma - 1}$$

for an isentropic expansion and rigid sphere gas molecules, where λ_{o} is the mean free path at stagnation conditions obtained from the expression given by Dushman(14)

$$\lambda_{o} = 0.11451 \quad \frac{\eta}{P_{o}} \left(\frac{T_{o}}{m} \right)^{\frac{1}{2}} \text{ millimetres}$$

η being the coefficient of viscosity in poise. However the mean

free path which is important in considering skimmer interaction is that of molecules scattered from the skimmer body back into the free stream. The mean free path of scattered molecules is obtained by assuming the molecules scattered from the skimmer body have accommodated thermally with the skimmer and are re-emitted with thermal energy equivalent to the temperature of the skimmer. The expression used was developed by Probstein[15] and is given below:-

$$\lambda_s = \frac{4}{\sqrt{\pi\gamma}} \left[\frac{T_b}{T_\infty}\right]^{\frac{1}{2}} \frac{\lambda_\infty}{M_\infty} = F\lambda_\infty$$

where:

$$F = \frac{4}{\sqrt{\pi\gamma}} \left[\frac{T_b}{T_\infty}\right]^{\frac{1}{2}} \frac{1}{M_\infty}$$

T_b = temperature of the body

T_∞ = static temperature of the gas

T_∞ is given by

$$\frac{T_o}{T_\infty} = 1 + \frac{(\gamma - 1)}{2} M^2$$

for an isentropic expansion from stagnation temperature T_o.

Table 2 shows the values of λ_∞, F, λ_s and hence Kn_s based on the skimmer entrance diameter, for the design case of a skimmer of entrance diameter 1.13mm placed 7OD downstream. Also shown is the value of the free stream Knudsen number $\left(\frac{\lambda_\infty}{d_s}\right)$ divided by the local Mach number $\left(\frac{Kn_\infty}{M}\right)$.

TABLE 2

P_o BAR	T_o ^oK	λ_o mm	M_s	γ	λ_∞ mm	F	λ_s mm	Kn_s	$\frac{Kn_\infty}{M}$
0.25	300	2.11×10^{-4}	12	1.31	5.46	.793	4.34	3.84	.403
1	300	5.29×10^{-5}	12	1.31	1.36	.793	1.08	0.955	.1
0.25	1000	1.19×10^{-3}	8.8	1.18	121	.365	44.2	39.1	12.4
1	1000	2.98×10^{-4}	8.8	1.18	30.4	.365	11.1	9.8	3.06

The value of T_b was taken as 300^oK. The assumption that $T_b = 300^oK$ leads to shorter scattered mean free paths than the real case when the skimmer will experience some heating from the flow, however this is a more stringent requirement for the skimmer orifice diameter and will be used in the absence of any information on the skimmer temperature.

The value of $\frac{Kn_\infty}{M} > 1$ for the two high temperature stagnation conditions indicating that skimmer interference should be minimal for these conditions.

The worst case conditions i.e. 0.25 and 1.0 Bar at 300^oK, are included here only as a lower bound and one of no real practical interest because no ammonia dissociation will occur at this temperature.

2.4.4 Attached Shock at Skimmer and Internal Geometry

To ensure an attached shock at the mouth of the skimmer the flow deflection caused by the skimmer must be less than the shock detachment angle. Conversely on the vacuum side of the skimmer the internal cone should have as large an angle as possible to allow the skimmed gas to be pumped away quickly and to minimise scattering by the walls. Thus a design compromise is necessary.

The internal angle of the skimmer can be made large enough such that few molecules have sufficient transverse random velocity to strike the walls. This has been expressed as

$$\theta i \geq \sin^{-1}(\bar{C}/M) = \sin^{-1} \frac{2(2/\pi\gamma)^{\frac{1}{2}}}{M} \quad \text{degrees}$$

by Kantrowitz and Grey[3] and as

$$\theta i \geq 3(\bar{C}/M) = \frac{6(2/\pi\gamma)^{\frac{1}{2}}}{M} \quad \text{Radians}$$

by Skinner and Moyzis[16]

Values of θi for the appropriate values of γ and M are shown in Table 3 for a skimmer placed 70D downstream.

The maximum external angle of the skimmer is more difficult to determine. The maximum cone half angle for an attached shock in hypersonic flow with $\gamma = 1.4$ is 55° for $M > 8$[17].

TABLE 3

P_o BAR	T_o $^\circ K$	M	γ	θi (Kantrowitz Grey)	θi (Skinner Moyzis)
0.25	300	12	1.31	6.6°	19.6°
1.0	300	12	1.31	6.6°	19.6°
0.25	1000	8.8	1.18	9.6°	28.7°
1.0	1000	8.8	1.18	9.6°	28.7°

The experience of workers[11] [18] in the production of molecular beams has been that one can expect an attached shock on the mouth of the skimmer for angles greater than the maximum derived from invicid flow calculations.

With the restrictions on the internal angle of the skimmer and from manufacturing considerations it was decided to make the internal half angle $\theta i = 30^{o}$ and the external half angle $\theta e = 40^{o}$. Another important consideration is the radius of curvature of the leading edge of the skimmer mouth. When the radius is of the order of the free stream mean free path of the gas one would expect molecules to be scattered into the incident flow with the possibility of a detached shock or attenuation of the skimmed beam. However in the present case the radius of curvature is of the order of 0.01mm which is three orders of magnitude less than the free stream mean free path thus this interaction is not expected to be important.

2.4.5 Second Orifice

Table I shows the expected skimmer chamber pressures for four limiting stagnation conditions, however these pressures are still too high to allow the gas to be introduced directly into a mass spectrometer (pressures typically 10^{-6} torr). It is necessary to expand the skimmed gas through a second orifice mounted downstream of the skimmer inside the skimmer chamber. This second orifice can be connected directly to the mass spectrometer and can be chosen in size and position to give the required mass flowrate.

The flux through the second orifice is given by Parker[10] in terms of stagnation conditions and local conditions at the skimmer mouth.

$$N_1 \underset{M \geq 3}{\approx} \frac{n_1 a_o S_1}{2} \frac{S_2}{\pi d_{12}^2} \frac{M(3 + \gamma M^2)}{\sqrt{\left\{1 + \left[(\gamma - 1)/2\right] M^2\right\}}} \quad \text{molecules/sec}$$

However this is the same expression as for the skimmer flux with the additional factor,

$$\frac{S_2(3 + \gamma M^2)}{2\pi d_{12}^2}$$

where S_2 is area of second orifice and d_{12} is the distance from the skimmer entrance to the second orifice. The distance d_{12} should be less than the mean free path of the gas in the skimmer chamber to minimise scattering, and with this restriction the diameter of the second orifice was chosen to give the required pressure at the mass spectrometer. The geometry of the second orifice is less critical than for the skimmer orifice, the mean free path of the gas in the skimmer chamber is much longer than at the skimmer, and the flow regime is molecular not transitional as at the skimmer. The second orifice was constructed as a hole in a thin membrane across the end of a 13mm internal diameter tube which is positioned inside the skimmer chamber (Figure 15).

The mass spectrometer was pumped by an Edwards 2M4 mercury diffusion pump with a cold trap and $\frac{1}{4}$ swing baffle valve giving a pumping speed of approximately 30 litres/sec for air at the mass spectrometer. The mass spectrometer and its pumping system was mounted outside the vacuum chamber and connected to the second orifice by a length of 13mm internal diameter tubing giving a pumping speed of 1.85 litres/sec of air at the second orifice.

The second orifice area was calculated to be 3.1 sq. mm for d_{12} = 80mm and a skimmer orifice area of 1 sq. mm for the lower mass flowrate stagnation conditions. However due to difficulty in manufacture the skimmer orifice was constructed with an area of 1.8 sq. mm giving a larger skimmer mass flow, to compensate for this the second orifice was reduced in area to 0.8 sq. mm.

The extra mass flowrate passing through the skimmer was still within the capacity of the pump to ensure correct operation of the skimmer. The skimmer is shown in position in Figures 16 and 17.

2.5 Assumptions and Simplifications made in the Design of the Skimmer

2.5.1 Mach Disc

It is important to know the position of the mach disc to ensure the skimmer inlet is always placed upstream, within the free jet. The position of the mach disc was calculated for a sonic orifice with the expression of Ashkenas and Sherman[4] however in this application the nozzle is of a convergent-divergent type and it was assumed the mach disc position would be at least as far downstream as for a sonic orifice. For sufficiently large pressure ratios across the nozzle and at large distance from the nozzle the flow is radial and appears to diverge from a point just downstream of the nozzle throat. This should apply equally for both convergent and convergent-divergent nozzles and should give a similar mach disc position in both cases especially in this case where the divergent section of the nozzle is short in comparison to the calculated mach disc-nozzle distance.

The divergent section of the nozzle is subject to boundary layer growth which will vary the effective nozzle size, and in the event of boundary layer closure at the nozzle exit plane, the mach disc position may vary from that given in the Ashkenas and Sherman expression. It has been predicted [19] that boundary layer closure will occur at nozzle Reynolds number (Re_{D^*}) of approximately 300 and below. In the production of molecular beams [13, 20] no change was observed in the beam intensity as the divergent section of a convergent-divergent nozzle was progressively cut back to its throat.

In the preceding discussion the mach disc was considered as a sharp discontinuity in the flow, however the shock has been estimated as 2 to 10 free stream mean free paths thick [21].

It has also been shown that at sufficiently low density in the test chamber the mach disc and barrel shock will tend to disappear as recognisable entities as a Knudsen number (Km) based on mach disc diameter (Dm) and mean free path of the gas behind the mach disc approaches unity. The latter mean free path (λc) is very nearly equal to that of the gas at tank ambient pressure and stagnation temperature. The diameter of the mach disc is given by Bier and Schmidt[22] as

$$Dm = 0.6\ xm \text{ for } \gamma = 1.3$$

Shown in Table 4 are xm, Dm, λc and Km for the four limiting stagnation conditions.

TABLE 4

P_o BAR	T_o ^oK	λc mm	xm mm	Dm mm	Km
1	300	1.73	120	72	0.024
0.25	300	3.04	100	60	0.05
1	1000	16	150	90	0.18
0.25	1000	26.4	130	78	0.34

Ashkenas and Sherman[4] show that for Km = 0.1 the impact pressure peaks ahead of the mach disc disappear and for Km = 0.3 the last recompression by the mach disc, visible by the sodium scattering technique, disappears. For the high temperature stagnation conditions $0.1 < Km < 0.35$ and the mach disc will tend to disappear for these conditions.

The effects mentioned above will tend to make the absolute position and strength of the mach disc shock more difficult to determine, however, in the present design it is only important that the skimmer be within the free jet, and not that the exact position of the mach disc is known. The design allows a large margin in mach disc position by selecting a position for the skimmer which is considerably upstream of its calculated position but it is recognised that any of the above effects may result in a mach disc closer to the nozzle than calculated. Should the design result in the skimmer being behind the mach disc it would be immediately obvious from the greatly reduced skimmer mass flowrate which would be a consequence of sampling from the diffuse flow behind the mach disc.

2.5.2 Axial Mach Number

The axial Mach number was calculated using an approximate relationship for a convergent-divergent nozzle exhausting into a vacuum. This was calculated using the geometric dimensions of the nozzle, i.e. 1mm diameter throat, 25:1 area ratio, 20° half angle. However at low Reynolds number (Re_{D*}) the nozzle boundary layer can be a considerable fraction of the geometric radius of the nozzle [19], the "effective" nozzle will be smaller than the geometric nozzle giving a different Mach number distribution.

In the free jet several relaxation processes occur which require collisions between gas molecules to maintain in equilibrium. For diatomic and polyatomic gases a considerable portion of the total energy can be in rotational and vibrational modes of the molecule and during the expansion this energy is transferred to translational motion. Transfer of energy takes place progressively slowly in an expansion because the collision rate falls until finally a limiting

region is reached in which further relaxation of the internal modes is inhibited because of an insufficient collision rate. Vibrational relaxation usually freezes first followed by rotational relaxation and finally a region is reached in the far field of a free jet expansion where the exchange of translational energy is frozen and the Mach number and temperature reach limiting values. The point at which the temperature and Mach number freeze has been investigated theoretically [23, 24] for monatomic and diatomic molecules and the freezing point has been expressed in terms of the source Knudsen number. Usually the translational freezing point is not observed because of finite pressure in the experimental vacuum facilities. Vibrational relaxation may freeze in the free jet, however it has been shown [19] that vibrational relaxation for NH_3 and $NH_3 - H_2 - N_2$ mixtures is very fast and vibrational energy may be near equilibrium in the nozzle. For high temperature stagnation conditions when considerable energy is in the vibrational modes of ammonia, vibrational freezing in the free jet will tend to increase the value of γ and hence increase the Mach number. The quantity most sensitive to Mach number and γ is the skimmer mass flowrate which can be experimentally measured to ascertain the possible effects of the above phenomena.

2.5.3 Condensation

The gas temperature in the free jet expansion falls very rapidly and, depending on stagnation conditions, after only a few nozzle diameters the gas can be below the temperature required for condensation under equilibrium conditions. Nozzle expansions have been used [37] to measure nucleation rates of ammonia in a dry air carrier gas. These experiments were carried out from stagnation conditions of 4 Bars and 284°K where condensation was observed to

occur at Mach numbers of 1.6. Condensation can occur, if nuclei are present, in the present experiments with room temperature stagnation conditions. However stagnation temperatures greater than 800°K are of interest and the possibility of condensation from these conditions will now be considered.

Figure 18 shows the isentropes for ammonia expansions from 800°K and pressures of 0.25 and 1 Bar for γ = 1.18 and 1.3, the numbers adjacent to the lines are the Mach numbers at that point. Also shown is the vapour pressure curve for ammonia. To the right of the vapour pressure curve is the vapour region and to the left below 195°K the region corresponding to the solid phase. It can be seen that the isentropes cross the vapour pressure at points which will be upstream of the skimmer; leading to the possibility of condensation. However condensation is a nucleation process, and, even if the thermodynamic conditions are right, proceeds at a rate proportional to the collision rate. Since this rate progressively falls as the gas expands the kinetic conditions for condensation worsen as the thermodynamic conditions become favourable.

The isentropes shown in Figure 18 cross the vapour pressure curve at points where the collision rate is decreasing rapidly which will inhibit the formation of a condensed phase. The subsequent experimental measurements gave no cause to believe condensation was occuring however lower temperature operation (below 800°K) could lead to condensation as has been observed from room temperature stagnation conditions.

2.6 Gas Mixtures

In the design analysis of the skimmer it has been assumed that the nozzle flow is pure ammonia, however the object of the experiments was to measure the degree of dissociation of ammonia so it is necessary to

consider the performance of the skimmer with $NH_3 - N_2 - H_2$ mixtures. To predict the performance of the skimmer for the complete range of $NH_3 - N_2 - H_2$ mixtures resulting from dissociated ammonia would be very difficult and because of approximations of limited value, so instead the effects of having other species present will be considered as a perturbation of the conditions for skimming pure ammonia.

2.6.1 Nozzle Flow and Position of the Mach Disc

The position of the mach disc, as given by Ashkenas and Sherman[4], has been shown to be independent of the gas and γ and only a function of the pressure ratio. Both the resistojet plenum pressure and vacuum chamber pressure increase with increasing dissociation and while it is possible to calculate the nozzle plenum pressure the vacuum chamber pumping speed as a function of pressure and gas composition would need to be experimentally determined. This was not done because of difficulty in measuring the pressure of gas mixtures with Pironi gauges and because Mcleod gauges could not be used since mercury and ammonia react.

Should the mach disc move towards the nozzle and in front of the skimmer with increasing dissociation it would become immediately evident because the skimmer mass flowrate would drop considerably when it entered the diffuse flow within and behind the mach disc.

2.6.2 Mach Number and Skimmer Mass Flowrate

The axial Mach number is a function of γ and increases as γ increases. The main dependences on Mach number are the skimmer mass flowrate and mass spectrometer flowrate, which are functions of γ also. The shock detachment angle for the flow past a cone is a function of Mach number and γ but the skimmer angle was chosen for the conditions $M > 8$ and $\gamma = 1.4$ which is a more stringent criterion than a lower γ. No attempt was made to calculate Mach number for $NH_3 - N_2 - H_2$ mixtures or to predict the skimmer mass

flowrate but instead, by interpreting the mass spectrometer readings, correct functioning of the skimmer could be inferred.

2.6.3 Separation Effect

A separation effect has been observed [11, 25] when sampling mixtures in a free jet. Enhancement of both light and heavy species has been observed to occur on the jet axis at certain nozzle skimmer distances and nozzle pressure ratios. The mechanism for this separation has been postulated as a radial migration of the light species away from the jet axis giving an enrichment of the heavy species on the axis and also a preferential invasion of the free jet by background molecules. Reis and Fenn[26] have explained the separation as a flow perturbation caused by the skimmer itself and found no separation when the shock was attached to the mouth of the skimmer. With correct design of the skimmer to ensure an attached shock at all times and a calibration procedure using gas mixtures it was hoped the effects of separation, if present, would be eliminated.

Chapter 3

INSTRUMENTATION

3.1 Ammonia Supply Pressure

The ammonia gas pressure was measured in the feed pipe upstream of the resistojet connection. Pressure was measured by a Bell and Howell pressure transducer type 4-326 which operated over the range 0 to 1 Bar absolute with a linearity of ± 0.15% of full scale. The output from the transducer (nominally 40mV at 1 Bar) was amplified to 100mV at 1 Bar. The amplifier with its offset and gain controls is shown in schematic form in Figure 19, also shown is the 10V DC supply for the transducer.

Interior parts of the transducer in contact with ammonia were constructed of stainless steel which was compatible with ammonia.

The amplified transducer output was read on a Solartron Digital Voltmeter model A220, 100mV corresponding to 1 Bar absolute. To enable the digital voltmeter to monitor both pressure and thermocouple signals a selector switch was installed such that the D.V.M. could be connected to one of 10 inputs. The input was selected by a 10 position edge switch the signal switching being performed by 10 dual reed relays. Reed relays were chosen as the switching elements because of their reliability and low contact resistance especially with low level signals. The schematic of the selector unit is shown in Figure 20.

3.2 Ammonia Mass Flow Rate

Ammonia mass flow rate was measured by timing the fall of a constant pressure gasometer. The gasometer, its filling valves and control system was described in Chapter 1.

The gasometer was of constant circular cross-section, the sliding seal being effected by an oil bath. A rod attached to the centre of the top face actuated the control microswitches. Attached to this rod was a metal strip with notches cut at 15mm intervals. A stationary lamp and phototransistor detected the presence of the notches. The signal from the phototransistor was used to gate a clock signal to a counter such that the time taken for the gasometer to fall between two successive notches could be counted and displayed. At the end of a timing period the contents of the counter were transferred to the display store and the counter reset for the next timing period. The time to transfer the contents of the counter and to reset it was made very short (100nS) in relation to the timing resolution ($\pm$ 100ms) to preserve accuracy. At the end of each timing period a separate indicator was advanced 1 digit to show a new count had begun. During gasometer filling a reed relay actuated from the gasometer fill valve inhibited the counter such that it would not display misleading information. Circuitry was also provided to reset the counter to zero before the first timing interval. The timing system was constructed using Transistor-Transistor-Logic (TTL) integrated circuits and cold cathode discharge indicators. The clock signal was obtained by digitally dividing the output from a 1MHz crystal oscillator, whose accuracy was 1 part in 10^5. The circuit is shown in block form in Figures 21, 22, 23 and 24.

The gasometer measured gas volume flow rate, which was converted to a mass flow rate. The ammonia gas density needed to convert volume flow rate to mass flowrates was calculated from the gas temperature and pressure in the gasometer. The temperature was measured with a thermocouple in the gasometer feed line and the pressure in the gasometer was atmospheric pressure plus the gasometer differential pressure, which was measured independently.

3.3 Resistojet Temperatures

Resistojet temperatures were measured with Chromel-Alumel thermocouples and the e.m.f.s. were measured with the digital voltmeter the appropriate thermocouple being selected by the reed relay selector unit.

3.4 Resistojet Plenum Pressure

Resistojet plenum pressure was measured with a Bell and Howell pressure transducer type 4-326 with a range 0 to 1 Bar absolute. The transducer output was conditioned by an amplifier identical to that used for the supply pressure transducer and the 10V D.C. supply for the supply pressure transducer also supplied the plenum pressure transducer. The amplified output was displayed on the D.V.M. via the selector switch.

3.5 Nitrogen and Hydrogen Supplies

Nitrogen and hydrogen required for calibration were obtained from gas storage bottles in which the gas was stored at pressures up to 170 bar absolute. These pressures were reduced by regulators to supply pressures of approximately 1.1 Bar absolute. The volume flow rate for both hydrogen and nitrogen was measured using rotameters. Two rotameters were used for each supply, with valves, such that the appropriate rotameter could be selected.

Hydrogen and nitrogen flow-rates could be measured in the ranges 10-1800cc/min and 5-600cc/min at N.T.P. respectively. To correct the measured readings to N.T.P. the supply temperatures were measured with mercury in glass thermometers and the rotameter outlet pressures measured with Bourdon type pressure gauges.

3.6 Vacuum Tank Pressure

Vacuum tank pressure was measured with an Edwards High Vacuum Pirani gauge model 9. The gauge head was mounted on a flange at the top of the chamber. The reading from this gauge was used to provide the chamber overpressure indication for the ammonia controller. The gauge head was calibrated for ammonia but did not give a true reading for

ammonia - hydrogen - nitrogen mixture, however it was accurate enough to show that the pumping system was functioning correctly.

3.7 Mass Spectrometer Analysing Systems

Two mass spectrometers were used to analyse the sampled gas. Two were not essential to perform the analysis but both were available at the beginning of the project. One mass-spectrometer was an Edwards High Vacuum E180-2 Residual Gas Analyser, the other an A.E.I. D18 mass spectrometer. Both analysers were of the 180^{o} magnetic deflection type the ion radii being 15mm and 10mm for the Edwards and A.E.I. instruments respectively. Partial pressure range for both instruments was 10^{-5} to 10^{-10} torr of nitrogen. The A.E.I. instrument was obtained without the necessary power supplies which were constructed to the circuit diagram supplied with the instrument.

Requirements for the mass spectrometer system were:-

(1) to provide a low pressure for the mass spectrometers to operate (less than 10^{-4} torr total pressure).

(2) to pump the gas from the second skimmer orifice.

This requirement was met by an Edwards 2M4 mercury diffusion pump backed by an Edwards 1SC 50 rotory vacuum pump. The diffusion pump was surmounted by a liquid nitrogen cold trap and a $\frac{1}{4}$ swing butterfly valve on which the mass spectrometers were directly mounted (Figure 23). This system had a pumping speed of approximately of 30 litres/sec. Connection to the skimmer was via a 12mm diaphragm valve. To prevent damage to the mass spectrometer filaments by inadvertent operation at too high a total pressure an Edwards Penning gauge Model 6 monitored the total pressure in the system. Use of a mercury pump with a liquid nitrogen cold trap prevented any contamination of the mass spectrometers by the pumping fluid.

Chapter 4

RESISTOJET DESIGN

4.1 Introduction

The resistojet design used for the experiments was specified by the Royal Aircraft Establishment (RAE) as having a geometry which was suitable for manufacture in a wide range of materials and would withstand the stresses imposed during launch and yet provide a good thermal design.

The criteria used for the design of a Resistojet suitable for flight use are very different from those used in the design of a laboratory test resistojet which may only need to operate for 20-30 hours. To provide RAE with information directly applicable to their own resistojet programme the internal flow geometry was made identical to their resistojets but the outside appearance and size were modified to allow simpler methods of construction and mounting. The nominal flow geometry is shown in Figure 27 and is the same for all the resistojets studied, the only differences between them being in materials and methods of construction.

4.2 Design

The RAE resistojet JP3, was designed to have a heating element inserted in the central core which was to provide the heat to keep the resistojet temperature maintained at approximately 1000^{o}K. This steady state temperature was determined by the available power input ($\approx$ 5 WATTS) and the various heat losses; nozzle radiation, radiation from the body, conduction along the fuel pipe and supports. Pulsed operation allowed the gas to be heated using the sensible heat contained in the resistojet body which would consequently suffer a drop in temperature during a pulse. In the time between pulses the body would be reheated to its equilibrium temperature.

To conduct the tests envisaged it was necessary to operate the resistojet continuously for up to two hours, which meant supplying the total power requirement for the gas continuously. ($\approx$ 100W at 1000^{o}K and 0.04gm/sec). This then meant the losses which are critical in low power pulsed operation become less important and much smaller in comparison with the total power requirement for continuous operation. To overcome the power supply problem the resistojet was designed to have two heaters, an inner core as in the original design and an outer heater sleeve. The outer heater provided a high temperature enclosure for the resistojet and as such supplied most of the heat lost by radiation and conduction along the supports. The outer heater was made by winding a Nichrome wire on a ceramic former and was capable of dissipating up to 300 watts. The inner heater was originally of similar construction and was designed to dissipate up to 150 watts. Because of limitations on wire temperature which restricted its maximum operating temperature the inner heater was changed for one constructed of tungsten wire on a ceramic former, which was capable of dissipating up to 100 watts but at a higher operating temperature.

To minimise radiation losses the resistojet was surrounded by a multilayer stainless steel radiation shield and then mounted in an aluminium housing, Figure 28. Supports consisted of eight 1.5mm wires, four at each end of the resistojet which were screwed into the resistojet body and supported in the housing on tubes as shown in Figure 28. The front and back faces of the resistojet were covered with stainless steel radiation shields with cut outs for the nozzle, feed pipe and heater supplies.

The first resistojet was constructed in stainless steel type AISI 321 and is shown in exploded forms in Figure 29 and as a sectional drawing in Figure 30. The nozzle and the inner section were interference fits in the main body but the fuel pipe was welded into the body on the back face.

End cheeks provided the support points and held the outer heater loosely in position and the inner heater was trapped in position by the rear end cheek. Both heaters were made loose fits to avoid problems of differing thermal expansions. Photographs of this resistojet are shown in Figures 31 and 32.

A second resistojet was constructed identically to the first except the body, nozzle and inner cone were made from nickel (commercially pure nickel; 99.5% nickel) all other parts including the feed pipe were of AISI 321 stainless steel.

The third resistojet was made demountable and sealed with metal "O" rings. This form of construction allowed a plenum pressure tapping to be incorporated to enable the pressure drop along the heated annular section to be measured. The method of construction of this resistojet is best seen in Figure 33 and the photographs of Figures 34 and 35.

The outside dimensions were made identical to the first two resistojets to enable it to be mounted in the existing housing and share the same heaters. This resistojet was made in AISI 321 stainless steel.

The fourth resistojet was identical to the first two except the material used was AISI 347 stainless steel.

4.3 Temperature Measurement

The temperature of the resistojet under test was measured by a chromel-alumel thermocouple welded to the end wall of the inner core as shown in Figure 36. The thermocouple leads passed through the centre of the heater in ceramic tubes. The two thermocouple leads were first welded together and then welded as a pair onto the end wall. To enable this welding to be performed a capacitor discharge welder was constructed similar to one designed by Colclough et al [27] except for the thyratron which was replaced by a thyristor. The circuit diagram is shown in Figure 37.

A sheathed thermocouple was also inserted into a pocket in the main body (except on the demountable resistojet) as shown in Figure 36.

4.4 Heaters and Power Supply

The heaters were originally constructed of a Nichrome wire helix wound on a ceramic former. Advantages of Nichrome wire are that it is easily worked, does not become brittle after heating and has an almost constant resistivity of 110 x 10^{-6} Ω - cm in the temperature range 300 to 1400°K. The disadvantage is that the maximum operating temperature is 1400°K. The maximum resistojet temperatures envisaged were 1100°K but because of poor thermal contact between the heaters and resistojet body (the heaters are in the vacuum space and heat is transferred by radiation alone) the heaters are operated at temperatures considerably higher than the resistojet.

The power supply designed for the Nichrome heaters was a switching A.C. controller and is shown in block form in Figure 38; advantages of this type of controller over a regulated D.C. supply of the same power level (400 watts maximum) are

(1) Greatly reduced dissipation especially at intermediate power settings, e.g. the power dissipation of a D.C. controller at quarter power is 100W, whereas for an A.C. controller it is proportional to current and a maximum of 10W at 10A.

(2) The power control could be made linear for a heater of constant resistance.

The controller works by switching the full supply to the heater for some fraction, set by the power control, of the sawtooth waveform period. This period was made approximately 2 seconds, which was sufficiently long to allow fine control but was considerably shorter than the thermal time constant of the resistojet.

Supply switching occurs at the zero voltage points of the A.C. waveform which leads to very low levels of interference generated by the controller. The transformer secondary voltage was chosen as 40V r.m.s., because:

(1) 40 volts is a low enough voltage to be handled safely in a vacuum system without risk of discharges.

(2) With 40V a current of 10A would produce a power of 400W. A current of 10A is easily handled without recourse to high current connectors and heavy duty cable.

(3) To dissipate 400W at 40V the heater needed a resistance of 4Ω. Heaters of the size required for the resistojet could be constructed to have a resistance of 4 Ω using easily available wire sizes.

4.5 Tungsten Inner Heater

The outer heating element performed satisfactorily, the wire temperature always being below the maximum safe temperature, but the inner heater failed several times due to overheating of the wire. Heat transfer between the inner heater and the resistojet body was by radiation alone and had the whole heater element (former and wire) been at the same temperature the heat transfer area would have been sufficient, however due to the loosely wound construction it became apparent that the wire operated at a much higher temperature than the ceramic core which led to its failure. Cementing the heater into the resistojet aggrevated the problem due to the poor thermal conductivity of the ceramic cement used. The solution adopted was to use a similar heater core but wound with tungsten wire which has a much higher operating temperature. Tungsten wire is more brittle than Nichrome wire, especially after heating, which necessitated cementing the sleeved lead out wires rigidly into position so as not to strain the heater section of the wire. The tungsten lead-out wires being sleeved with stainless steel tube, dissipated less power and

operated at a much lower temperature than the unsleeved element.

The wire size and length were chosen to give a resistance of 1 Ω at 1400°K (estimated operating temperature) which would then be capable of dissipating 144 watts from a 12V, 12A variable A.C. supply. In practice the wire temperatures obtained were higher than 1400°K. This restricted the maximum power that could be dissipated to approximately 100W because the resistivity of tungsten increases with temperature. At a supply voltage of 12V the current drawn was 8A. No attempt was made to shorten the heater to enable it to dissipate more power because 100W was found to be sufficient for the experiments performed. The power supply for the tungsten heater is shown in schematic form in Figure 39.

Chapter 5

EXPERIMENTAL METHOD AND MEASUREMENTS

5.1 Skimmer Mass Flow Rates

The expressions used in the design of the skimmer predict the mass flowrate through the second orifice to the mass spectrometer as a function of resistojet plenum conditions. The diameter of this orifice was chosen to give a gas flow at the mass spectrometer such that the range of partial pressures produced were within the linear dynamic range of the mass spectrometers. For a resistojet mass flowrate of 0.025gm/sec at 1000°K the second orifice diameter had been calculated to give a partial pressure of 4×10^{-7} torr of ammonia at the mass spectrometer. This partial pressure was a factor of five greater than the background at mass number 17 due to dissociated water vapour, such that any corrections necessary would be small. In order to cover the range of mass flowrates (0.022 → 0.033gm/sec) and the temperature range (900 → 1070°K) only one orifice of 1mm diameter was needed.

Skimmer mass flowrates which were inferred from the pressure at the top of the diffusion pump evacuating the skimmer agreed closely with the calculated values as given in Table I Chapter 2, which confirmed correct opeation of the skimmer.

5.2 Resistojet Pressure Drop

Pressure drop in the heater section of the resistojet is important for performance predictions, the predicted performance would be based on plenum pressure and not supply pressure. It was possible to measure both the plenum and supply pressure on the demountable stainless steel resistojet and hence pressure drop. Pressure drop was not measured

directly because it was not possible to obtain a differential pressure transducer which was compatible with ammonia. The pressure drop was measured as a function of mass flowrate and temperature and is shown in Figure 40. The pressure drop measurements were the first test on this resistojet, before any significant amounts of nitride had formed, (this is explained in Chapter 6), and were for undissociated ammonia.

5.3 Attached Shock at Skimmer Lip

Correct operation of the skimmer required an attached shock at the skimmer lip. To try to provide evidence as to whether or not the shock was attached optical flow visualization studies in the free jet were investigated.

Of the various optical techniques the two which were applicable to the present experiment were electron beam fluoresence and nitrogen fluoresence or afterglow [28, 29]. Electron beam fluoresence enables detailed studies within the free jet and nozzle region but requires considerable expertise and equipment, and was not considered for these reasons. The electron beam method is potentially applicable to all gases, however the afterglow technique is only applicable to nitrogen or similar gases (e.g. oxygen). The mechanism involved is the afterglow or fluoresence from excited nitrogen molecules produced by atomic recombination, the shock wave being a region of higher density shows as a brighter region due to increased recombination rates. Although the skimmer had not been designed for operation with nitrogen it was expected that the shock at the skimmer lip would still be attached, providing the skimmer was inside the mach disc and the flow did not choke in the skimmer entrance. The position of the mach disc was calculated for nitrogen as a function of plenum pressure and temperature (Figure 41) using the measured pumping speed of the vacuum chamber for nitrogen. For a skimmer placed 7OD downstream the mach disc was always expected to be downstream of the skimmer entrance, however to provide a greater margin and to avoid any possible condensation effects

the tests were conducted with the resistojet heated to approximately 750°K. Stable discharges were only possible for plenum pressures below 400m Bar the corresponding vacuum chamber pressure was 2×10^{-2} torr.

A brightened shock region around the skimmer was visible but due to the low gas density and poor contrast the photographs taken were not suitable for reproduction. Figure 42 shows a line drawing taken from the original photograph which shows the shock position and the electrode configuration. The conditions for Figure 42 were plenum pressure = 350m Bar, discharge voltage = 5KV, resistojet temperature = 753°K and the vacuum chamber pressure = 2×10^{-2} torr.

Previously calculated mean free paths at the skimmer entrance predicted a shock thickness of several millimetres which makes it difficult to determine the exact position of the shock at the skimmer mouth but from Figure 42 the shock originates from the skimmer lip and not from in front of the skimmer as it would if it were a bow shock.

Evidence from the nitrogen afterglow experiments and the good agreement between the calculated and measured partial pressures of ammonia at the mass spectrometer inferred that an attached shock was present at the skimmer lip.

5.4 Method of Calibration of the Mass Spectrometers

The mass spectrometers were not equally sensitive to all gases. As well as the mass spectrometers having different sensitivities for ammonia hydrogen and nitrogen, the tube connecting the mass spectrometers to the skimmer and the mass spectrometer pumping system had different conductivities for the three gases. The free expansion flow from the nozzle is also susceptable to mass separation effects [26, 11].

To overcome all these effects it was necessary to calibrate the mass spectrometers by introducing known mixtures of ammonia, hydrogen and nitrogen into the resistojet. However because some of the separation

effects depend on relative concentrations and total pressure, thus requiring a large matrix of calibrations, it was found simpler to calibrate after each experiment by varying the input gas mixture to reproduce the readings obtained during the run. This method of calibration did not require either a knowledge of the absolute sensitivity of the mass spectrometers nor any corrections because of the different conductivities of the gases.

To ensure the free expansion flow was not substantially different during the calibration and the actual measurements, the calibration were carried out with the resistojet at a temperature of 820°K. This temperature was well below that at which dissociation was initiated (900°K) but was sufficiently high to avoid any condensation effects in the free expansion.

This method of calibration also simplified corrections due to background pressures in the mass spectrometers. The most predominant of these backgrounds was that due to water vapour which due to fragmentation by the electron beam was observed at H_2O (mass 18) OH (mass 17) and O (mass 16). For each mass spectrometer there was a fixed ratio between the masses 18, 17 and 16 peaks due to water vapour such that the water vapour contribution to an ammonia reading at mass 17 could be determined from the water vapour present at mass 18.

This correction to the ammonia readings was not always necessary because the water vapour background did not change appreciably between the time of the test and calibration, which were usually within two hours of each other. Ammonia was also observed in the mass spectrometer as mass numbers 16 (NH_2), 15 (NH), 14 (N), 28 (N_2) and 2 (H_2) due to fragmentation by the electron beam. The calibration method adopted did not require a knowledge of the relative intensities of the fragmentation peaks because during the calibration the partial pressure of ammonia present was identical

to that during the actual measurements and hence made an equal contribution to the fragmentation peaks. The peak at mass number 16 (NH_2 + O from water vapour) was also recorded with that at mass number 17, as representative of the ammonia present because the background at mass 16 due to water vapour was over an order of magnitude lower than the peak due to ammonia.

The peaks recorded at masses 2 and 28 (hydrogen and nitrogen) were not corrected for background readings because of the very low and substantially constant background pressures at these mass numbers.

The operating parameters for the two mass spectrometers are shown in Table 5.

TABLE 5

	Electron Beam Current μA	Electron Beam Accelerating Potential V	ION BOX Potential V	ION Path
EDWARDS	60	76	-36	1.5cm radius
A.E.I.	5	70	-20	1.0cm radius

Chapter 6

EXPERIMENTAL RESULTS

This section presents the experimental results obtained with the various resistojets. The results will be analysed in the next section in relation to other theoretical and experimental reported works.

6.1 First Stainless Steel Resistojet

The first resistojet had been run for some considerable time (tens of hours) before the measurements presented here were taken, and in the light of the results from the later stainless steel resistojets this explains their apparent inconsistent behaviour. Considerable running time was needed to set up the mass spectrometers, skimmer, and to arrive at a satisfactory design for the inner heater, before dissociation measurements were made.

Measured values of dissociation at various temperatures and two mass flowrates are shown in Figure 43. It was proposed to perform further measurements at two more mass flowrates, however when attempted it was found that, at constant mass flowrate and temperature, the supply pressure was slowly rising with time. The measured supply pressure was considerably higher than the theoretical prediction for the required plenum conditions and also higher than it had been on an earlier test at otherwise identical conditions.

On investigation it was found that the nozzle surfaces had become coated with a black deposit. At first it was thought to be caused by hydrocarbons from the oil filled gasometer dissociating in the heater and nozzle and depositing carbon. However on examination it was suspected of being a nitride of either iron or chromium. No further tests were conducted with this resistojet which was cut in half (at right angles to the axis into the gallery) to examine the inner heater surfaces. The

metal surfaces in the heater were very hard and covered by a loose black scale which had partially blocked the flow passage. When the scale was removed and the dimensions of the heater assembly checked it was found that the metal surfaces had been eroded, more at the nozzle end than the inlet end, such that the central plug diameter had been reduced from 13.5mm to 13.35mm at the nozzle end. This was consistent with nitride formation, the metal would be consumed as nitride was formed, nitride having a larger specific volume than the parent metal would tend to close the flow passages as it grew resulting in the observed pressure increase.

6.2 Nickel Resistojet

In an attempt to study an elemental high temperature metal, nickel was chosen as the material for the second resistojet. This choice was made before the nitriding behaviour of the first resistojet had been observed.

When the nickel resistojet was first installed the experimental apparatus was functioning perfectly such that measurements of dissociation could be made immediately. Measurements were made at temperatures in the range 905 - 1053^{o}K for four different mass flowrates. Dissociation was evident during the first test and the results shown in Figure 44 were obtained. These results showed consistency and no evidence of blocking was found during the course of the experiments.

On conclusion of the experiments the resistojet was cut in half to examine the internal surfaces, which were covered with a thin white deposit. The metal surface had a very thin hard layer but no pitting or erosion was observed.

6.3 Demountable Stainless Steel Resistojet

This resistojet was designed after the results from the first stainless steel resistojet had been obtained. The objective was to enable the internal surfaces to be examined without having to cut the

resistojet in half so that if necessary it could be used again. With the design adopted it was also possible to insert a plenum pressure tapping to measure pressure drop through the heater.

Initial experiments were performed to measure the heater pressure drop at various temperatures and mass flowrates. The temperature range chosen was between 825 and 900°K, this was below the temperature at which dissociation had been observed on the earlier stainless steel resistojet, because dissociation may have resulted in nitride formation and possible blockage.

The subsequent tests were to measure the dissociation of ammonia at temperatures up to 1050°K. However the first time the temperature was taken up to 1050°K no dissociation was observed. This behaviour was inconsistent with either the nickel or earlier stainless steel resistojets, and suggested that dissociation and nitride formation might be associated and could possibly change with time. Subsequent tests involved holding the resistojet at a constant temperature of 1075°K and monitoring the dissociation.

The results obtained are shown in Figure 45, dissociation below 3% was difficult to measure accurately. When dissociation become evident, the pressure drop through the heater and plenum pressure both increased.

After $8\frac{1}{2}$ hours running the resistojet was dismantled for examination. Both surfaces of the annulus showed grey blister like formations, more at the nozzle end than the feed end. These surface crustations were examined with an electron beam probe the photographs taken shown in Figure 46. The top photograph shows a portion of the surface with a blister to left hand lower corner of the photograph. The middle photograph shows the same area but the pattern of dots is a measure of the nitrogen concentration in that area. This indicates a fairly uniform nitrogen concentration across the surface. The lower photograph indicates iron concentration and clearly shows a higher concentration in

the region of the blister.

The conclusions to be drawn from these photographs is that the blister is a build up of surface iron nitride, which had been suspected on the first stainless resistojet.

No further tests were performed on this resistojet because of the time dependent nature of the dissociation and the possibility of blocking precluded the use of this material for an operational resistojet.

6.4 A.I.S.I. 347 Stainless Steel Resistojet

This resistojet was similar to the first resistojet in construction except for the different grade of stainless steel used. The results shown in Figure 45 are similar to those of the demountable resistojet and when cut apart also showed a similar blistered surface.

6.5 Analysis of Nickel Resistojet Results

Of the results obtained with the various resistojets only those from the nickel resistojet readily lend themselves to analysis in terms of an activation energy. Various other workers had measured dissociation of ammonia on metal surfaces, however Miles[30] fitted his results into an equation of the form

$$\frac{d}{1-d} = K \left(\frac{S}{G}\right)^{c} e^{-B/RT}$$

where d = fraction of dissociated ammonia

K = constant

S = active area

G = mass flowrate

C = constant

B = activation energy

The results from the nickel resistojet were reduced to the form of the above equation and the best fit gave the equation

$$\frac{d}{1-d} = 2.98 \times 10^{7} \left(\frac{S}{G}\right)^{1.16} e^{-65,550/RT}$$

where G = mass flowrate gm/sec

S = area m^2

R = 4.1868 KJ/kg. ^{o}K.

The results are shown plotted in Figure 47. The relationship derived above includes a dependence on area as in the expression of Miles, however in the present experiments it was not possible to check this dependence.

The expression derived by Miles for stainless steel is equivalent to

$$\frac{d}{1-d} = 1.06 \times 10^{6} \left(\frac{S}{G}\right)^{0.5} e^{-51,900/RT}$$

Comparing the two equations, the activation energy is higher for nickel than stainless steel. This compares well with the results of Rabiere[31] who found less dissociation on Inconel (80% nickel) than stainless steel and Miles who also found less dissociation on nickel.

The mass flowrate exponent is also much higher for nickel than stainless steel, the reason for this is unclear, but the space velocity (mass flowrate per unit surface area) is much higher in this investigation than in Miles's experiment (1.33 - 2.66 x 10^{-5} gm/sec. mm^2 in this experiment and 2.09 - 43.5 x 10^{-7} gm/sec. mm^2 in Miles's experiment) which may account for the effect.

Catalytic dissociation of ammonia is believed[32] to be dependent upon the absorption of ammonia molecules on the catalyst surface and this in turn is dependent upon the number of available surface sites per unit mass of gas. Hence one might expect a dependence on space velocity. In this investigation the surface area of the resistojet was constant and

an overall dependence on space velocity could not be found. No dependence on pressure was found which varied from 354 to 548 m Bar.

The experimental data points were used as input data in a computer program supplied by I. Edwards[19] which predicts the flow through small nozzles. The calculated performance figures, thrust, and specific impulse versus temperature are shown in Figures 48, 49, 50 and 51. Experimental input data required for the program is plenum pressure which was supply pressure minus the heater pressure drop (measured for the stainless resistojet), temperature and degree of dissociation. The program then calculated thrust, specific impulse, mass flowrate and electric power to the gas. The calculated and measured mass flowrates agreed to within 2%. Shown in Figure 52 is the calculated power to the gas (Watts) as a function of temperature for the four mass flowrates and Figure 54 shows the specific power plotted against temperature. Figure 53 shows specific power ($^{W}/_{mN}$) plotted against specific mass flowrate ($^{gm}/_{N.sec}$), since both of these quantities need to be minimised for efficient operation the lower left hand corner represents more efficient operation. The highest mass flowrate shows most efficient operation because of reduced losses in the nozzle (higher Reynolds number).

For all four mass flowrates the specific impulse is approximately 210 seconds at 1050°K compared with 187 seconds at 1050°K if no dissociation occurs. This will be discussed further in the next chapter with respect to satellite mission requirements.

6.6 Analysis of Stainless Steel Resistojet Results

The results from the three stainless steel resistojets cannot be analysed in the same way as for the nickel resistojet, however their behaviour warrants some investigation. Had the demountable and 347 stainless steel resistojets been held at high temperature long enough it is likely they would have become blocked as did the first resistojet. From the results presented here it is obvious stainless steel is an unsuitable material for ammonia resistojets.

The blisters formed on the demountable resistojet were found to be an iron nitride which was ultimately responsible for blocking the first resistojet. Iron nitride is an intermetalic compound Fe_3N, thought to be formed in the presence of atomic nitrogen. Atomic nitrogen is formed in the dissociation of ammonia and some is dissolved into the metal matrix which can then form a nitride with the metal. Nitrogen has a much lower solubility in nickel than in iron which is why thick nitride layers were not found on the nickel resistojet within the time scale of the experiment. However had the experiment with the nickel resistojet continued, ultimately, thick nitride layers as on the stainless steel may have formed.

Both Rabiere and Miles have reported results of dissociation on stainless steel, the expression derived by Miles was quoted in the previous section and the results of Rabiere reduced to a similar expression are:-

$$\frac{d}{1 - d} = 3.17 \times 10^8 \left(\frac{S}{G}\right)^{0.5} e^{-75,800/RT}$$

The measurements of Rabiere were in the same temperature range as the present experiments and for a similar experimental configuration, two concentric tubes with flow through the annulus, however the space velocity was over an order of magnitude lower. In Miles's experiment dissociation was produced on a 30mm internal diameter tube 620mm long which was the preheater section to a catalyst bed.

The time dependent nature of the dissociation found on the stainless steel resistojets can be quantified in the following relationship:-

$$d = 0.345 \left(\log_{10} t - \log_{10} t_o\right)$$

for $t > t_o$

where d = degree of dissociation

t = time in hours

t_o = an induction time in hours

t_o = 2.91 hours for the 321 stainless steel resistojet and 2.7 hours for the 347 stainless steel resistojet.

This relationship would predict no dissociation in the induction time period, this however is unlikely, the observed behaviour suggests that in this period the metal surface is conditioned, perhaps by the formation of a thin surface nitride layer, and at later times it is this modified surface which is responsible for the dissociation. Since neither Rabiere nor Miles found dissociation to be time dependent it may be that their experiments were performed in the induction period on a partially conditioned surface. This could explain the difference in the activation energy of the two expressions for dissociation on stainless steel, however the time dependent nature of the rate of dissociation as found in the present experiment suggests caution in interpreting an expression of this form because the relationship may only hold for a sample of material with the same history.

Table 6 lists the conditions present in the experiments of Miles, Rabiere and the present investigation.

TABLE 6

	Resistojet	Miles's Experiment	Rabiere's Experiment
Mass flowrate gm/sec	$20 \rightarrow 40 \times 10^{-3}$	$12 \rightarrow 250 \times 10^{-3}$	$0.5 \rightarrow 5 \times 10^{-3}$
Volume mm^3	1.835×10^{2}	4.29×10^{5}	5.5×10^{2}
Area mm^2	1.5×10^{3}	5.74×10^{4}	1.1×10^{3}
Space Velocity gm/sec mm^2 $(\frac{G}{S})$	$1.33 \rightarrow 2.66 \times 10^{-5}$	$2.09 \rightarrow 43.5 \times 10^{-7}$	$4.55 \rightarrow 45.5 \times 10^{-7}$
Mass flowrate per unit volume gm/sec mm^3 $(\frac{G}{V})$	$1.09 \rightarrow 2.18 \times 10^{-4}$	$2.8 \rightarrow 58.3 \times 10^{-8}$	$0.91 \rightarrow 9.1 \times 10^{-6}$
Temperature Range	$900 \rightarrow 1050^{\circ}K$	$650 \rightarrow 810^{\circ}K$	$900 \rightarrow 1150^{\circ}K$

The mass flowrate per unit volume is a measure of residence time in the heater.

Corrosion behaviour of stainless steel and nickel alloys in ammonia atmospheres has been reported[33] and it was found that corrosion was a minimum for 80% nickel, 20% chromium alloys (similar to Inconel) in the temperature range 720 - 820°K. Figure 55 shows the results they obtained at a temperature of 770°K in an ammonia plant line. Those alloys containing chromium that suffered corrosion were shown by X ray diffraction to have a brittle outer layer of chromium nitride and an inner layer of nitrogen dissolved in the metal matrix. The higher nickel alloys were more resistant although not pure nickel, and some stainless steel specimens were completely destroyed, the higher nickel content alloys showed a lower solubility for nitrogen.

The above evidence suggests that stainless steels form brittle nitride surface layers in hot ammonia atmospheres, the time taken to form these layers being dependent on both space velocity and temperature. The present experiment had both the highest temperature and space velocity of the three investigations compared and was the only one where nitride formation was observed.

Chapter 7

DISCUSSION ON RESISTOJET DESIGN

This chapter deals with resistojet design in general and is divided into three main sections, heat input, heat losses and dissociation. This design study is by no means exhaustive not covering for example material selection or mechanical design. It has concentrated on the thermal aspects of resistojets which should be applicable to any subsequent design adopted. Where necessary reference has been made to the performance of resistojets with no dissociation and full dissociation. The resistojet in these two limiting cases is assumed to have the same geometry as the nickel resistojet, whose performance is used as a realistic measure, having been achieved in practice. The performance parameters, thrust, power to the gas, specific impulse, etc. have been computed using the program of Edwards[19].

7.1 Heat Input

The average power transferred to the gas in a thermal storage resistojet operating in the pulsed mode can be very low, consequently the power consumption is dominated by heat losses incurred in maintaining the steady state temperature of the resistojet. A typical resistojet producing 0.05N thrust at an operating temperature of 1000°K and for a 0.1% duty cycle only requires an average power of 80mW yet it needs approximately 5W to maintain a constant temperature of 1000°K. During the period of thrusting the power requirements are much higher (80W for the above example). Energy given to the gas during a pulse is taken from the sensible heat of the metal which consequently drops in temperature. To ensure that the temperature drop is not excessive the heater must have sufficient sensible heat to accommodate this energy consumption during the length of the pulse. For example approximately 1gm of Nickel

is required to limit the temperature drop to 10°K in a resistojet pulsed for 50ms and producing 0.05N thrust at 1000°K.

The heat may be supplied to the resistojet in two different ways, direct resistance heating of the resistojet or indirect heating from a separate resistance heater. Direct heating dispenses with a separate heater and heats the metal surfaces directly, but because the resistojet has a low resistance and therefore requires a low voltage high current supply extra power conditioners are required. These conditioners whose efficiency is approximately 90% at best further reduce the available payload of the satellite. Fast heat up resistojets, in which power is supplied only during a pulse, have been constructed using direct heating where it is necessary to minimise the thermal time constant and consequently the mass of material in the resistojet. A separate heater element can be tailored to the satellite power supplies thus dispensing with power conditioners and can allow the designer more scope by, for example not requiring electrical continuity of the resistojet.

To produce short (approximately 50ms) well defined repeatable pulses from a resistojet the heater passage volumes must be kept to a minimum to ensure the filling time is considerably shorter than the pulse length. Heat transfer to the gas requires a large surface area to minimise the temperature difference between the gas and heater. However the pressure drop through the heater which represents a loss and will ultimately limit the pulse response, will be greatest for those designs which both minimise the included volume and maximise the surface area, therefore a design compromise is necessary.

The flow geometry adopted for these experiments originated from the Royal Aircraft Establishment (R.A.E.) Farnborough as a possible design which could be constructed suitable for flight duty.

The annular passage, heated internally by a separate heater results in a very compact design with a small external surface area for lowest radiation loss.

The flow through the annular passage is fully developed laminar flow (Reynolds number = 19.75 at T = 1000°K, and Thrust = 0.05N for undissociated ammonia). Treating the annular passage as two flat plates it is possible to calculate the heat transfer rate to the gas. Assuming a temperature profile of the form

$$t = t_w + ay + by^2 + cy^3$$

where t = gas temperature

t_w = wall temperature

y = distance from centre line of flow at right angles to walls

a, b and c are constants.

The local Nusselt number can be calculated, using a method similar to that of Rogers and Mayhew[34], to be 3.25. The overall Nusselt number is the same as the local Nusselt number except for the entry length, where the temperature profile is changing, and can initially be neglected.

Now

$$Nu = \frac{h\,d\,Pr}{\mu\,Cp}$$

where Nu = Nusselt number

Pr = Prandth number

μ = viscosity of gas

Cp = Specific heat at constant pressure

h = overall heat transfer coefficient

d = distance between plates

Taking values of Pr, μ and Cp at a mean gas temperature of 650°K one obtains

$$h = 0.1132 \text{ Watts cm}^{-2}\ {}^{o}K^{-1}$$

Now $$\dot{Q} = \dot{m}\,Cp\,(t_{out} - t_{in})$$

and $\dot{Q} = h A \Delta \dot{T}_{LM}$

where A = heat transfer area

ΔT_{LM} = log mean temperature difference

Equating one obtains

$$\ln \left\{ \frac{t_w - t_{out}}{t_w - t_{in}} \right\} = - \frac{hA}{\dot{m}Cp}$$

Using the value of Cp at 650°K and a representative mass flowrate one obtains:-

$$\ln \left\{ \frac{t_w - t_{out}}{t_w - t_{in}} \right\} = - 20.9$$

Now $t_w - t_{in} = 700^{\circ}K$

therefore $t_w - t_{out} = 6.3 \times 10^{-7}\ ^{\circ}K$

This demonstrates that the heat transfer is very good for the R.A.E. designed resistojet, the outlet gas temperature being almost identical to the wall temperature. The entry length which was neglected in the above analysis is given by Schlichting[35] as

$$Le = 0.04.d.Re.$$

for the above case where Re = 19.75

$$Le = 0.79d$$

This result implies fully developed pipe flow at one channel width downstream. The value of Reynolds number used above was for gas at 1000°K but within the entry length the temperature will be considerably less and changing which will give a higher Reynolds number, however the entry length will still be of the order of a few channel widths.

If the heat transfer analysis is repeated with $t_w - t_{out}$ equal to 10°K the resulting area corresponds to a length of 3.45mm or 14 channel widths. It would therefore seem possible to reduce the heater length of the present design from 17mm to 5mm and still have adequate heat transfer.

The overall heater surface area may be determined not from heat transfer considerations but from the surface area required to obtain sufficient dissociation of ammonia. In cases where it may be advantageous to suppress dissociation a heater of minimum area, from heat transfer requirements, would help in this respect.

7.2 Heat Losses

A thermal storage resistojet will attain a temperature which will be determined by the heat input, the heat losses which increase with temperature and the power supplied to the gas. With operation at low duty cycles most of the heat supplied is used to maintain the temperature of the resistojet and only a small proportion of the heat input is actually transferred to the gas. Low power operation requires that the losses be minimised to obtain the highest temperatures and consequently better performance.

Operation in a vacuum environment allows only two heat transfer mechanisms, conduction and radiation. Convection however could be important if the nozzle flow were allowed to permeate the insulation but this would be as a result of bad design and will not be considered further. The conduction paths available are the supports, fuel pipe, heater leads and instrumentation leads (e.g. thermocouples) if any, the first two being the most important. A typical resistojet configuration might have three mounting wires each 0.5mm diameter, 15mm long and a fuel pipe 3.0mm outside diameter, 2.5mm inside diameter, 25mm long and would expect the conduction losses as shown in Table 7.

TABLE 7

Temperature °K	Heat Losses by Conduction WATTS	
	Stainless Steel	Molybdenum
1000	2.15	8.79
1100	2.46	10.0
1200	2.77	11.3
1300	3.07	12.55
1400	-	13.8
1500	-	15.1

The losses for molybdenum are obviously very high and unacceptable, those for stainless steel are more realistic up to the temperature limit of 1300°K. By careful design it should be possible to achieve conduction losses of the order of 1 watt at 1000°K.

Radiative heat loss is more important than conductive losses especially at high temperatures. A typical resistojet at 1000°K would radiate approximately 50 watts of heat if uninsulated, which emphasises the need for some form of insulation. Radiation shielding applied to the body of the resistojet can reduce these losses to approximately 3.5 watts at 1000°K[36] however the nozzle which cannot be insulated and will be at or near the heater temperature will still radiate appreciable amounts of heat. An estimate of nozzle radiation losses was made assuming the nozzle throat was a black body and the rest of the nozzle was a grey body with an area equal to the exit plane and an emissivity appropriate to the material at that temperature. The calculated losses are shown in Table 8 for nickel and molybdenum for a typical resistojet nozzle.

TABLE 8

	Heat losses by radiation. Watts.					
	1000°K	1100°K	1200°K	1300°K	1400°K	1500°K
Molybdenum	0.17	0.24	0.35	0.48	0.65	0.85
Nickel	0.22	0.32	0.46	0.64	0.85	1.13

The high levels of heat loss by nozzle radiation is a significant factor. By using nozzles with small expansion ratios to give a small exit plane area low radiation losses can be obtained. Ideally to expand the flow into a vacuum an infinite area ratio nozzle is needed, however, because of boundary layer growth which increases with nozzle wall length and large radiation losses nozzles are truncated; 25:1 area ratio in the present design. For higher temperature operation it may be necessary to further truncate the nozzle to an expansion ratio as low as 5:1 to reduce radiation losses. Alternatively it may be possible to reduce the overall nozzle size whilst maintaining the same area ratio, this technique must however be applied with caution because of increased losses incurred in smaller nozzles due to thick boundary layers. In truncated nozzles increased incomplete expansion loss is traded for higher temperatures and hence higher specific impulse.

Radiation loss from the body of the resistojet can be reduced as already indicated by insulation. This can either be solid fibrous insulating material or for much better performance multilayer metal foil shields are used. Typically the shields would be made of molybdenum or nichrome, essentially a high temperature low emissivity material, and would be separated by either a thin insulating material or they would be "dimpled" to space them. Single shields of high reflectance (low emissivity) gold have been tried, but are very susceptible to damage by

evaporation of material from the resistojet to the shield, which would dramatically reduce its reflectance. Further radiation loss is incurred through the fuel pipe, for a fuel pipe without bends the resistojet would appear as a black body at heater temperature. To reduce this loss baffles installed in the fuel pipe act as radiation shields.

To illustrate the effects of heat losses on performance for a power limited resistojet it is necessary to compare the specific impulse (S.I.) obtained for different power inputs. Total power input is the sum of heat losses and power to the gas, which depends on the product of pulse length, thrust level and pulse rate i.e. impulse per unit time. Heat losses for thermal storage resistojets have been measured by Dixon[36] and by using his results it is possible to plot S.I. versus power input for various values of impulse per unit time. This is shown in Figure 57 for two values of impulse 5×10^{-2} and 5×10^{-1} mNs/sec which correspond to duty cycles of 10^{-3} and 10^{-2} at a nominal thrust of 50mN. For duty cycles less than 10^{-3} the power to the gas can be neglected and only losses need be considered. The nickel resistojet results were used to compile Figure 57 which explains the increase in gradient with increasing power level, it is in this power (temperature) range that dissociation is increasing and having a marked effect on performance. To illustrate the dominating effect of heat losses on performance attained at constant power the losses measured by Dixon were multiplied by a factor of 0.9 and 1.1 and Figure 57 redrawn for the 5×10^{-2} mNs/sec case. The effect is seen in Figure 58, the three lines corresponding to the heat loss multiplied by the factor 0.9, 1.0 and 1.1. The general shape of Figure 57 is maintained except the curves are shifted with respect to one another, at a power level of 5 watts a change of + 10% in the heat losses changes the S.I. by -8.5 and a -10% change by + 15.

For resistojets which are power limited and operated at low duty cycles the performance will depend critically on the degree of dissociation and the efficiency of the thermal insulation. The conclusions drawn from Figures 57 and 58 will hold true for both undissociated and fully dissociated ammonia although the shape of the curves will change and the effect will be less marked. Power levels of the order of 5 watts have been considered realistic for ammonia resistojets and the current state of the art in thermal insulation enables temperatures of the order of 1000°K to be attained at this power. It is at these temperatures that dissociation increases significantly, therefore small improvements in thermal insulation can lead to significant performance improvements.

7.3 Dissociation

In almost any practical application of pulsed resistojets the system will be power limited and the temperature will be determined by the various loss mechanisms. To dissociate ammonia requires energy which is not subsequently recovered in the nozzle expansion. However the average power to the gas is only a small fraction of the total power supplied (at low duty cycle) therefore for maximum performance (maximum specific impulse) it is advantageous to operate at as high a temperature as possible and to promote dissociation. Were continuous operation, or operation at high duty cycles required the overall power level would then be determined by power to the gas and at low power levels it may be advantageous to inhibit dissociation if this is possible. This will allow operation at higher temperatures with undissociated ammonia which may produce a higher specific impulse than operation at a lower temperature with partially dissociated ammonia. The amount of ammonia dissociated in any particular resistojet will depend on temperature, material, geometry and possibly pressure and can best be determined by an experiment as the present one.

The effect of promoting dissociation is to lower the mass flowrate required for the same thrust at the expense of a higher power consumption. It has already been mentioned that for duty cycles of 10^{-3} or less the total power consumption is almost independent of the power to the gas, thus if one can promote more dissociation at a particular power level a decrease in fuel requirements is obtained at no expense. An increase in dissociation at a constant power level can be obtained in several ways, one is to improve the thermal insulation and operate at a higher temperature as was demonstrated in the previous section, another is to use a material which promotes more dissociation at the same temperature, others include altering the geometry of the resistojet but this may incur a penalty in either pressure drop or transient response.

It is instructive to consider a typical satellite application to illustrate the significant mass savings which are made when dissociation occurs in the resistojet. A small satellite (100kg) in near earth orbit will require approximately 10^4 Ns yr^{-1} of total impulse(40) for attitude control and drag make up. The beneficial effects of dissociation can be illustrated by comparing the fuel requirements for 1 year of operation for undissociated, dissociated and partially dissociated ammonia. The partially dissociated ammonia case was taken to be the nickel resistojet to represent a performance that has been achieved in practice. Figure 59 shows how fuel requirements drop with increasing temperature, the fuel requirements for the nickel resistojet approaches the full dissociation case at high temperatures and the undissociated case at low temperatures. However fuel requirements do not represent the only changes in mass, extra solar cells are required to operate at the higher temperature. To enable the mass of the solar cells to be taken into account a variable system mass is defined which includes the mass of fuel and solar cells but neglects the mass of the resistojets, fuel tanks and control systems whose mass will not vary greatly over the temperature range considered.

The variable system mass will depend on the life of the satellite, the performance of the resistojet and the efficiency of the thermal insulation. Assuming an impulse requirement of 10^4 N.s.yr^{-1} as before for a 100kg satellite having 12 resistojets, for 3 axis control, a projected life of 1 year and thermal insulation as described in the previous section, the variable system mass then shows an increase with increasing temperature as shown in Figure 60. This is because the solar cell mass increases faster than the decrease in fuel requirements as the temperature is increased, however if a 5 year life is assumed the variable system mass then falls with increasing temperature as can be seen in Figure 61. At a temperature of 1000°K there is a difference of over 8kg between the fully dissociated and undissociated case, this represents a saving of 25% in the variable system mass.

In the design of satellites it will not be the temperature of operation which will be specifically limited but the power level, it is therefore instructive to compare the variable system mass for the three cases considered as a function of power level per resistojet and not temperature. This is shown in Figure 62 for the 5 year lifetime case, which shows the same behaviour as Figure 61, but it now becomes easy to see that it is operation at higher power levels which will lead to the lowest mass in this case. As the power level (and consequently temperature) is increased the fuel requirements will continue to fall, however the mass of the solar arrays needed to supply the power will increase more quickly (radiation which is the main loss is proportional to T^4) and a power level will be reached at which the system mass will be at a minimum for that particular configuration. The power level and temperature at which this minimum occurs will depend on mission requirements, degree of dissociation and the efficiency of the thermal insulation. It can be seen in Figure 60 that system mass rises for both undissociated and full dissociated ammonia with increasing temperature,

but falls for the nickel resistojet. The optimum temperature and power level is therefore lower than 900°K for the two limiting cases but higher than 1050°K for the nickel resistojet. For satellites with short projected lifetimes the extra complexity of resistojets may not be warranted to obtain small mass savings over a cold jet system especially if the optimum temperature of the resistojet is low and the ammonia is undissociated. It is for satellites whose lifetimes are of the order of 5 to 10 years that considerable mass savings can be made by using resistojets operating at high temperatures. It is only by knowing the performance of the resistojet and thermal insulation as a function of temperature and the mission requirements that an analysis of this type, which leads to the concept of an optimum power, can be undertaken.

To facilitate the prediction of performance of the nickel resistojet over the temperature range studied, a carpet plot of thrust versus S.I. has been prepared and is shown in Figure 63. This carpet plot has been reduced to the equation:-

$$F = 2.42\ \dot{m}\ T^{1.3} \times 10^{-4} \quad \text{Newtons}$$

where $\dot{m}$ = mass flowrate gm/sec

T = Temperature °K

The carpet plot and equation will only hold for the particular resistojet configuration which was used in this work, any other configuration will need to be investigated experimentally, either directly by measuring thrust or by predicting the performance from the measured nozzle stagnation conditions as has been done here.

To be considered for operational use on a satellite a resistojet system would need extensive testing to show it could operate satisfactorily during the life of the satellite; typically 1 to 10 years. The

behaviour of the stainless steel resistojets obviously precludes their use on an operational satellite. The nickel resistojet performed repeatabily and reliably in the tests conducted but they only lasted about 10 hours, however at a mean thrust level of 0.05N this represents approximately 2×10^3 Ns of impulse or the impulse requirements for 1 year for the satellite considered above.

7.4 Overall Design Considerations for Electrothermal Thrusters

When a particular mission requirement is specified for a satellite the total attitude control impulse will also be determined and also at which thrust level and individual impulse bit this total impulse is required. This requirement is then translated into a provisional thruster design at the required thrust level. In the case of ammonia resistojets the work of I Edwards[19] on the analysis of small nozzles would provide invaluable design information.

However once a preliminary design has evolved it is then necessary to construct and then evaluate the particular design.

In the initial design stage one relies on experience obtained with previous designs and parametric data applicable to the proposed design. It was with the intention of providing data on ammonia dissociation, to simplify thruster design, that the present project was undertaken. It was decided to start with easily fabricated materials, stainless steel and nickel to gain experience, and then proceed to materials which on past experience were serious contenders for ammonia resistojets (molybdenum, rhenium, Haynes 25). The results of the short duration tests on the stainless steels obviously exclude them from further consideration for use as ammonia resistojets. Similar scale formation has been found on electrothermal hydrazine thrusters of stainless steel where atomic nitrogen formed when hydrazine decomposes into ammonia and nitrogen could have been responsible. Materials which have been considered for the

construction of electrothermal thrusters are platinum, rhenium, molybdenum and Haynes 25. Unfortunately each of these materials has its own particular drawback. Platinum suffers from high temperature embrittlement, rhenium is very expensive and the only satisfactory method of fabrication is by chemical vapour depositon followed by electron beam welding, but, because it is the only material which retains strength and ductility to high temperatures (> 2000°K) may be the final choice. Molybdenum is difficult to fabricate and suffers embrittlement, Haynes 25 is a cobalt alloy which has been used for hydrazine resistojets operating at temperatures up to approximately 1000°K and has shown good long term properties at these temperatures. Haynes 25 can be machined with difficulty, it was not used in the present experiments because the material was not available in this country and the equivalent British alloy was not available in the billet size necessary to construct the resistojet design adopted here. Larger billet sizes were to be available but not within the time scale of the present experiments.

Sufficient information is available to design a thruster with respect to mechanical performance, heat transfer, pulse response and pressure drop, however very little information exists on ammonia decomposition and the actual performance of the resistojet would have to be measured and could be considerably different from that calculated depending on the degree of ammonia decomposition assumed and that actually achieved.

An extension of the work performed here is a parametric study of ammonia decomposition in resistojets constructed of the materials listed above. Armed with this information the thruster designer could make a much more accurate initial guess and would also enable a more rigorous design optimisation to be performed.

During testing of a proposed thruster simultaneous monitoring of both thrust and dissociation would give a more complete understanding of the processes which lead to changes in thruster performance. For example

the stainless steel resistojets tested here would have shown an increase in thrust with time as shown in Figure 56, but the reason for this change is apparent, only when one measures dissociation. For pulse testing of resistojets it has been found difficult to measure low (0.05N) transient thrust but with modification to the skimmer arrangement to allow an in line mounting of a quadrapole mass spectrometer it would be possible to measure the species present during a 50ms pulse and relate this to thrust. This modification would also allow the measurement of the change of exhaust gas composition of hydrazine thrusters as the heat from hydrazine decomposition heated the thruster into the temperature range for decomposition of ammonia.

It can be seen that measurement of exhaust gas species as well as the more usual parameters (pressure, temperature, mass flowrate, thrust etc.) allows a more complete understanding of the processes taking place in resistojets and will enable designers to make better resistojets whose predicted and actual performances compare more favourably.

References

1. W. P. S. Tan. PhD Thesis 1971 Southampton University.

2. D. J. Buckingham. PhD Thesis 1966 Southampton University.

3. A. Kantrowitz, J. Grey. A High Intensity Source for the Molecular Beam. Part I Theoretical. "The Review of Scientific Instruments" Vol. 22 No. 5 pp. 328-332.

4. H. Ashkenas, F. S. Sherman. In Rarefied Gas Dynamics. J. H. de Leeuw Ed. (Academic Press Inc. New York 1966) Vol. 2 pp. 84-105.

5. I. Edwards, R. E. W. Jansson. Gasdynamics of Resistojets: Initial Modelling and Preliminary Results. AASU Report No. 304.

6. G. F. Greenwald. Approximate Far-Field Flow Description for a Nozzle Exhausting into a Vacuum. J. Spacecraft Vol. 7 No. 11 pp. 1374-1376.

7. M. Sibulkin, W. H. Gallaher. Far Field Approximation for a Nozzle Exhausting into a Vacuum. AIAA Journal Vol. 1 No. 6 pp. 1452-1453.

8. J. A. F. Hill, J. S. Draper. Analytical Approximation for the Flow from a Nozzle into a Vacuum. J. Spacecraft, Vol. 3 No. 10 pp. 1552-1554.

9. U. Bossel. Investigation of Skimmer Interaction Influences on the Production of Aerodynamically Intensified Molecular Beams. Report No. A5-68-6. University of California, Berkeley.

10. H. M. Parker, A. R. Kuhlthau, R. Zapata, J. E. Scott. The Application of Supersonic Beam Sources to Low Density High-Velocity Experimentation. Rarefied Gas Dynamics (1960) pp. 69-79.

11. R. Camparque. Aerodynamic Separation Effect on Gas and Isotope Mixtures Induced by Invasion of the Free Jet Shock Wave Structure. Journal of Chemical Physics Vol. 52, No. 4 pp. 1795-1802.

12. J. B. Fenn, J. Deckers. Molecular Beams from Nozzle Sources. Rarefied Gas Dynamics. J. Lourmonn Ed. (1964) Vol. 1 pp. 497-515.

13. R. Camparque. High Intensity Supersonic Molecular Beam Apparatus. Rarefied Gas Dynamics Vol. II 1966 pp. 279-298.

14. S. Dushman. Scientific Foundations of Vacuum Technique.

15. R. F. Probstein. Shock Wave and Flowfield Development in Hypersonic Re-entry. A.R.S. J. Vol. 31 p. 185 (1961).

16. G. T. Skinner, J. Moyzis. Experimental Study of the Collimation Problem in a High Intensity Molecular Beam. Physics of Fluids Vol. 8, No. 3 (1965) pp. 452-458.

17. J. W. Macoll. Proc. Royal Society A Vol. 159 (1937) p. 459.

18. K. Bier, O. Hagena. Optimum Conditions for Generating Supersonic Molecular Beams. Rarefied Gas Dynamics Vol. II 1966 pp. 260-278.

19. I. Edwards. PhD Thesis. A Theoretical Study of the Performance of Resistojet Nozzles. Southampton University September 1972.

20. E. W. Becker, K. Bier. Z. Naturforsch Vol. 9a p. 975.

21. J. B. Anderson, R. P. Andres, J. B. Fenn. Supersonic Nozzle Beams in Molecular Beams. Advanced Chemical Physics Vol. 10 p. 275.

22. K. Bier, B. Schmidt. Z. Angew Phys. Vol. 13, p. 493.

23. J. W. Brook, R. A. Oman. Steady Expansion at High Speed Ratio using the B-G-K Kinetic Model. In Rarefied Gas Dynamics. Vol. 1 (1966) pp. 125-139.

24. B. B. Hamel, D. R. Willis. Physics of Fluids Vol. 9 pp. 829-841 (1966).

25. F. T. Greene, J. Brewer, T. A. Milne. Mass Spectrometric Studies of Reactions in Flames I. Beam Formation and Mass Dependence in Sampling 1 - Atm. Gases. Journal of Chemical Physics Vol. 40 pp. 1488-1495 (1964).

26. V. H. Reis, J. B. Fenn. Separation of Gas Mixtures in Supersonic Jets. Journal of Chemical Physics Vol. 39 pp. 3240-3250 (1963).

27. C. D. Colclough, J. Smillie. Welding Fine Thermocouple Wires to Large Metal Bodies. The Engineer November 1959 pp. 696-698.

28. S. C. Metcalf, D. A. J. Walliker, C. J. Berry. A New Method of Afterglow Visualization for Low-Density High Mach Number Flows. N.P.L. Aero Report 1291.

29. O. Leuchter. Flow Visualization at Mach Number 14 by the Glow Discharge Method. La Recherche Aerospatiale No. 110, Jan/Feb 1966 p. 59.

30. G. A. Miles. An Investigation of the Catalytic Dissociation of Ammonia. Allison Division of General Motors Report Number R.N. 65-47.

31. J. Rebiere. Etude Experimentale De La Dissociation De L'Ammoniac En Ecoulement Laminaire Dans Des Espaces Annulaires. Commissariat A L'Energie Atomique. Report Number CEA CEN-G ASP/69-16.

32. Catalysis. R. Emmett (Editor) Volume 7 1960.

33. J. J. Moran, J. R. Mikalisin, E. N. Skinner. Behaviour of Stainless Steels and Other Engineering Alloys in Hot Ammonia Atmospheres. Corrosion Vol. 17 pp. 191t-195t (1961).

34. G. F. C. Rogers, Y. R. Mayhew. Engineering Thermodynamics Work and Heat Transfer p. 525.

35. H. Schlichting. Boundary Layer Theory, p. 171.

36. J. C. Dixon, P. J. Musgrove. Thermal Insulation for Electrothermal Thrusters. Electric Propulsion of Space Vehicles Conference Proceedings held at UKAEA Culham 10-12 April 1973 pp. 166-170.

37. H. L. Jaeger, E. J. Willson, P. G. Hill. Nucleation of Supersaturated Vapours in Nozzles. I. H_2O and NH_3. Journal of Chemical Physics Vol. 51 pp. 5380-5388 (1969).

38. R. F. Sawyer. The Homogeneous Gas Phase Kinetics of Reactions in the Hydrogen-Nitrogen Tetroxide Propellant System. AFOSR Sci. Rep. No. 66-0855 (1966).

39. S. R. Logan, C. Kemball. The Catalylic Decomposition of Ammonia on Evaporated Metal Films. Trans. Faraday Soc. Vol. 56 pp. 144-153 (1960).

40. J. Porter. Satellite Attitude and Orbit Control Systems Based on Ammonia or Hydrazine. RAE Tech. Memo Space 128 (1969).

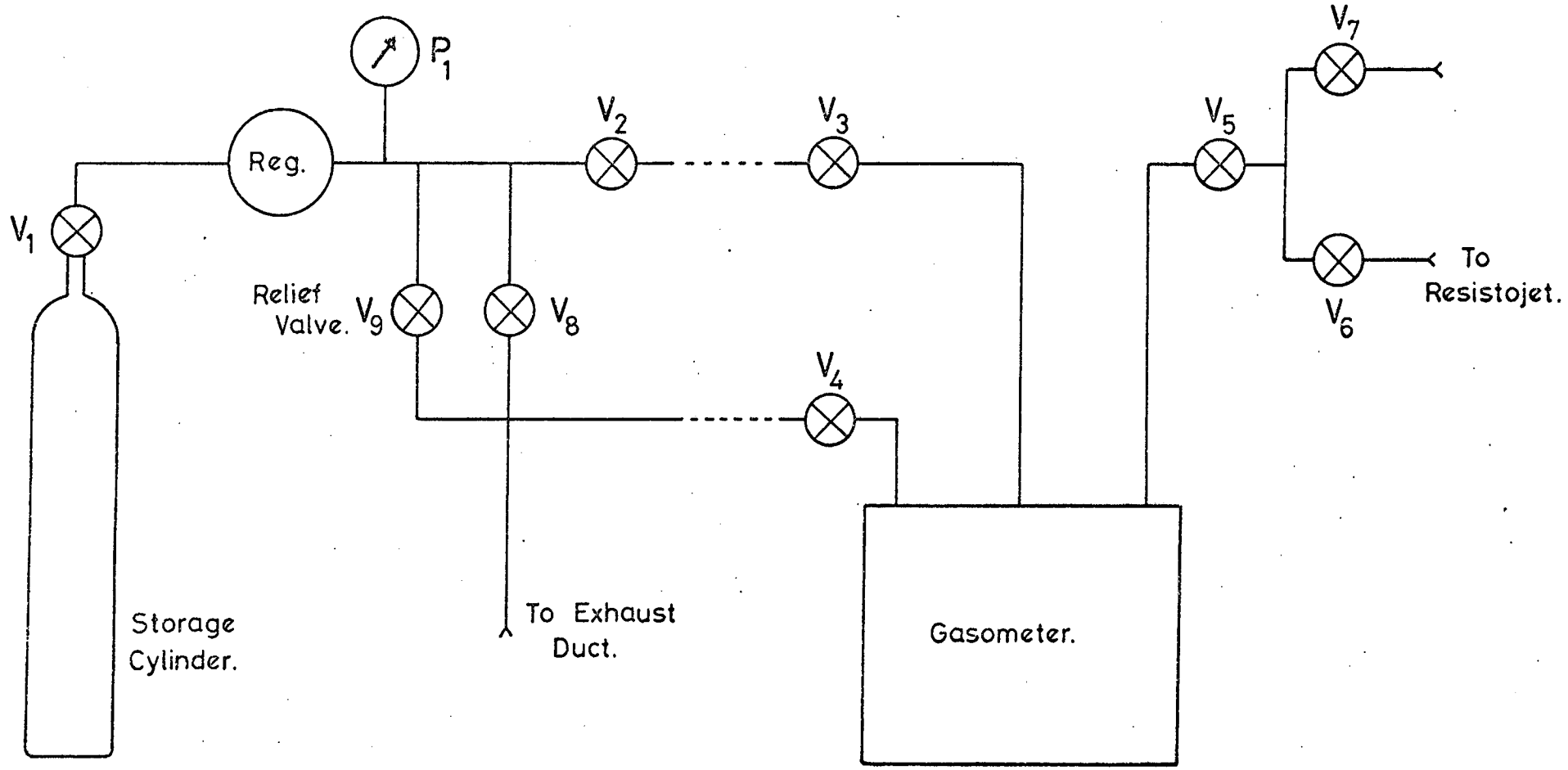

Fig. 1 Ammonia Flow System Schematic.

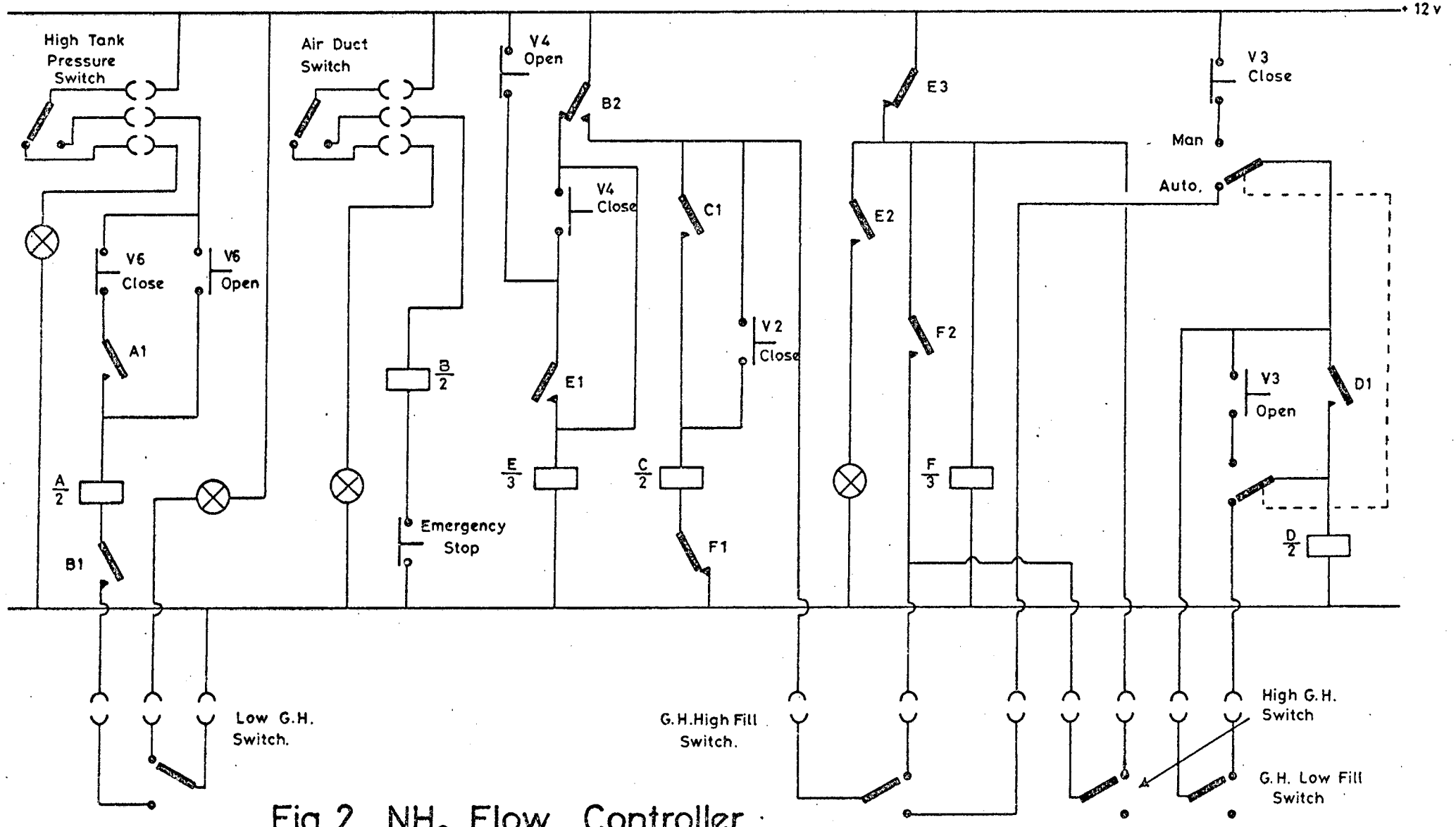

Fig. 2 NH_3 Flow Controller.

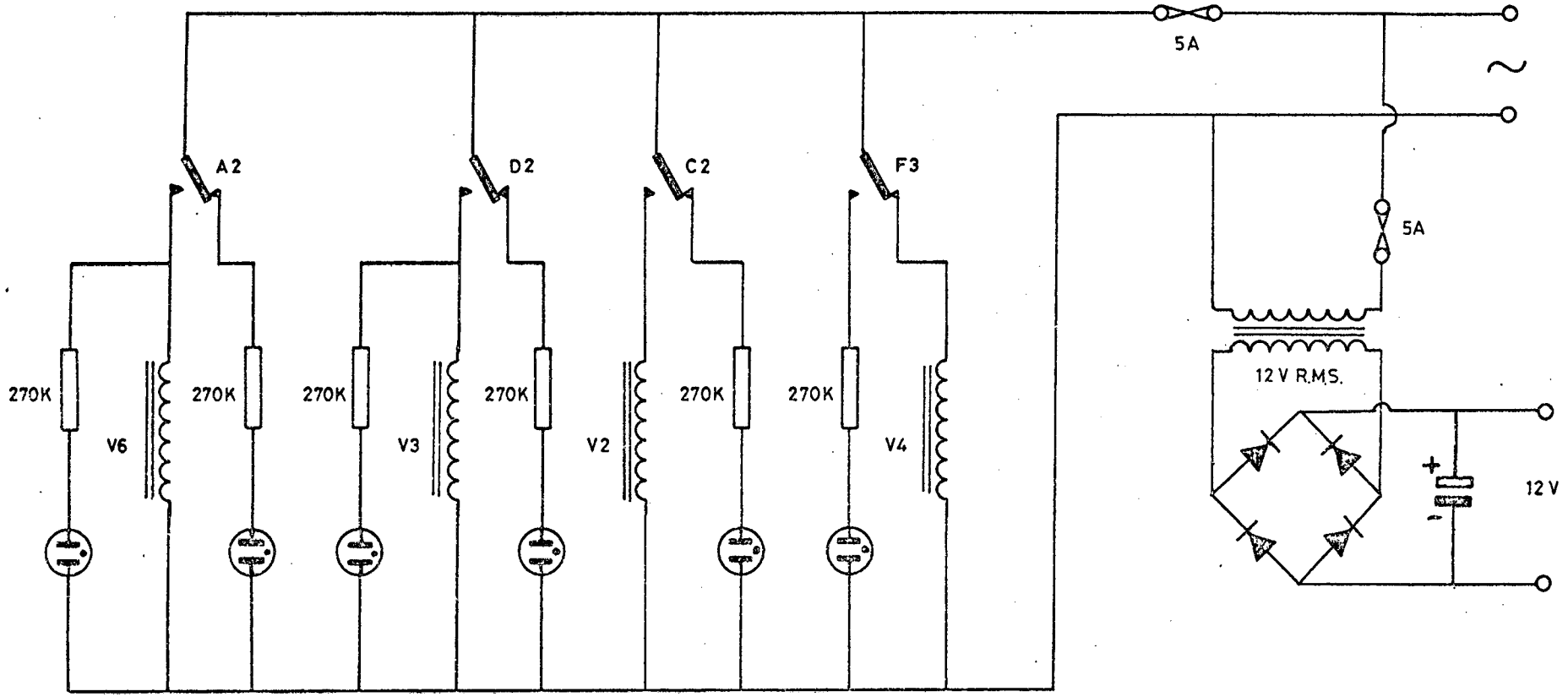

Fig. 3 Ammonia Flow Controller.

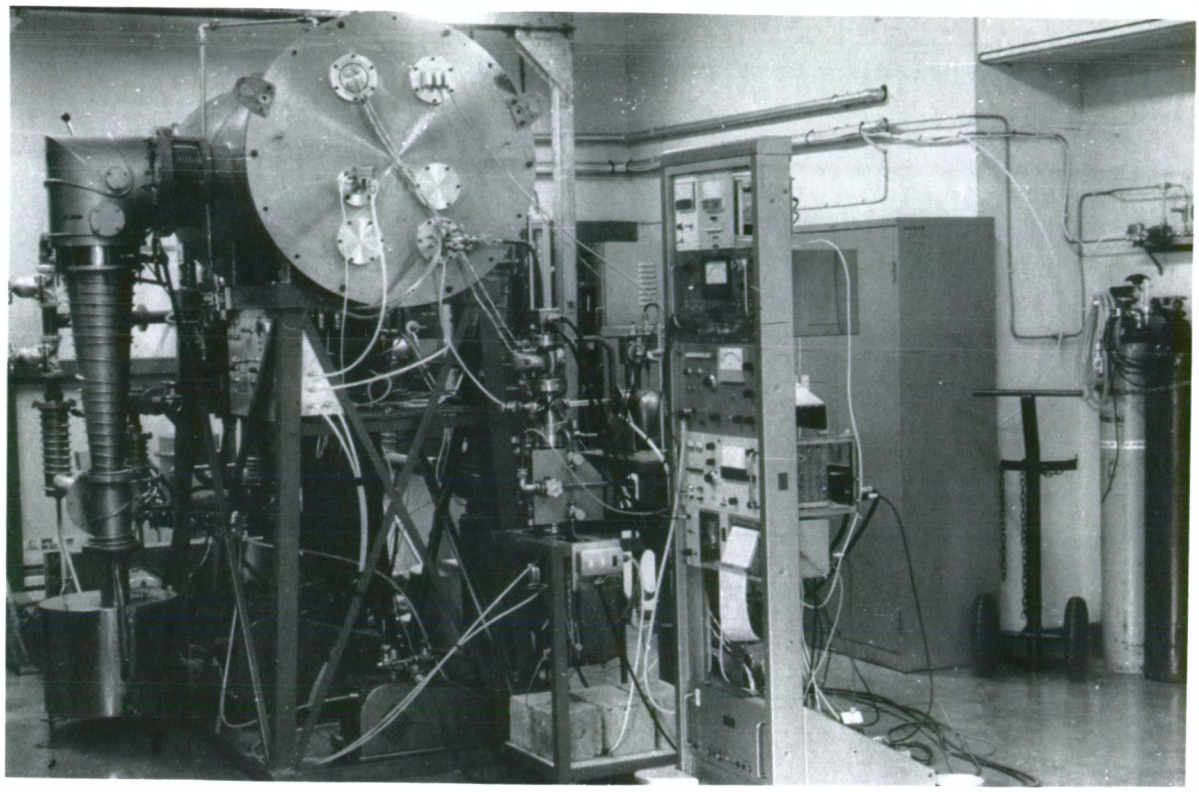

Fig. 4 Vacuum Chamber.

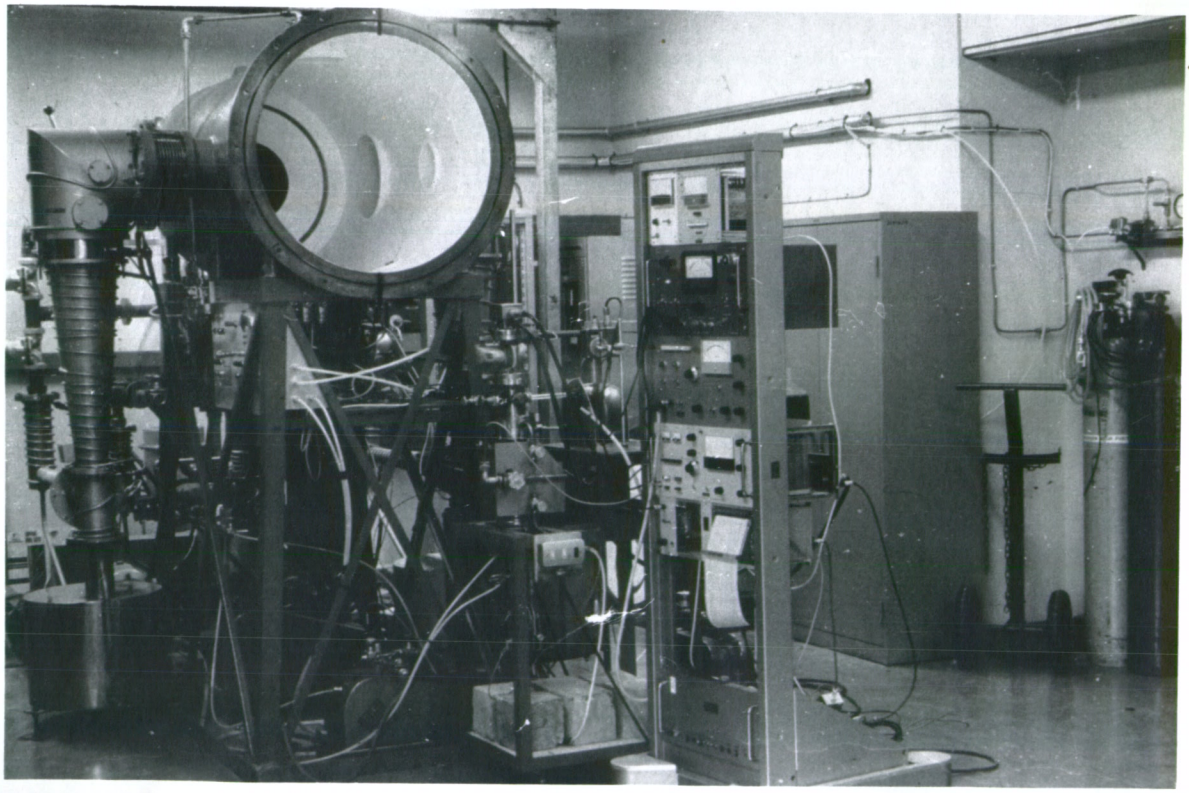

Fig. 5 Vacuum Chamber.

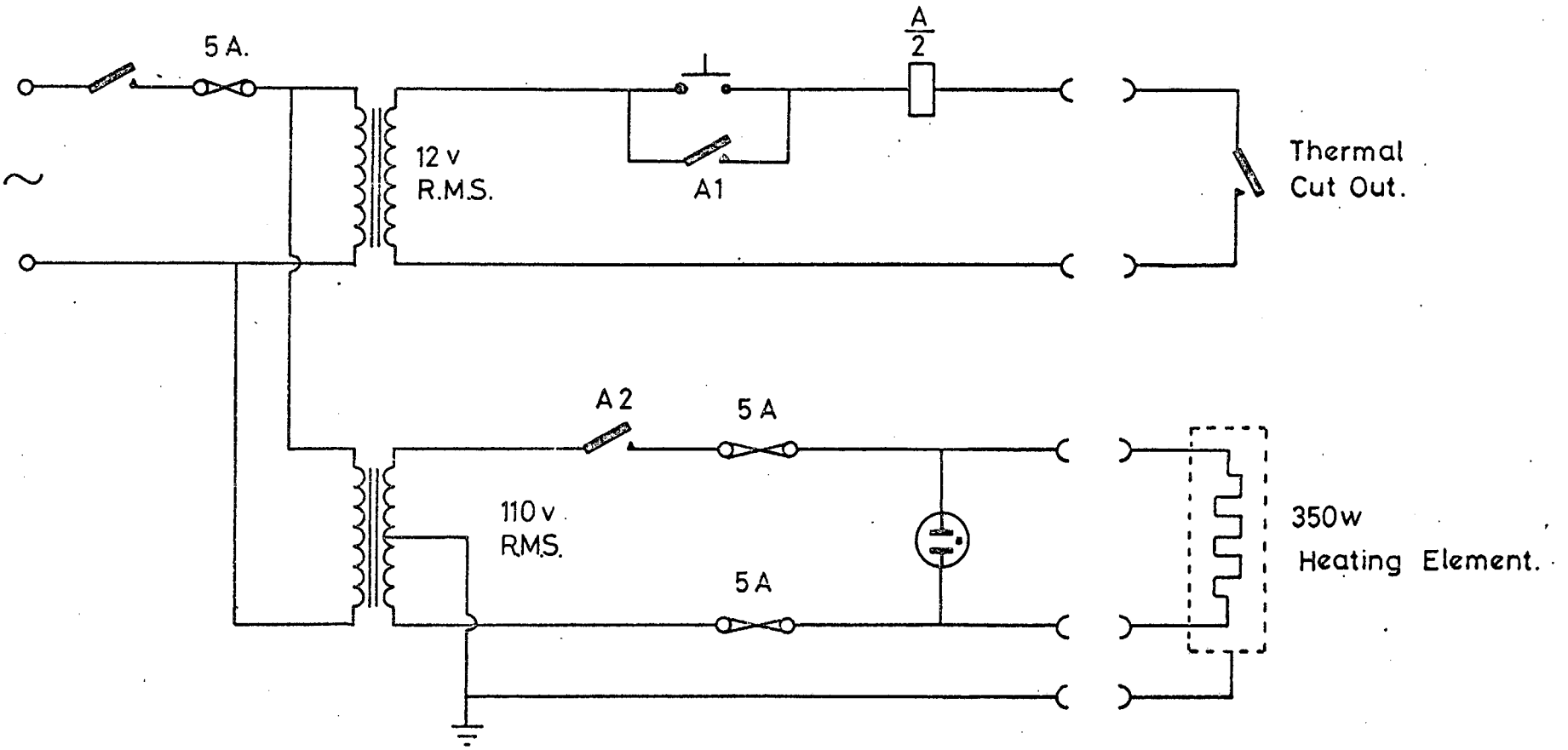

Fig. 6 Skimmer Pump Wiring Schematic.

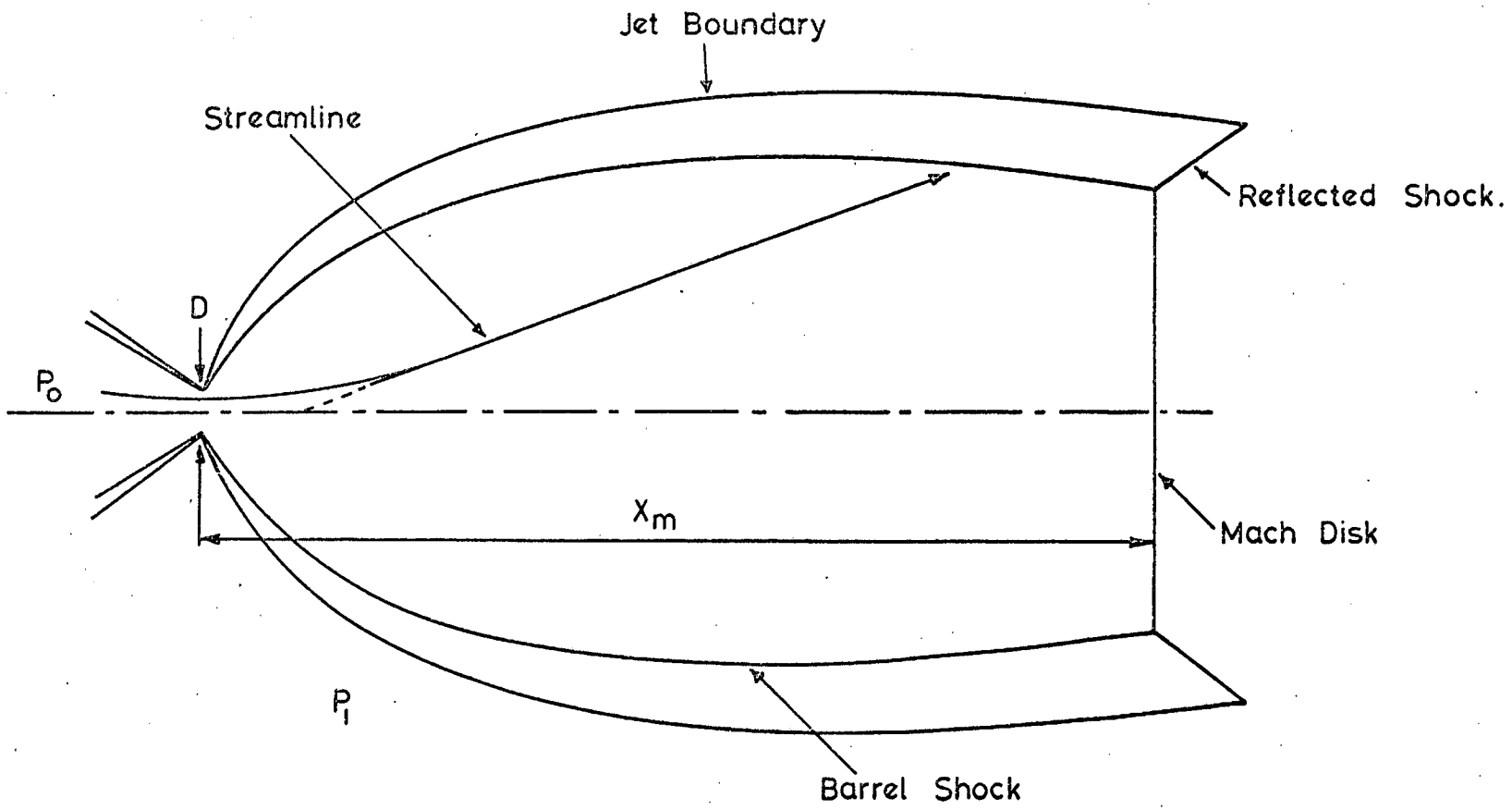

Fig. 7 Underexpanded Free Jet Structure.

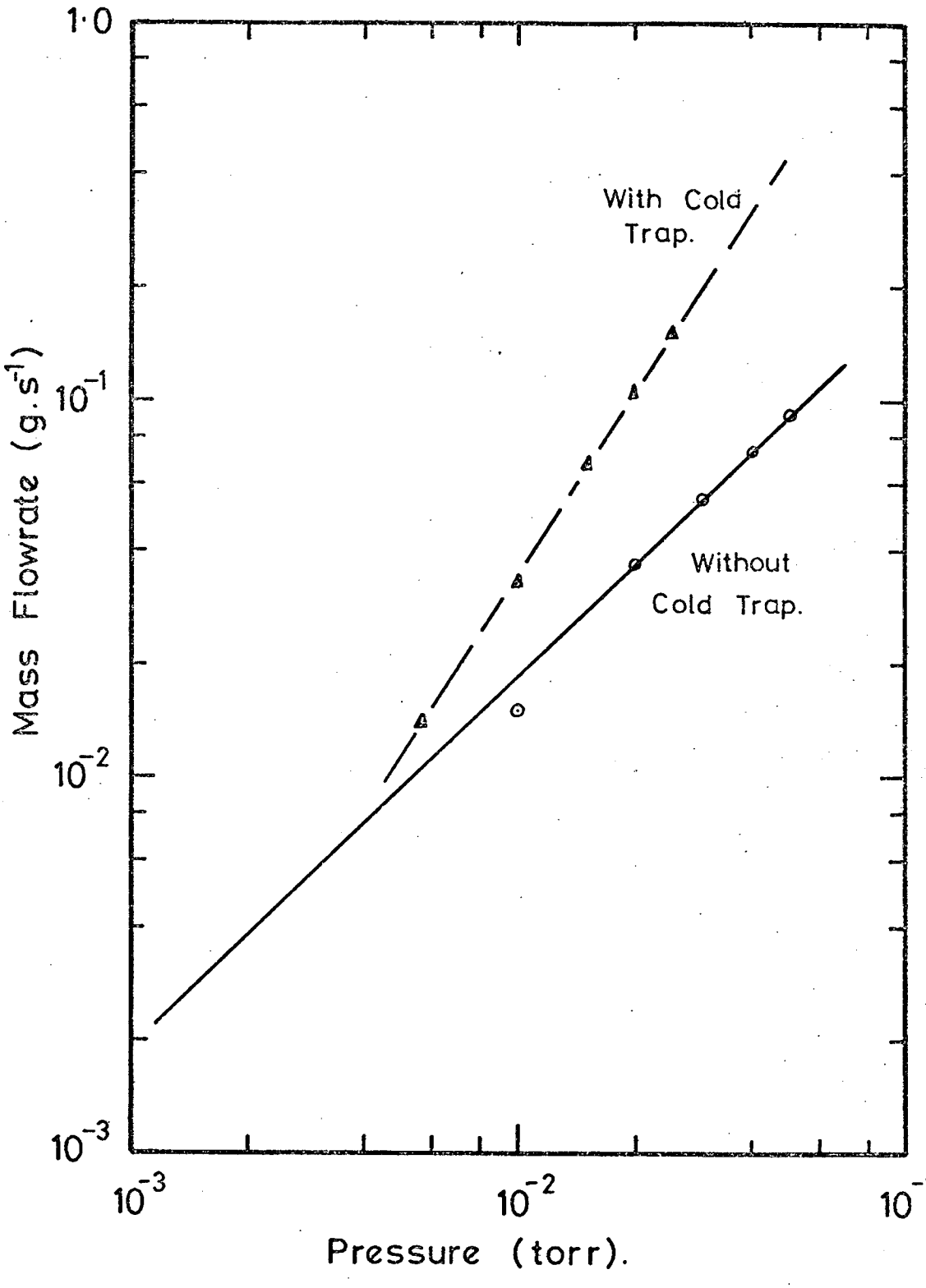

Fig. 8 Pumping Capacity of Vacuum Tank.

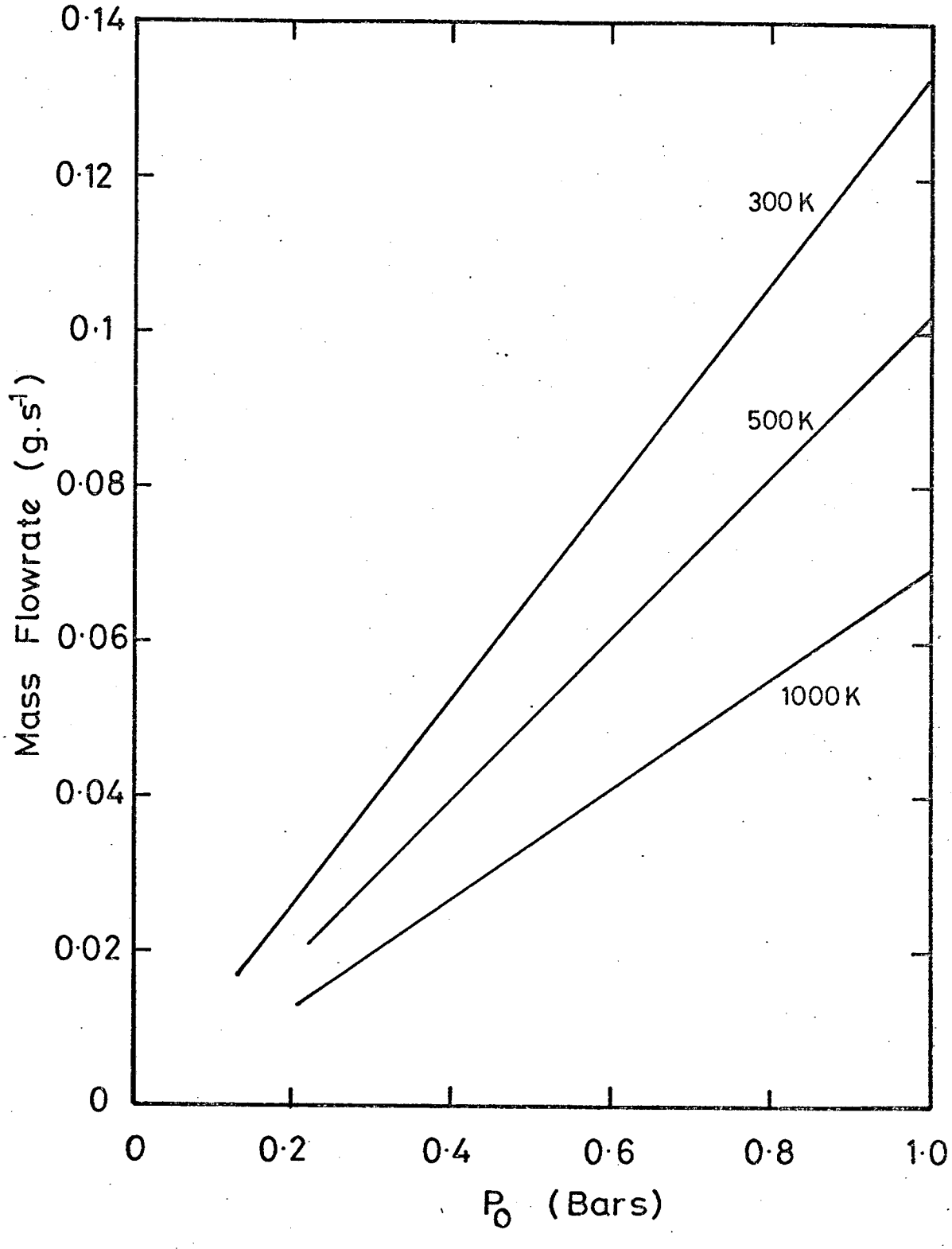

Fig. 9 Variation of Mass Flowrate with Stagnation Pressure.

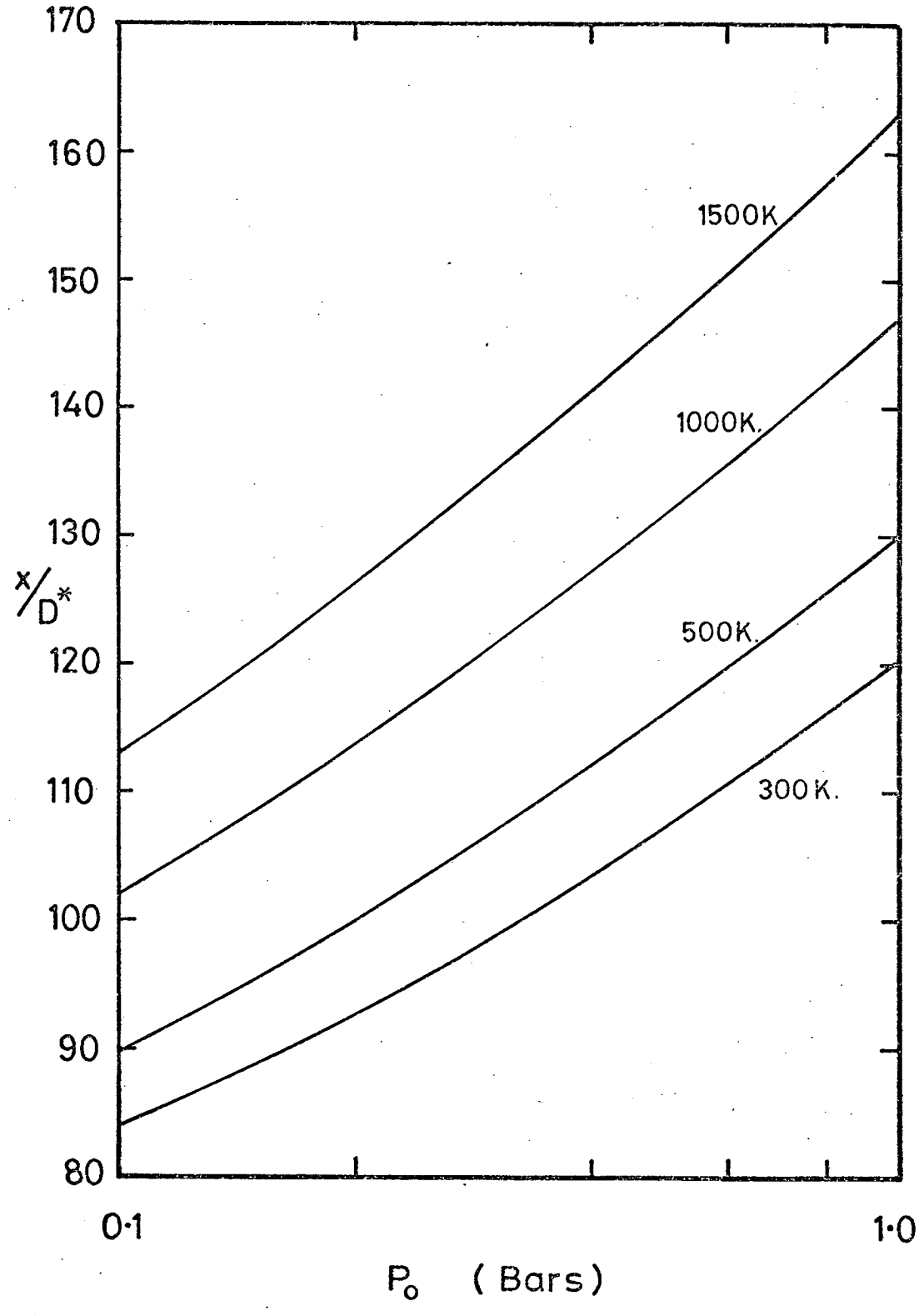

Fig. 10 Mach Disc Position with Changing Stagnation Pressure.

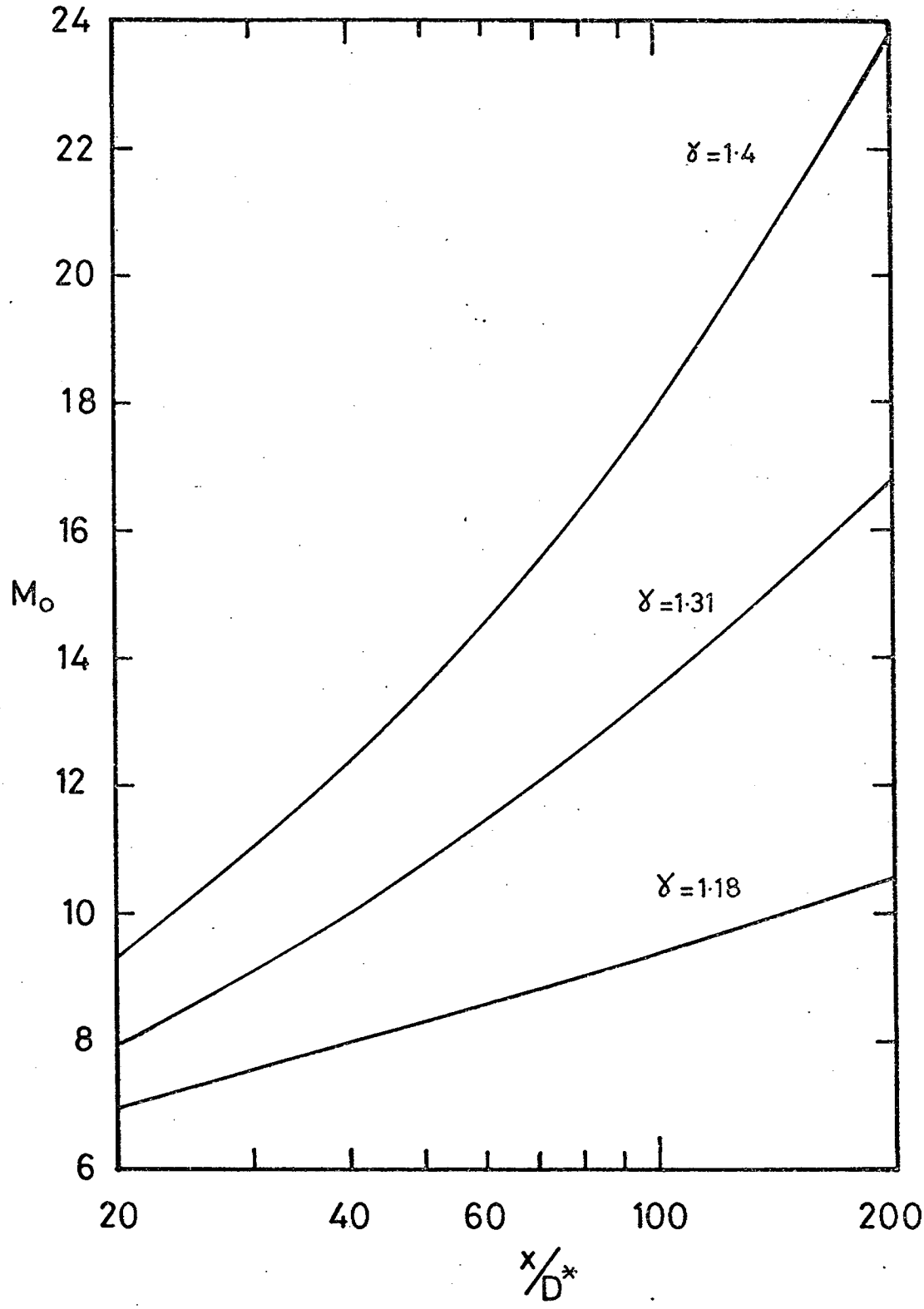

Fig. 11 Variation of Mach Number with Downstream Distance.

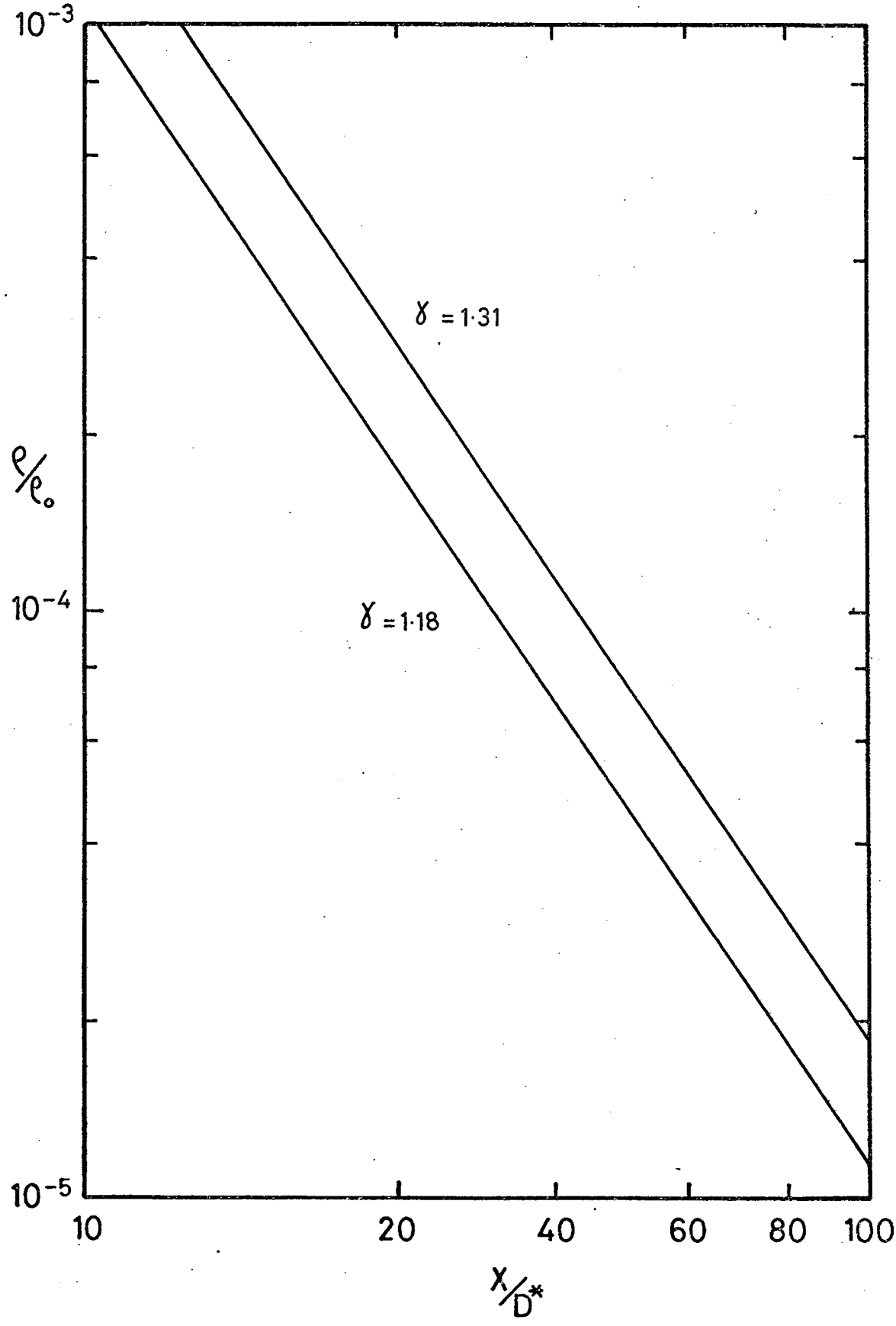

Fig. 12 Variation of Density with Downstream Distance.

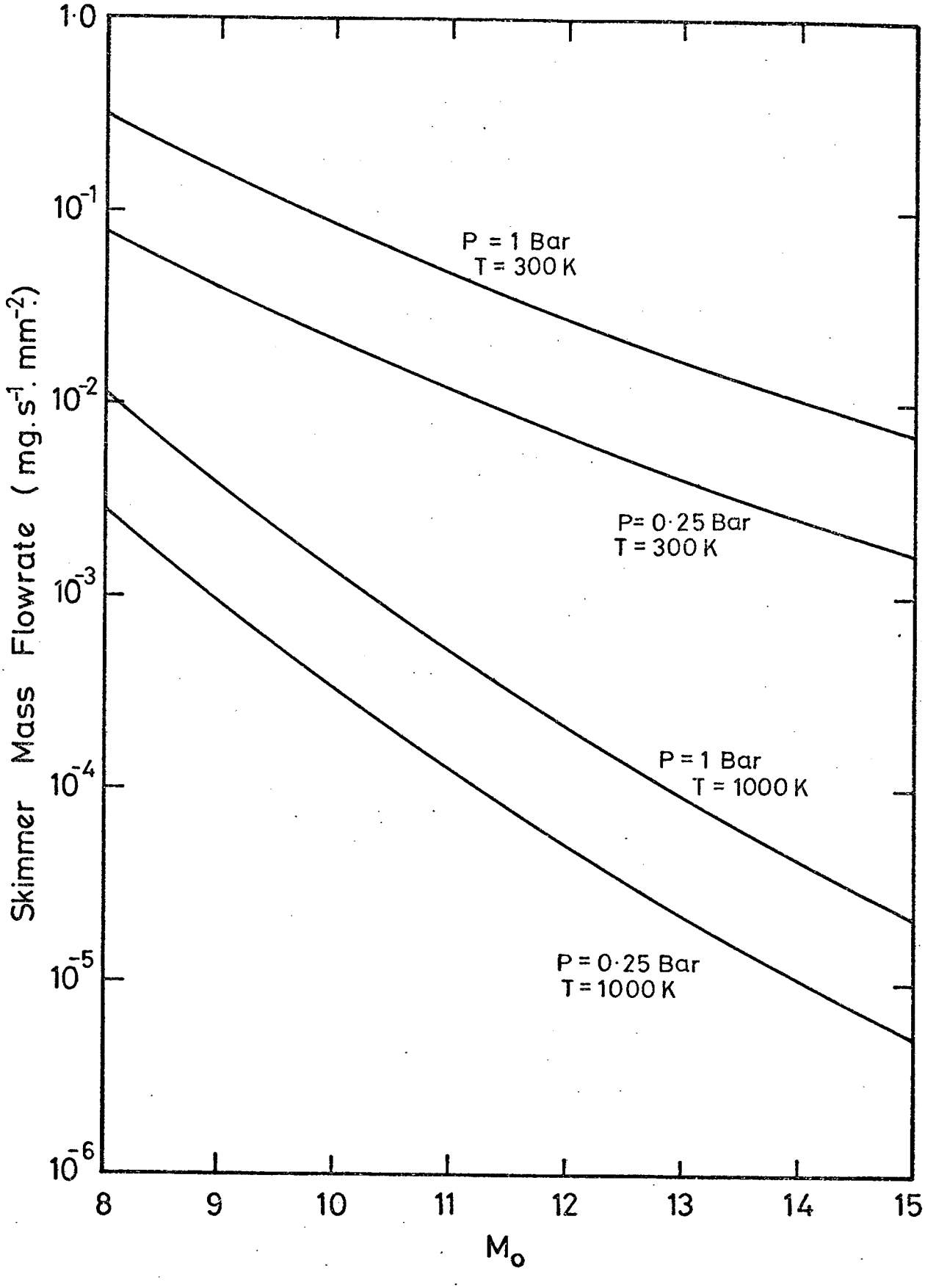

Fig. 13 Variation of Skimmer Mass Flowrate with Mach Number.

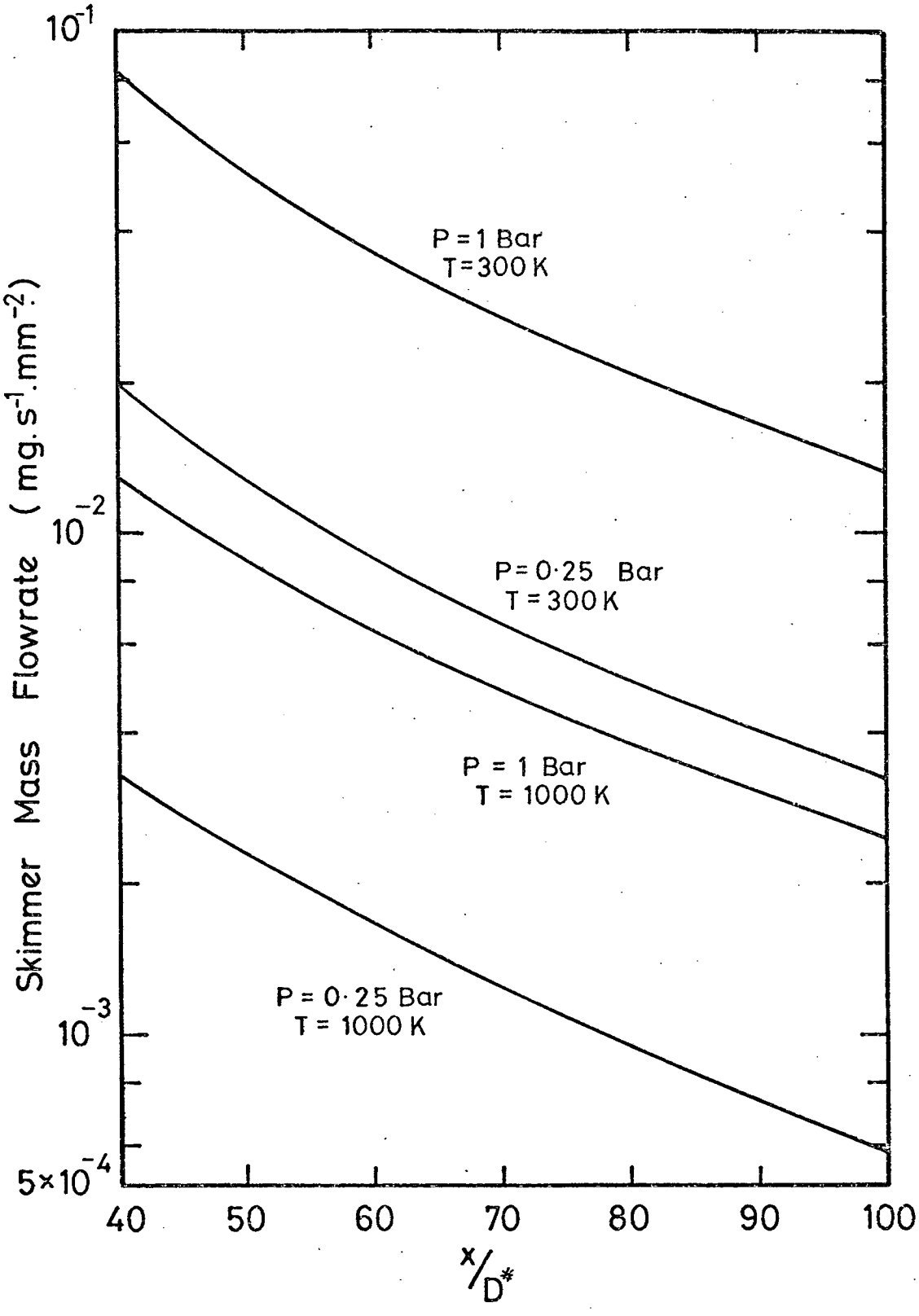

Fig. 14 Variation of Skimmer Mass Flowrate with Dowstream Distance.

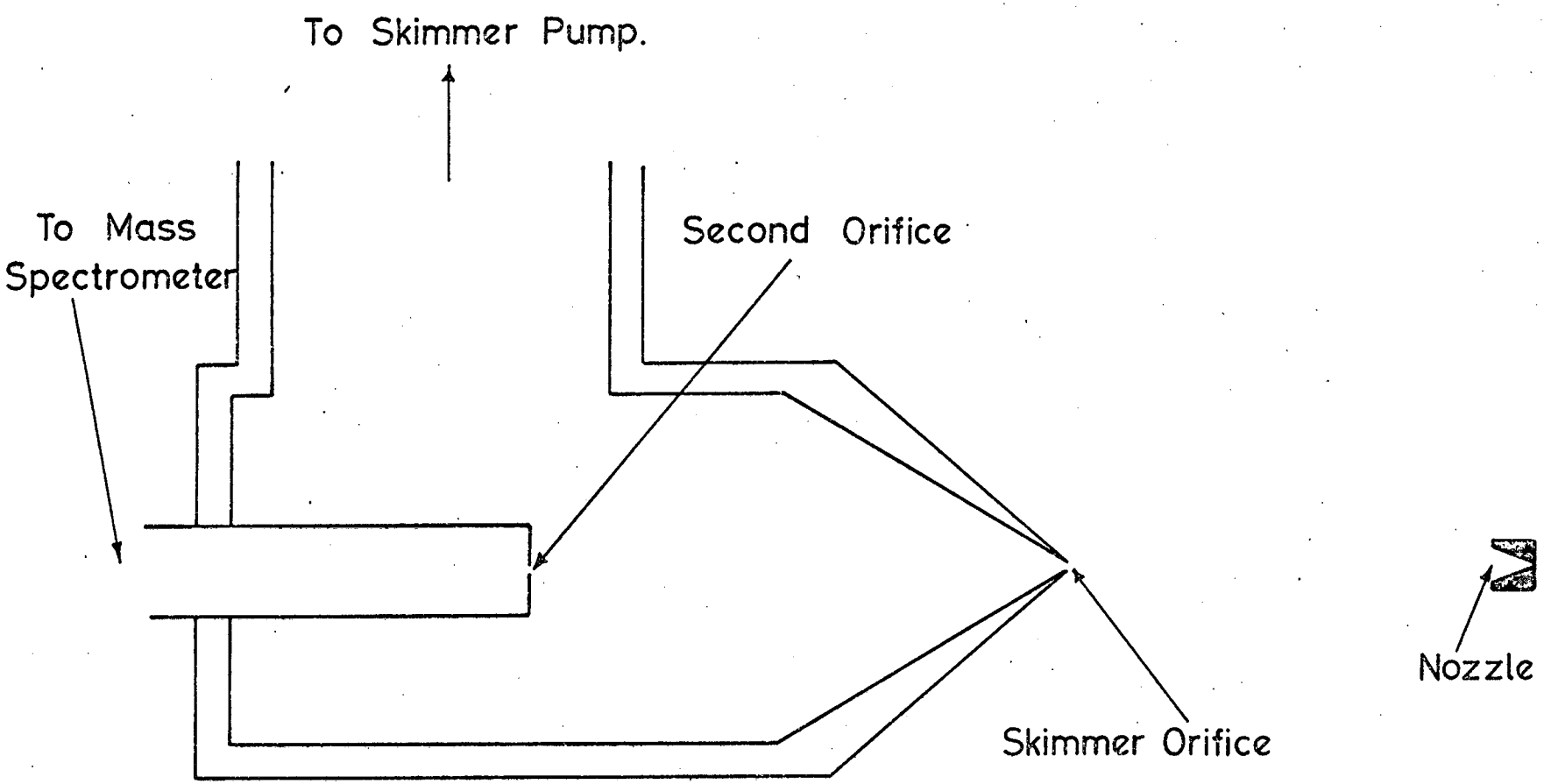

Fig. 15 Diagram of Skimmer Chamber.

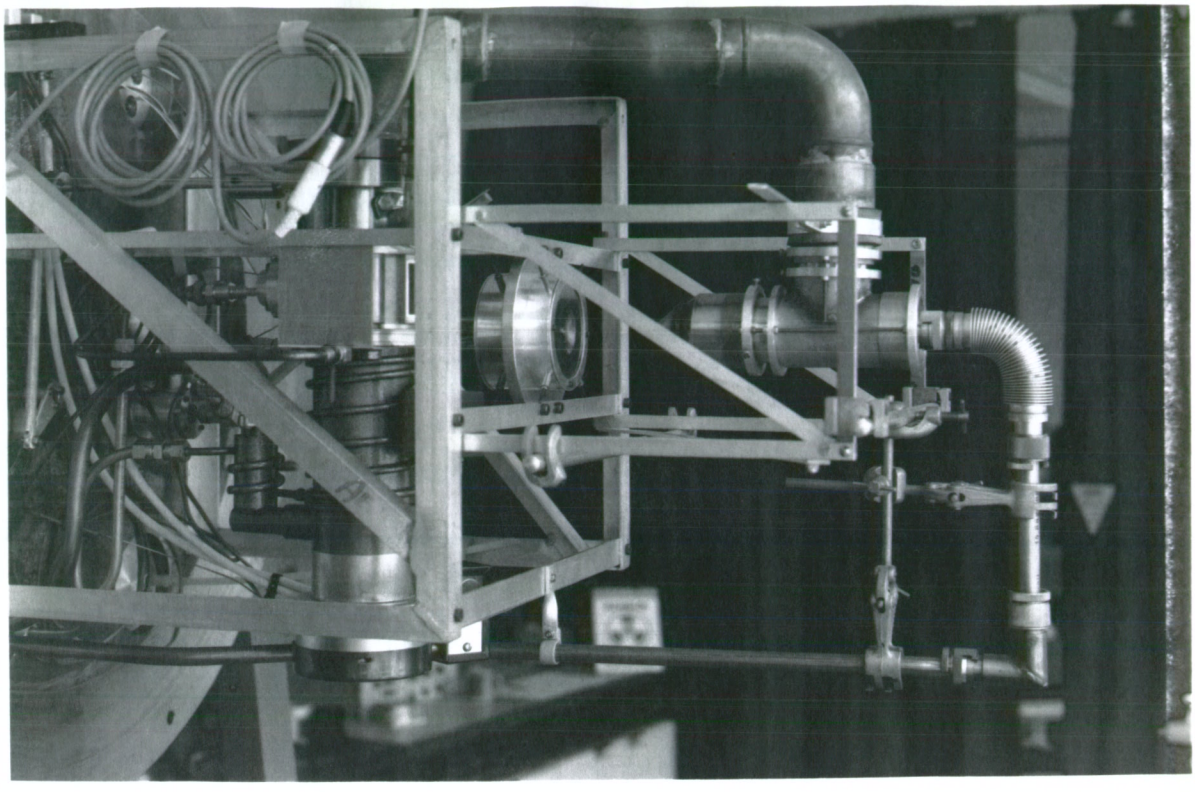

Fig. 16 Experiment Mounted on Door.

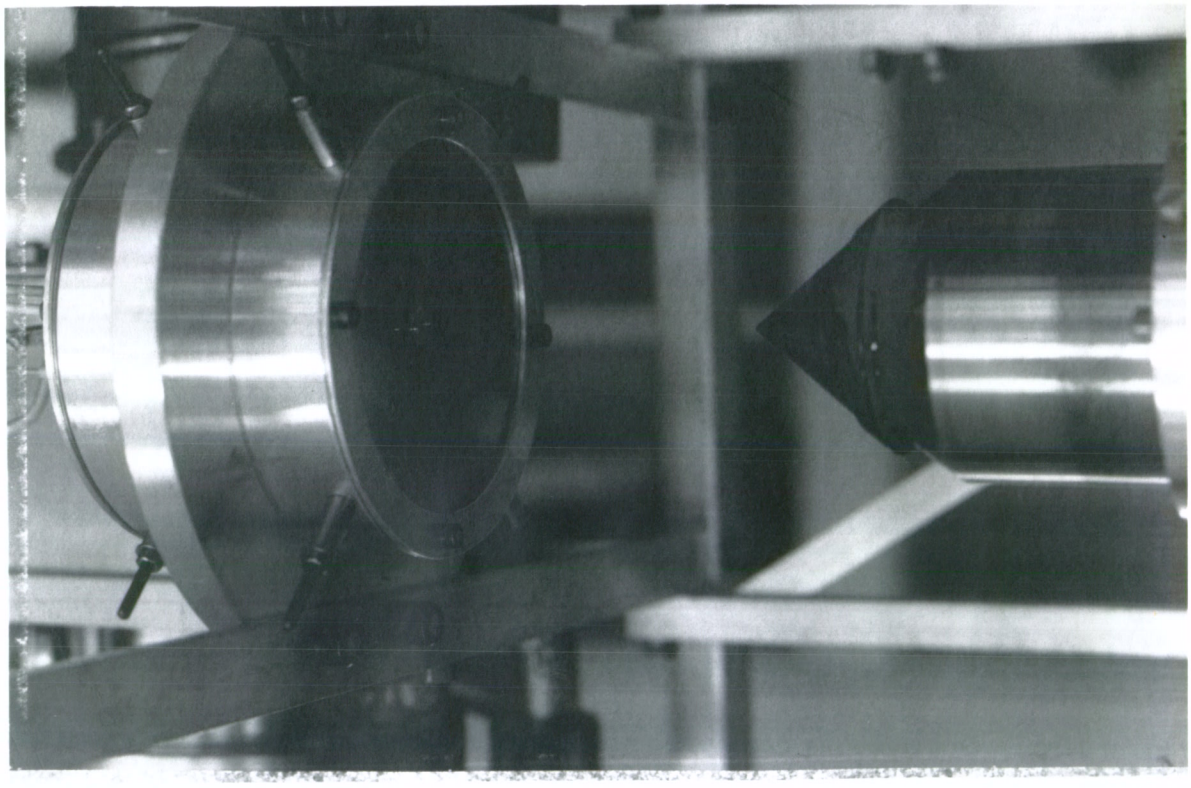

Fig. 17 Skimmer in Position.

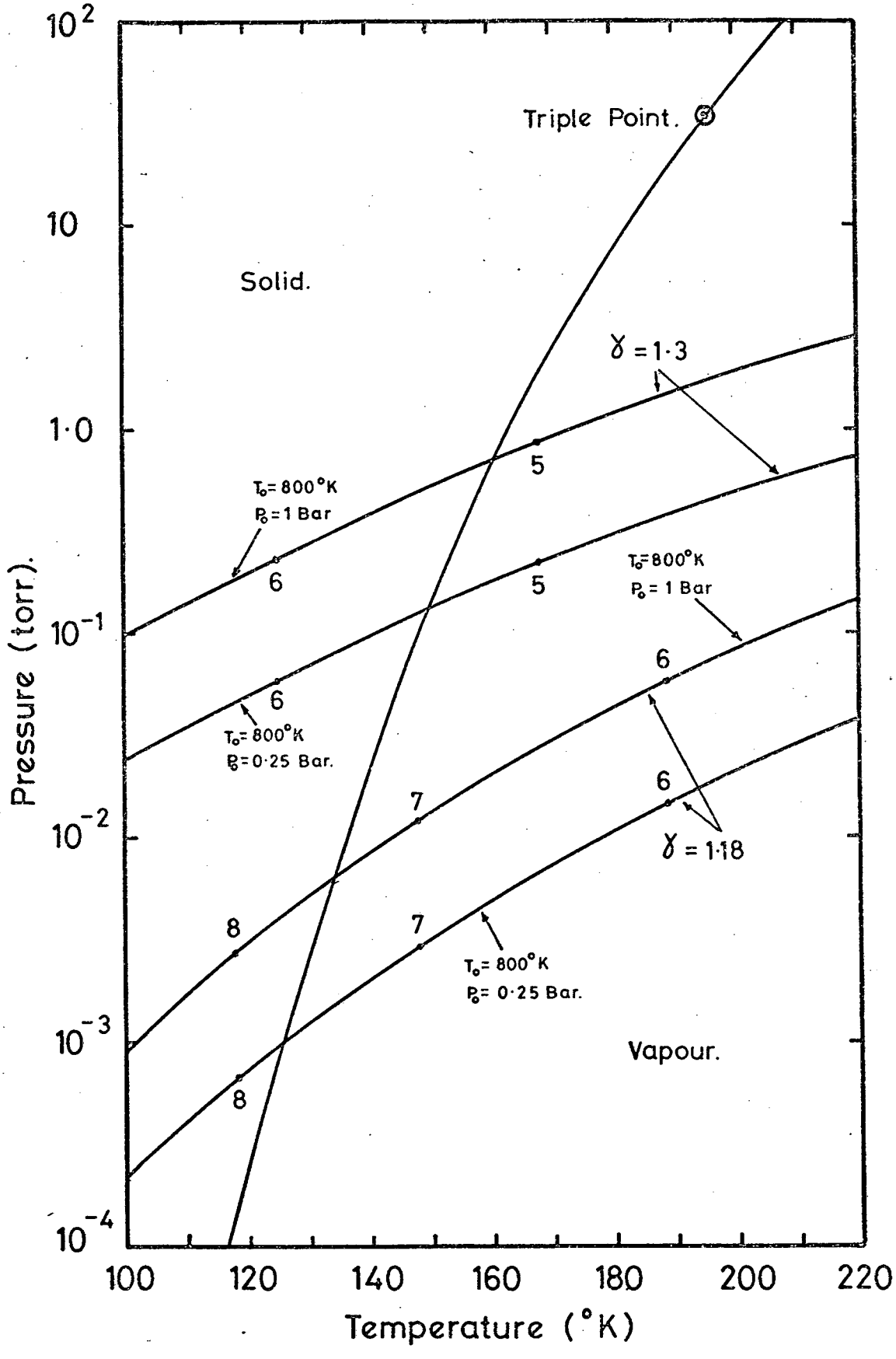

Fig. 18 Thermodynamic Conditions for Condensation of Ammonia.

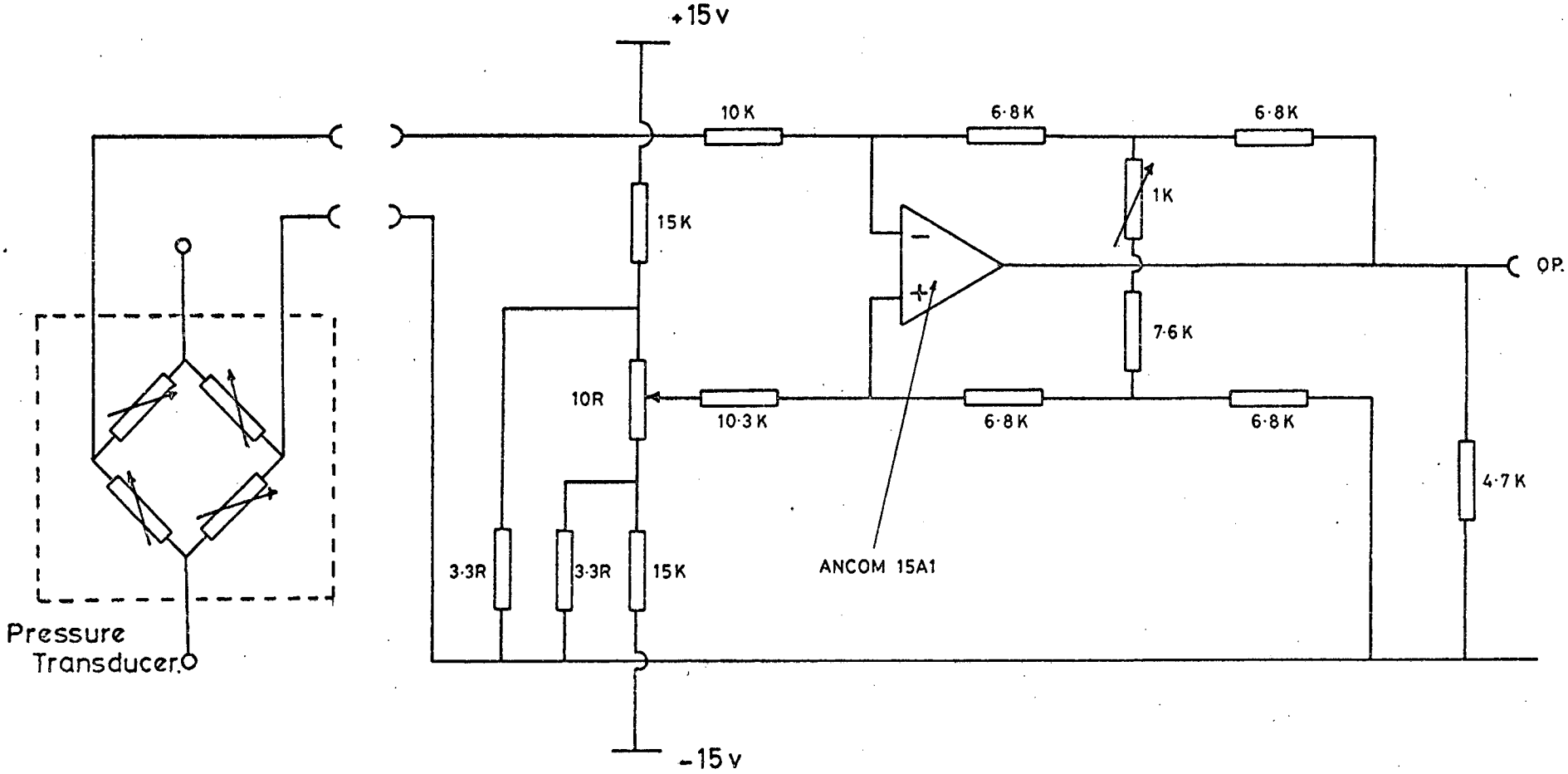

Fig. 19 Pressure Transducer Amplifiers.

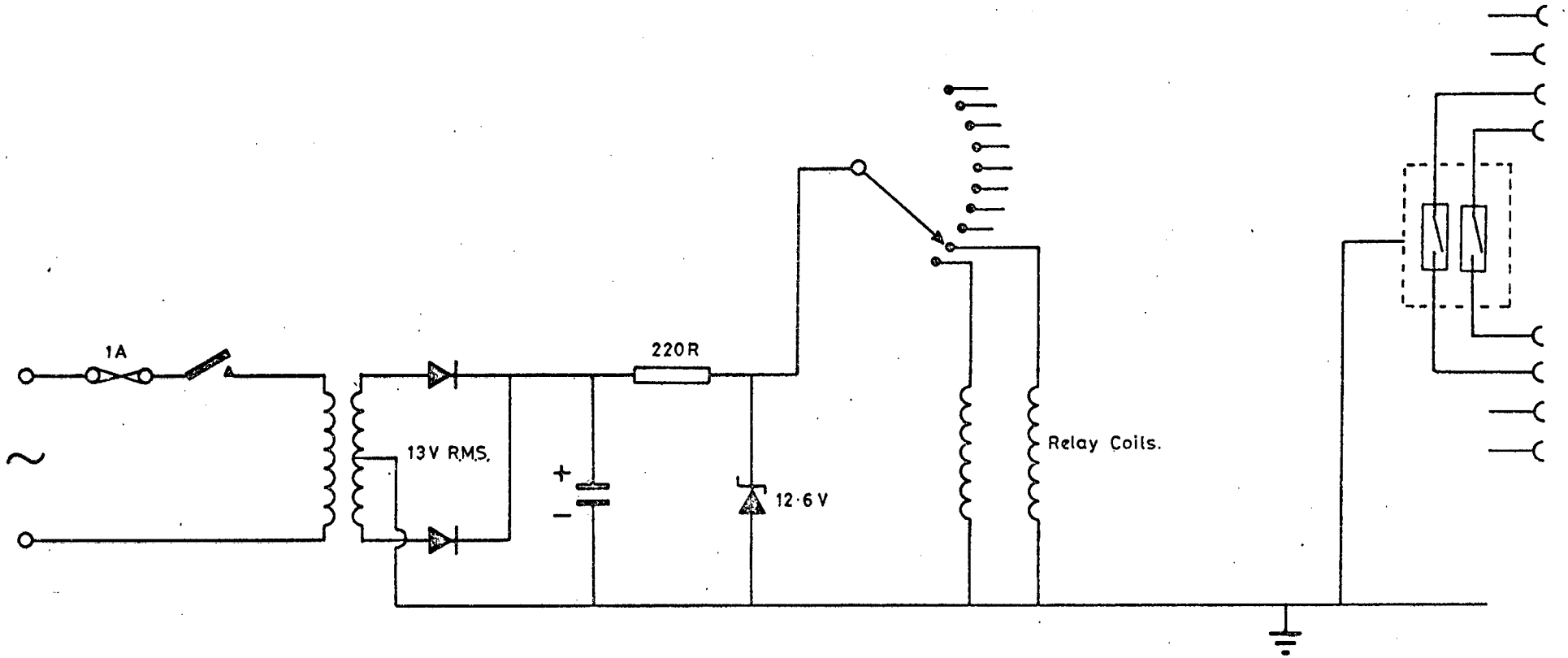

Fig. 20 Selector Switch Wiring Schematic.

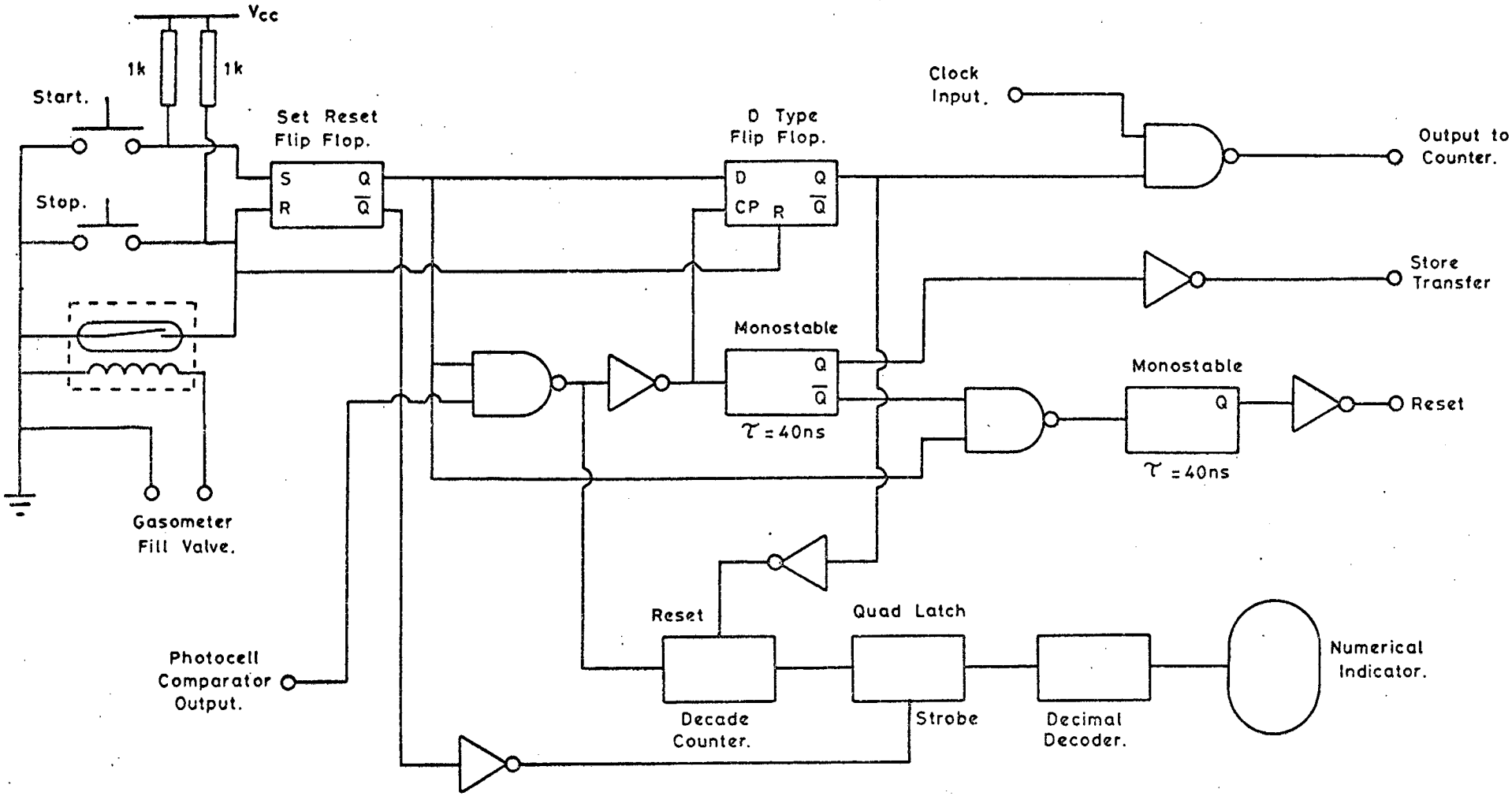

Fig. 21 Gasometer Timing Circuit.

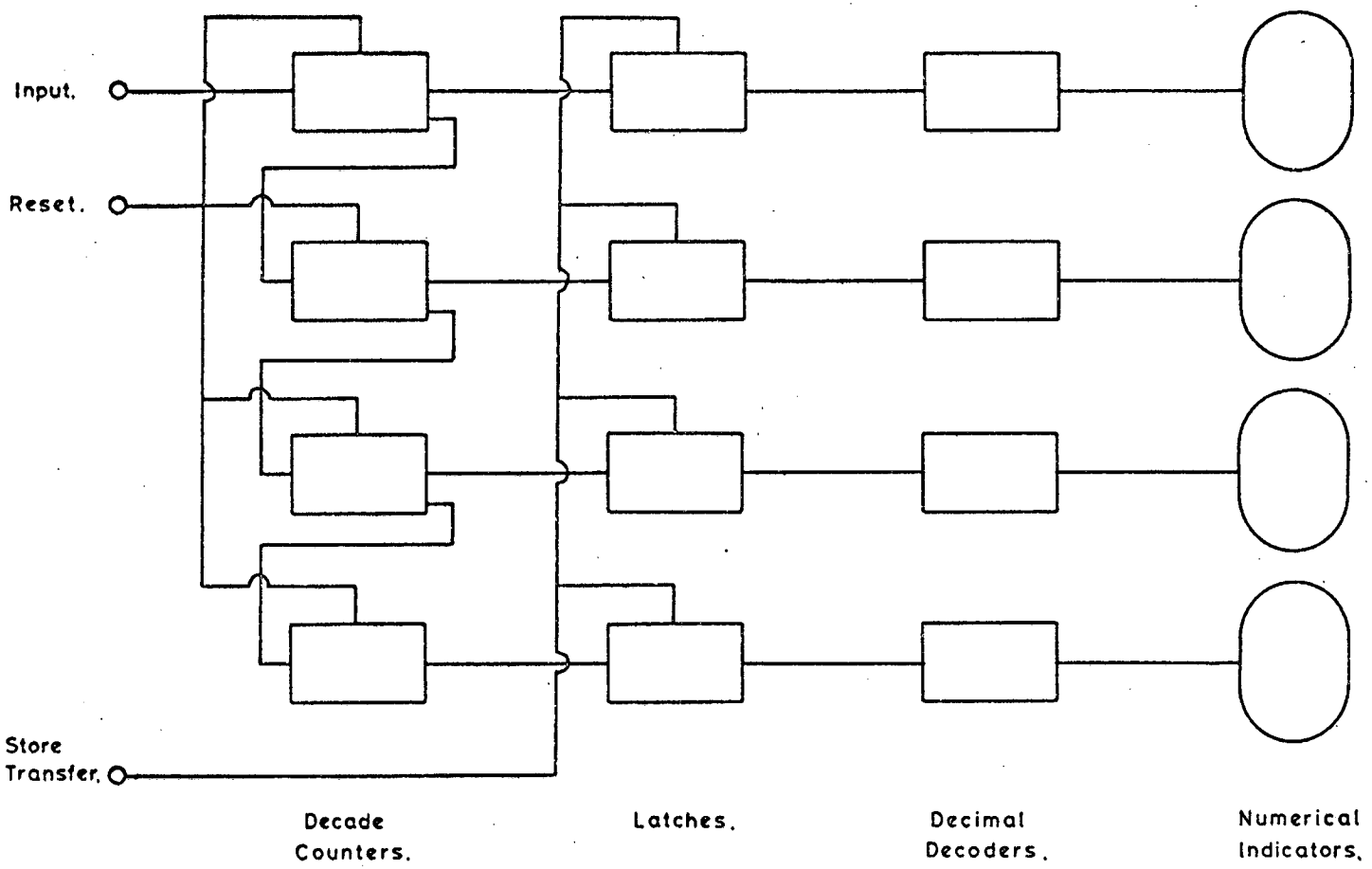

Fig. 22 Gasometer Timing Circuit.

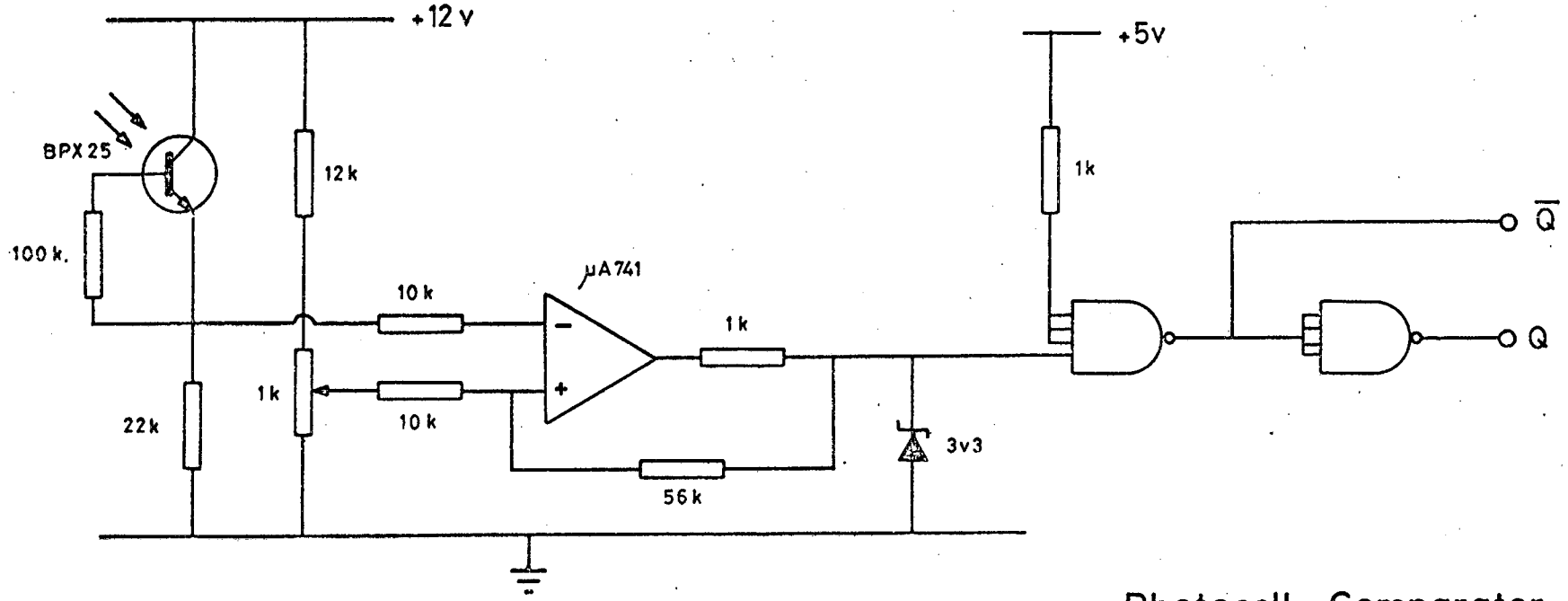

Fig. 23 Gasometer Timing Circuit.

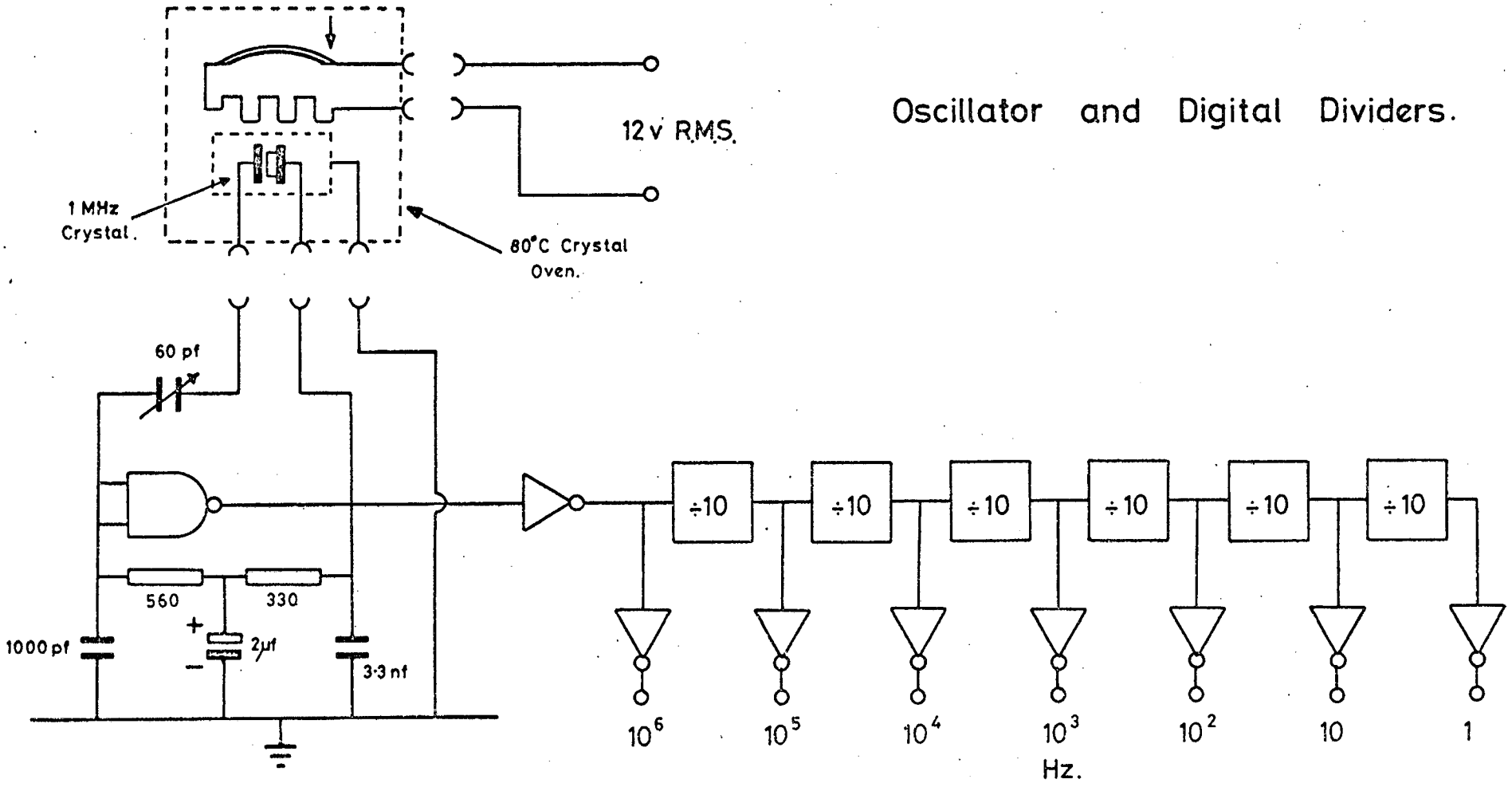

Fig. 24 Gasometer Timing Circuit.

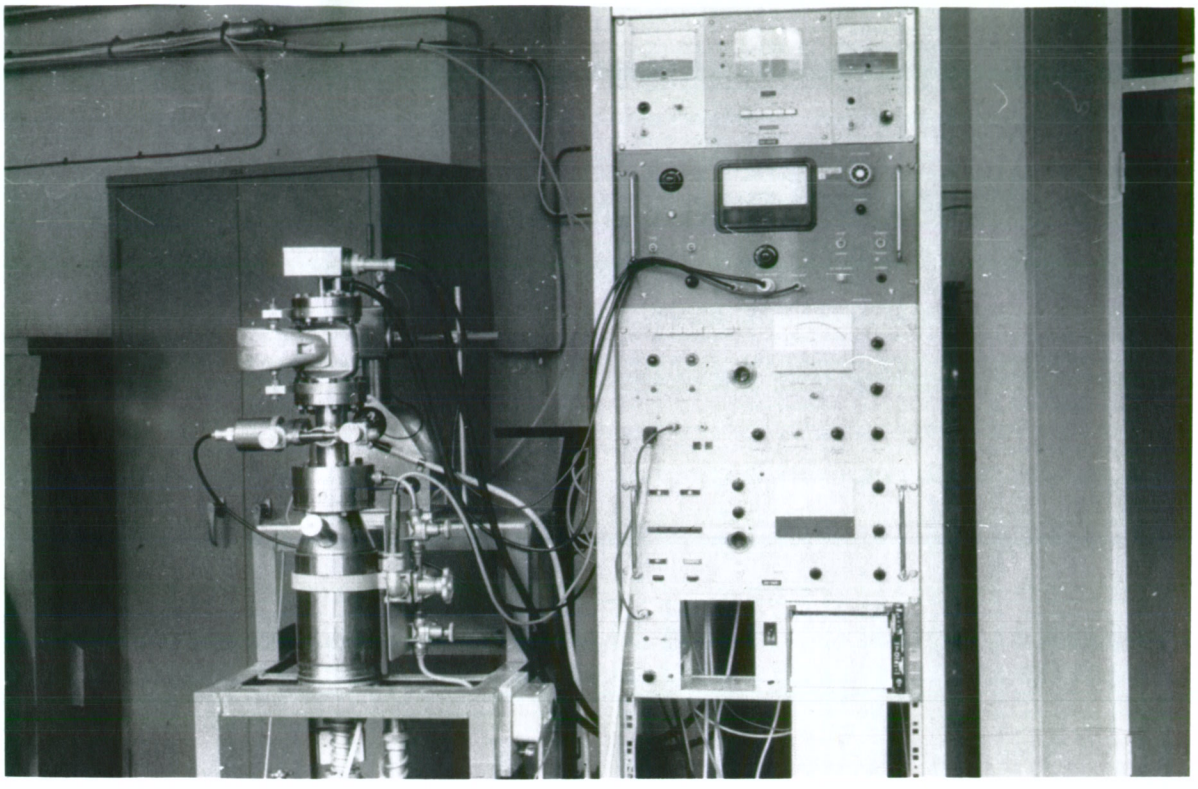

Fig. 25 Mass Spectrometers.

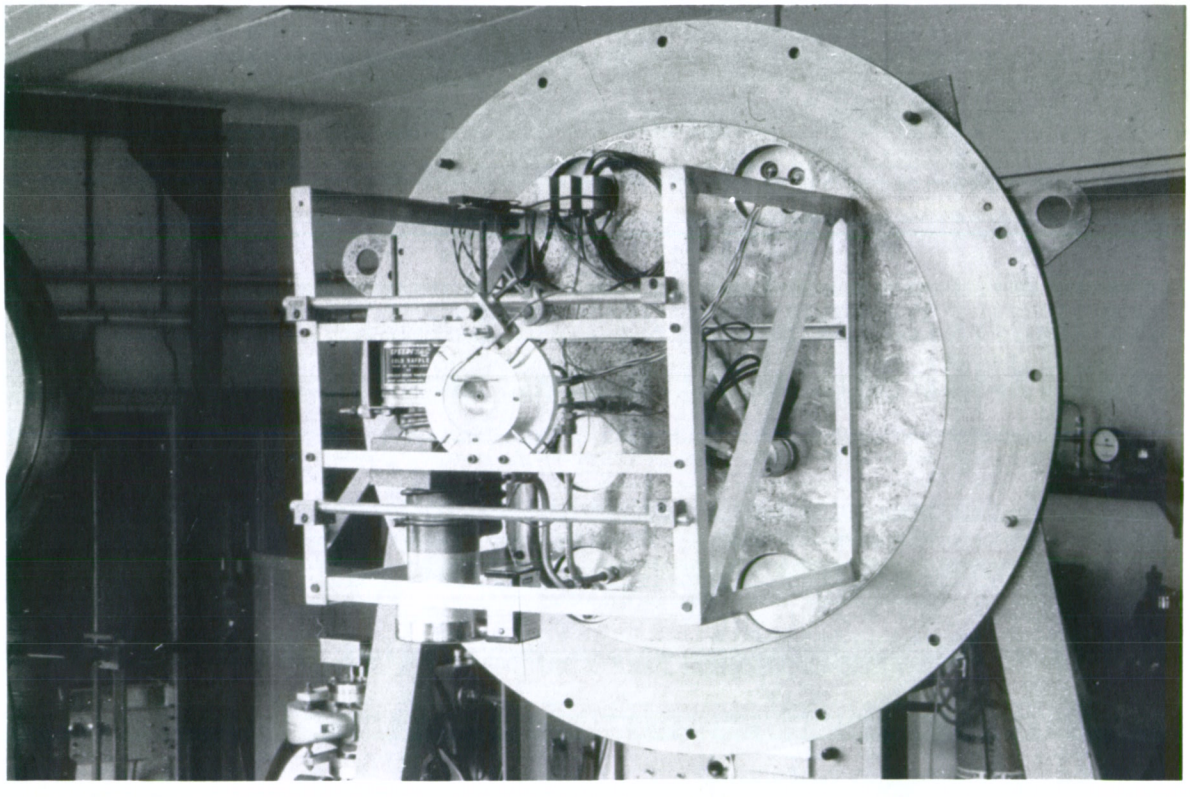

Fig. 26 Experiment on Door.

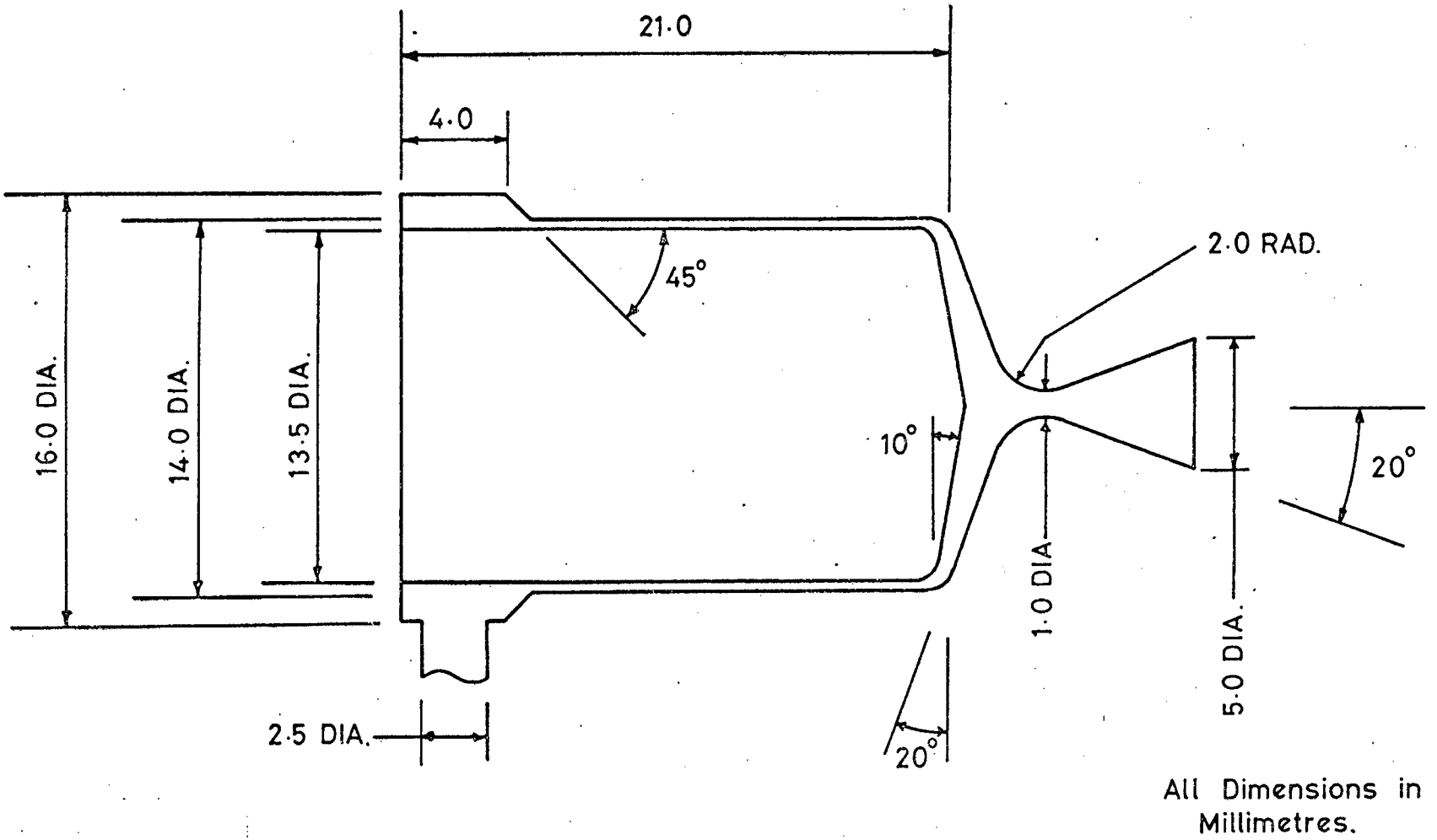

Fig. 27 Resistojet Flow Geometry.

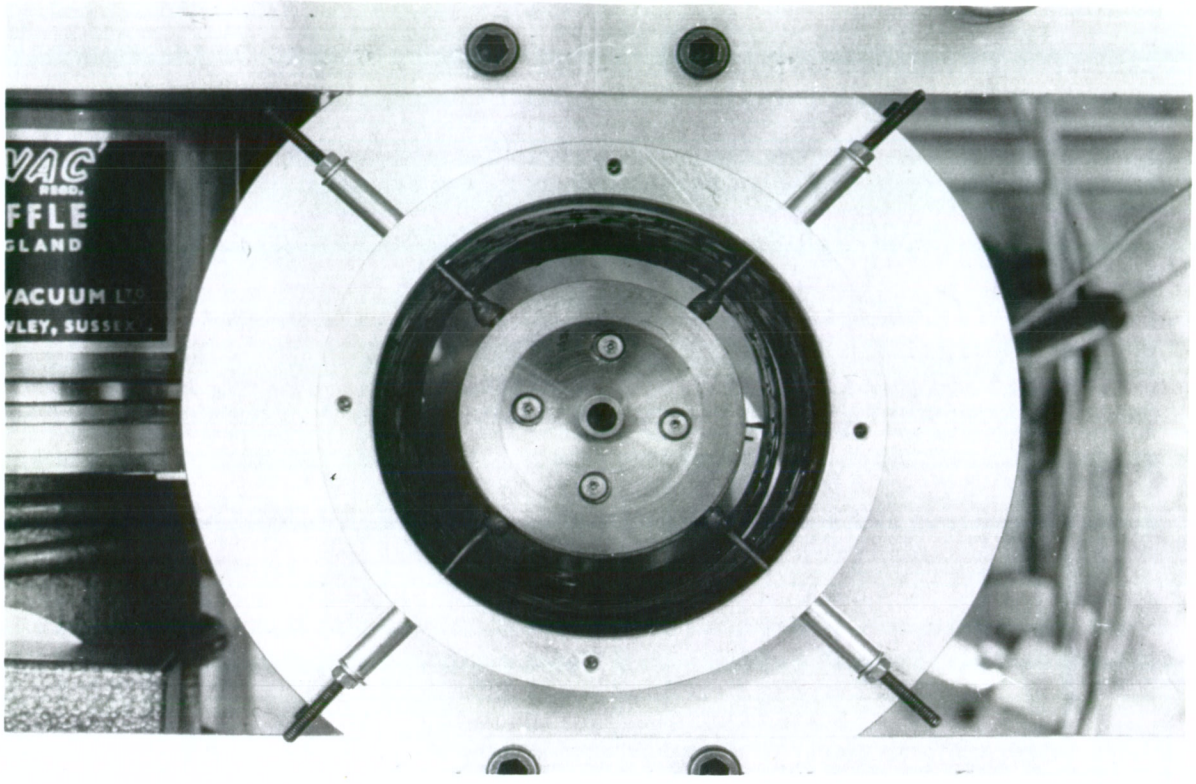

Fig. 28 Resistojet in Mounting.

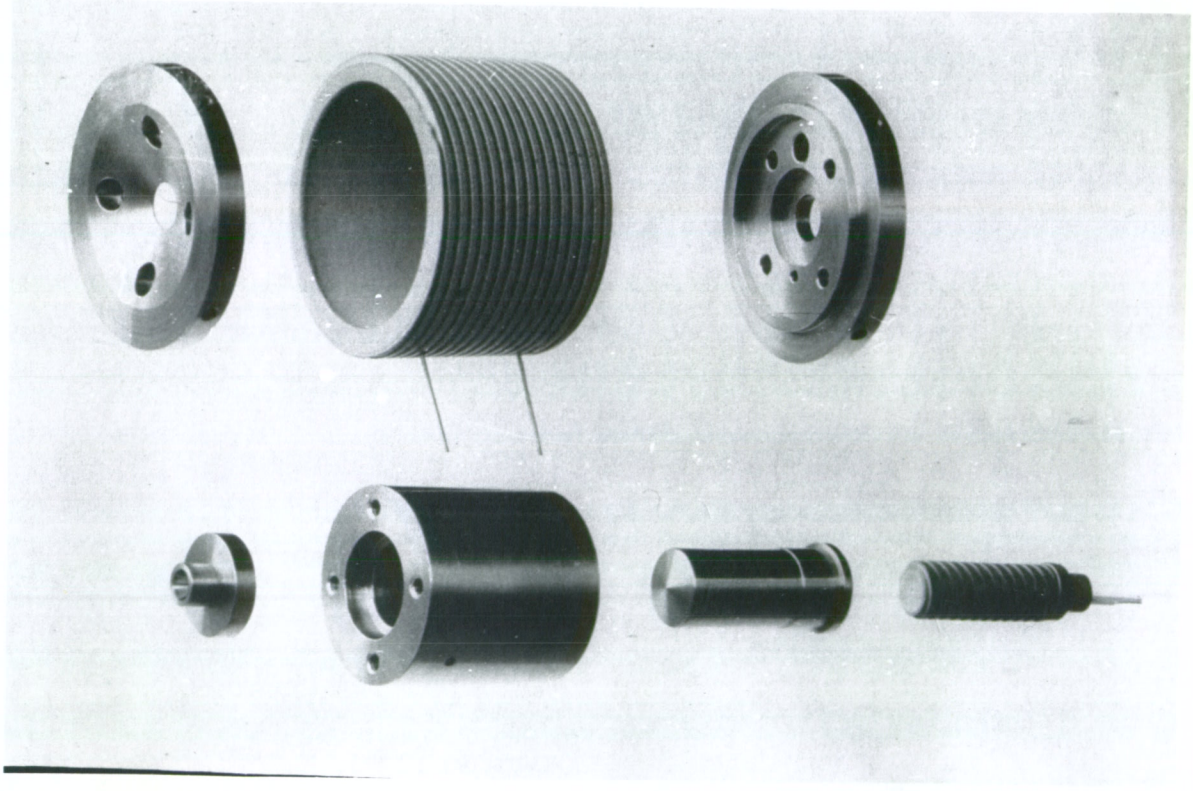

Fig. 29 Exploded View of Resistojet.

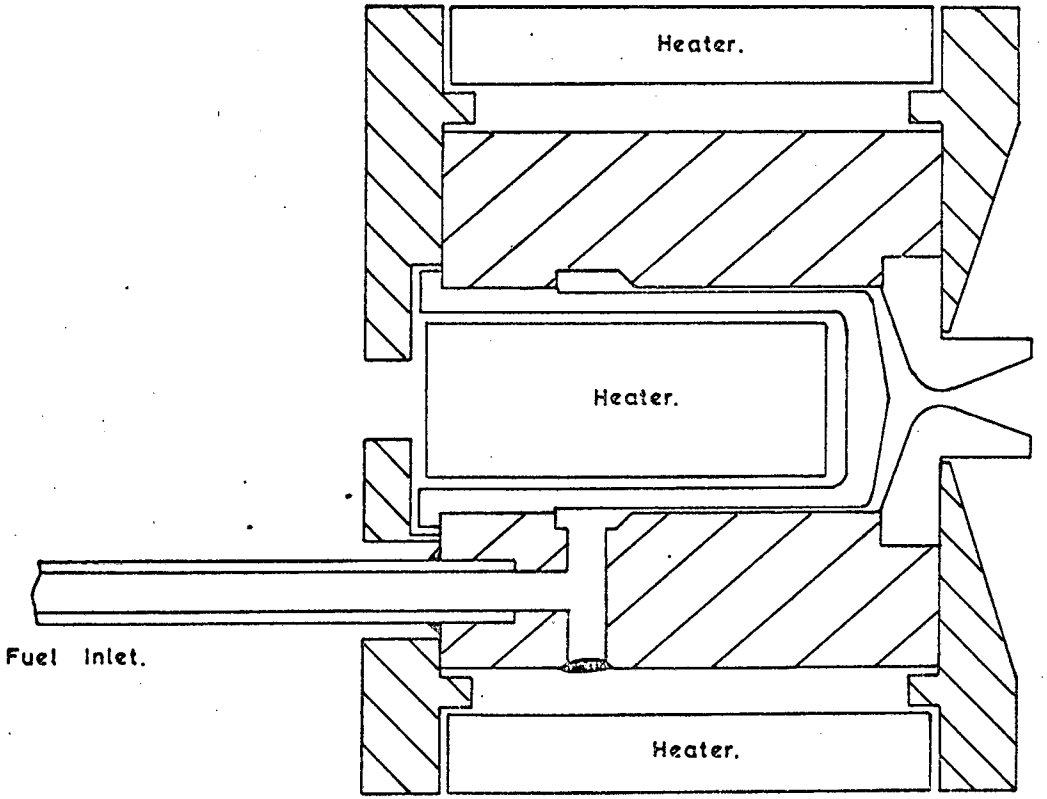

Fig. 30 Cross-Sectional Diagram of Shrink Fit Resistojet.

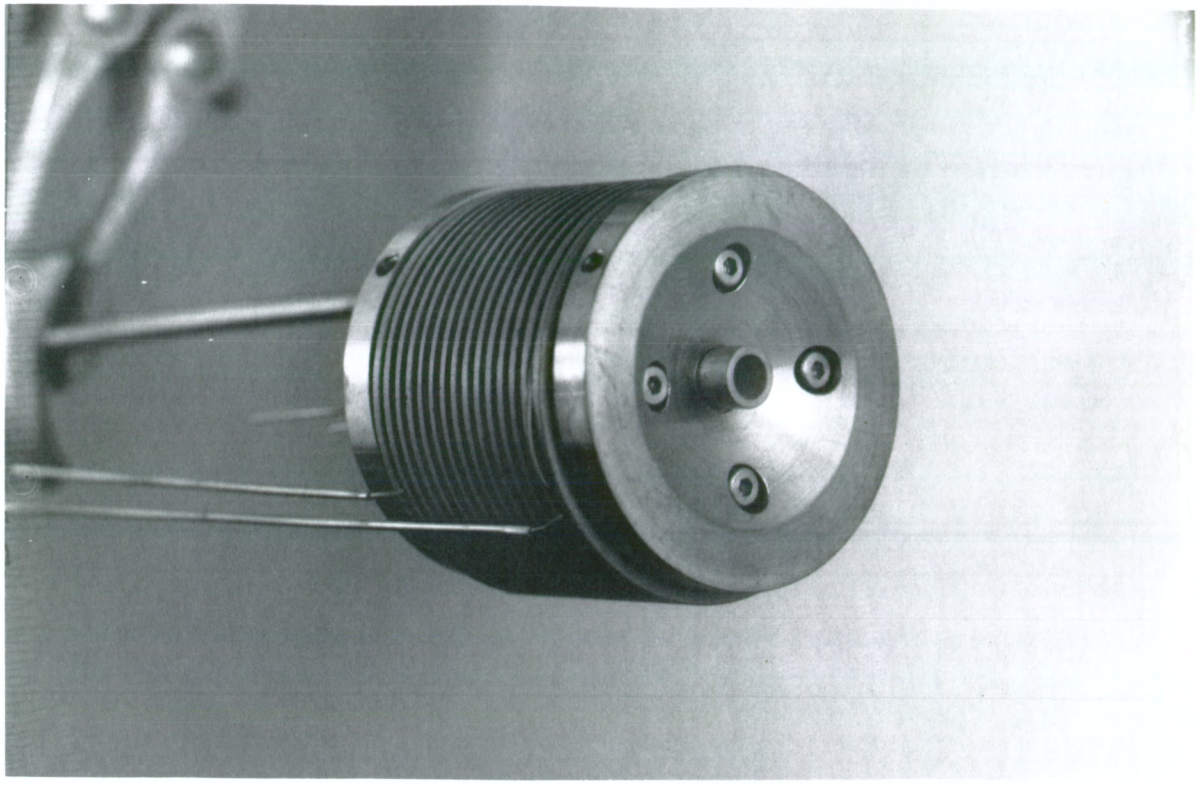

Fig. 31 Shrink Fit Resistojet.

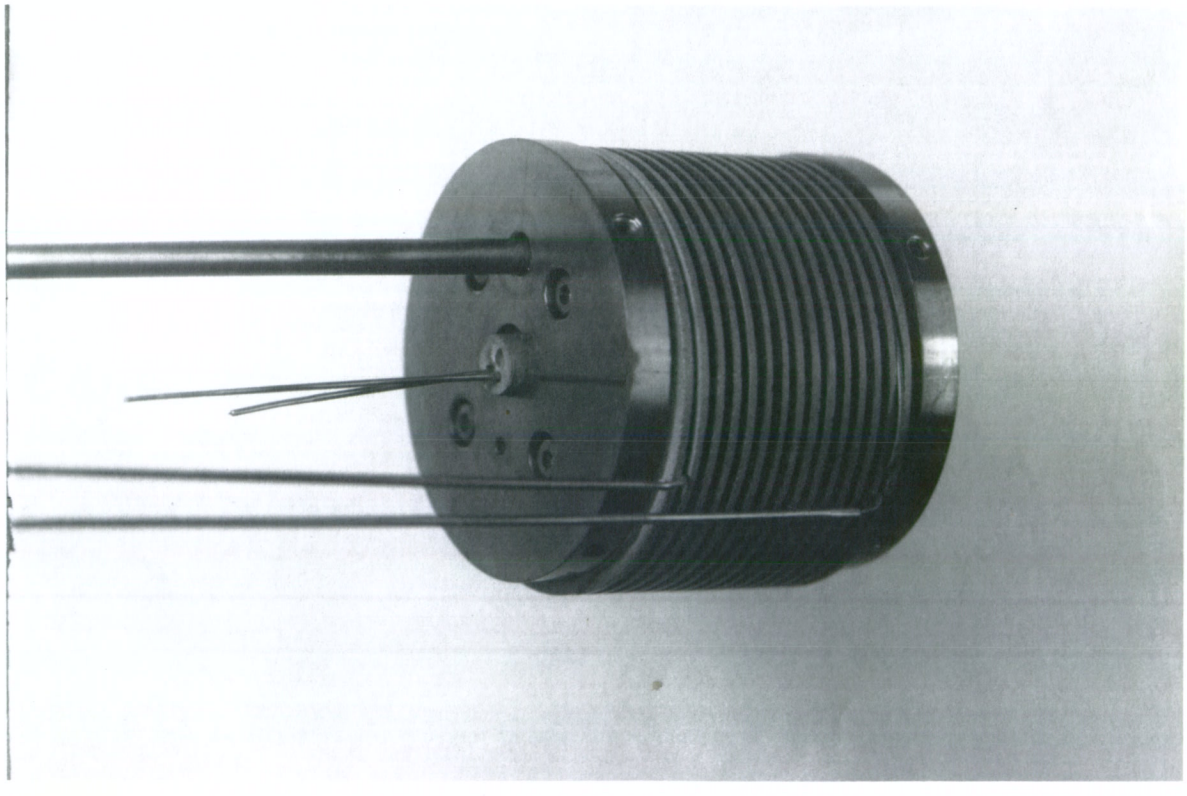

Fig. 32 Shrink Fit Resistojet.

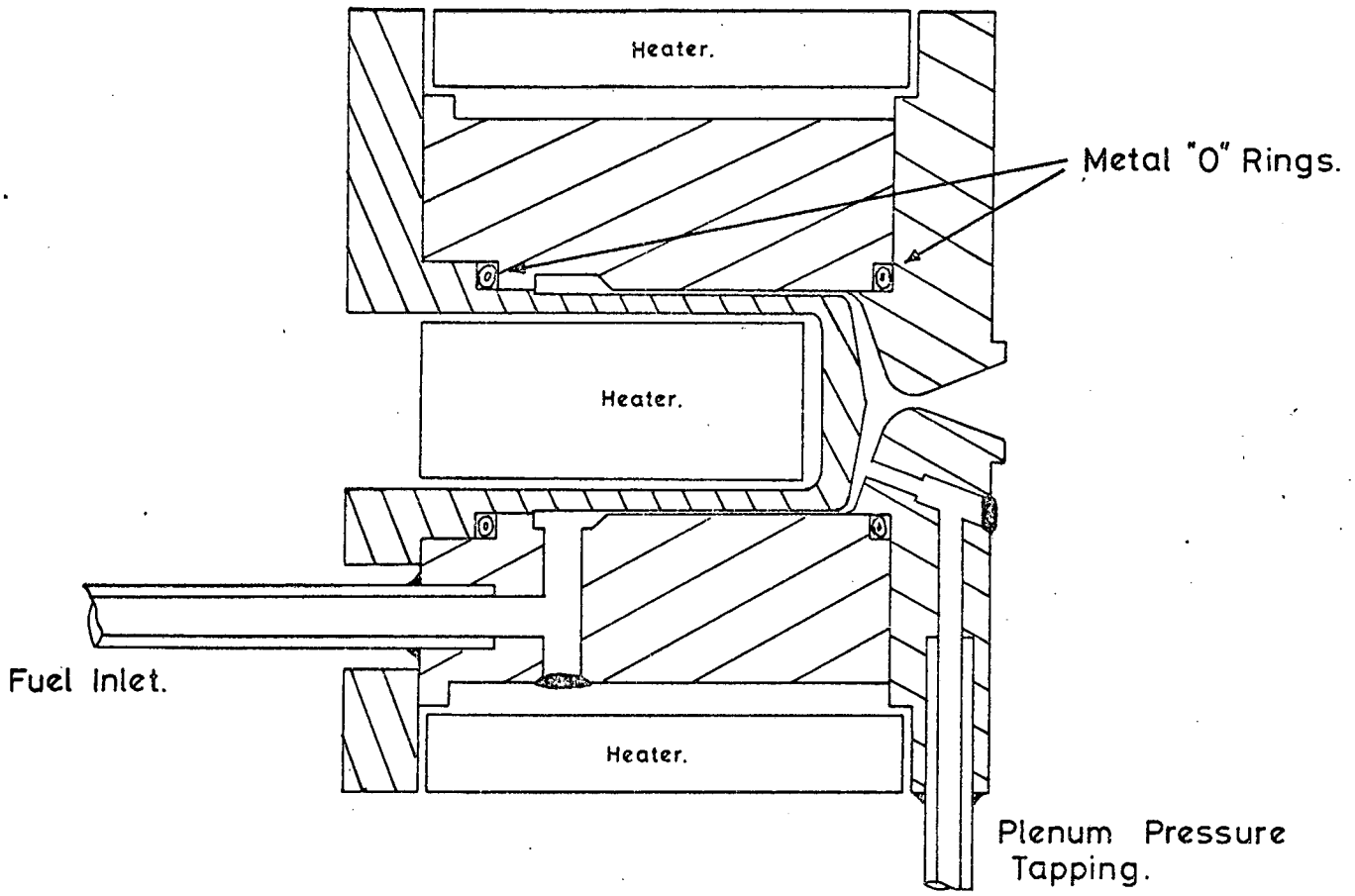

Fig. 33 Cross-Sectional Diagram of Demountable Resistojet.

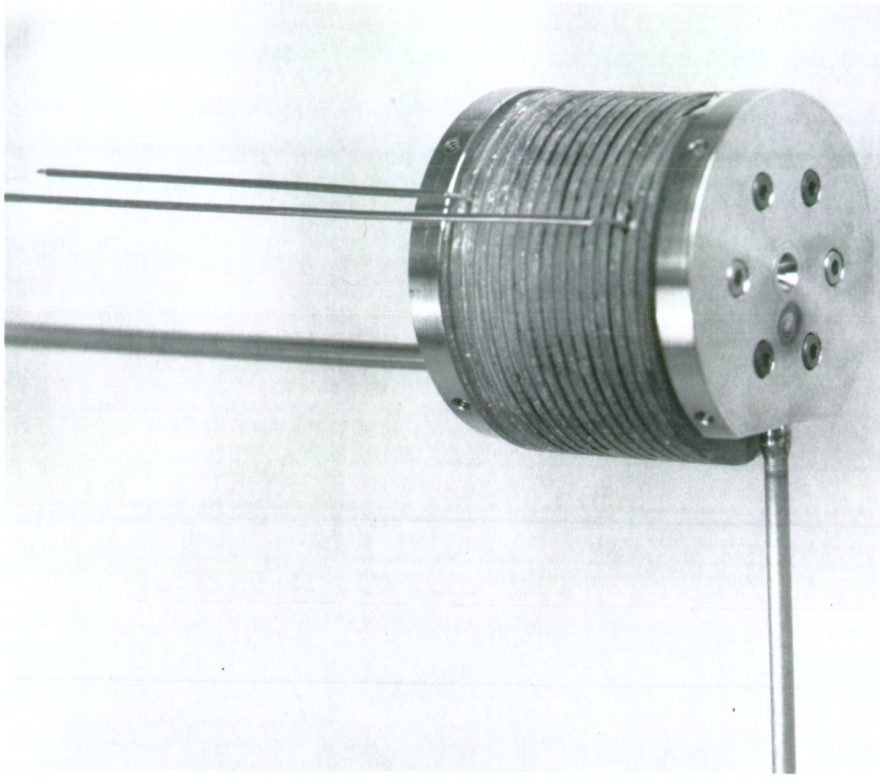

Fig. 34 Demountable Resistojet.

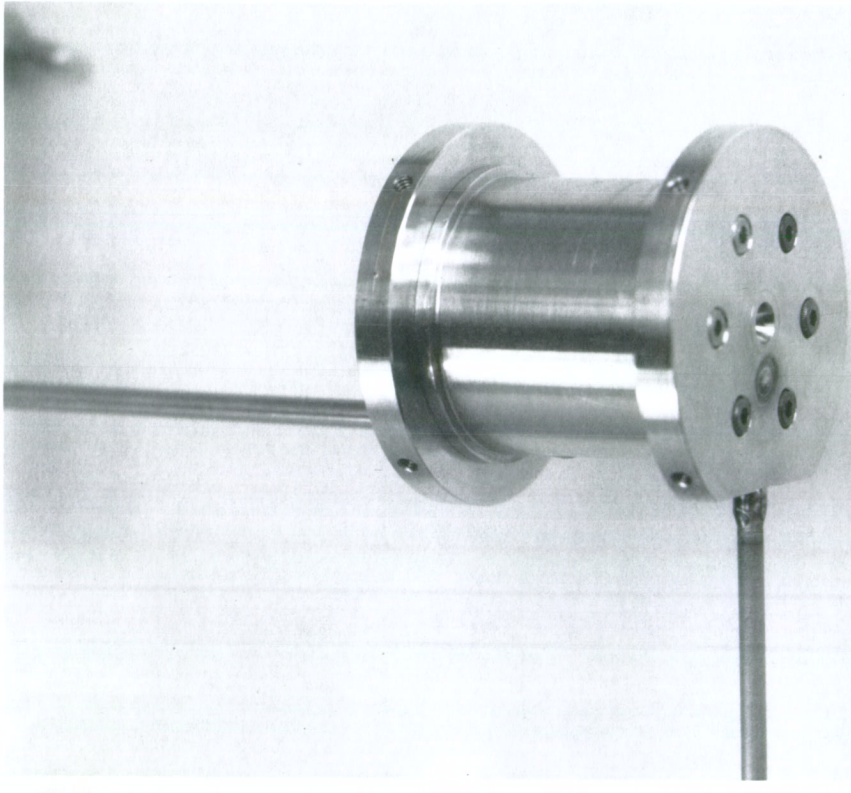

Fig. 35 Demountable Resistojet.

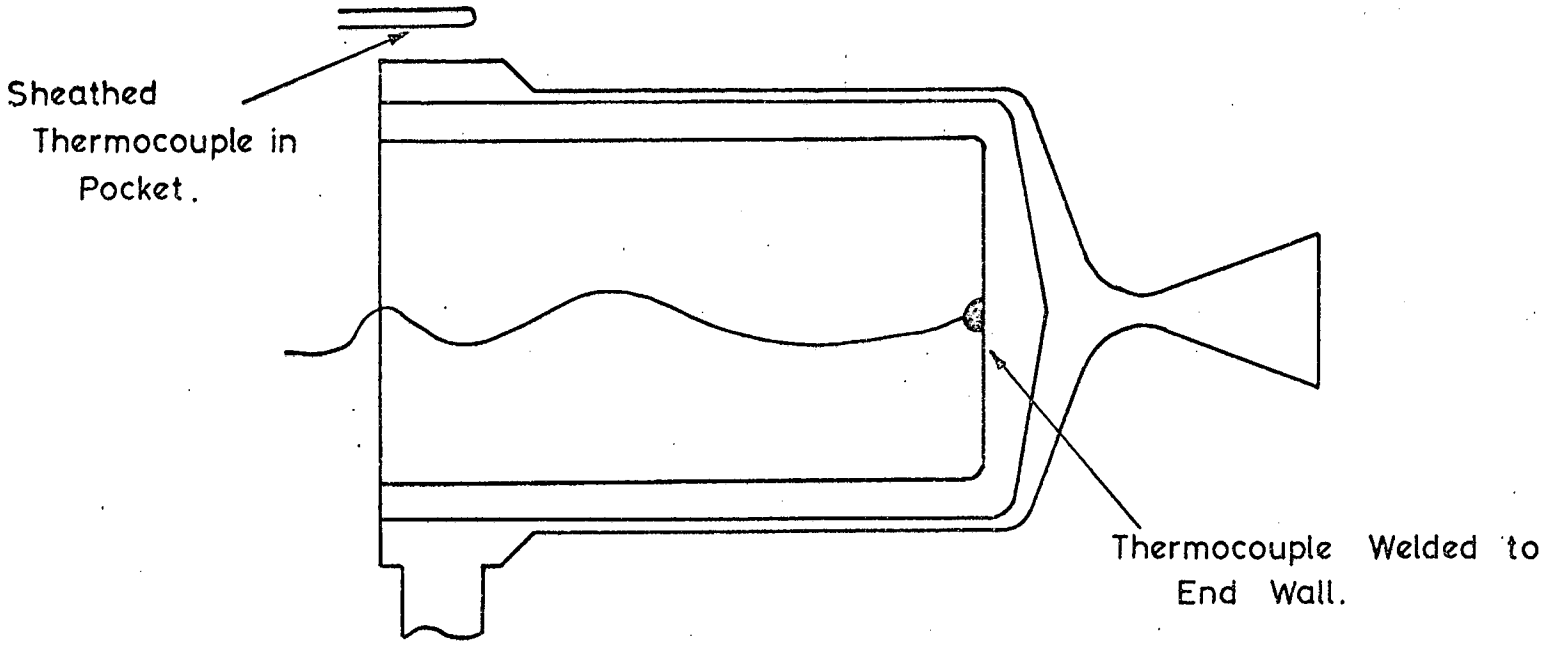

Fig. 36 Position of Thermocouples in Resistojet.

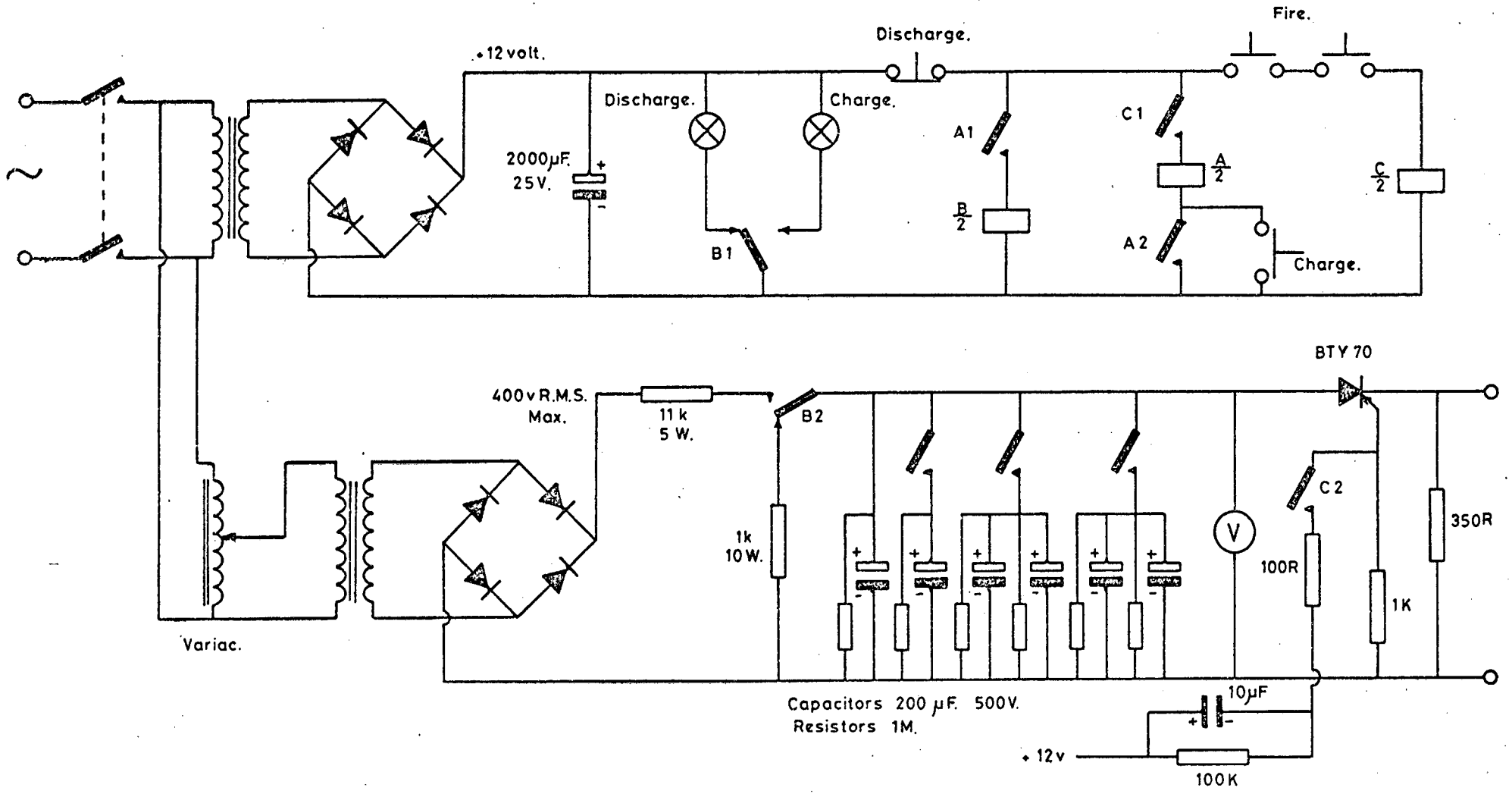

Fig. 37 Circuit Diagram of Thermocouple Welder.

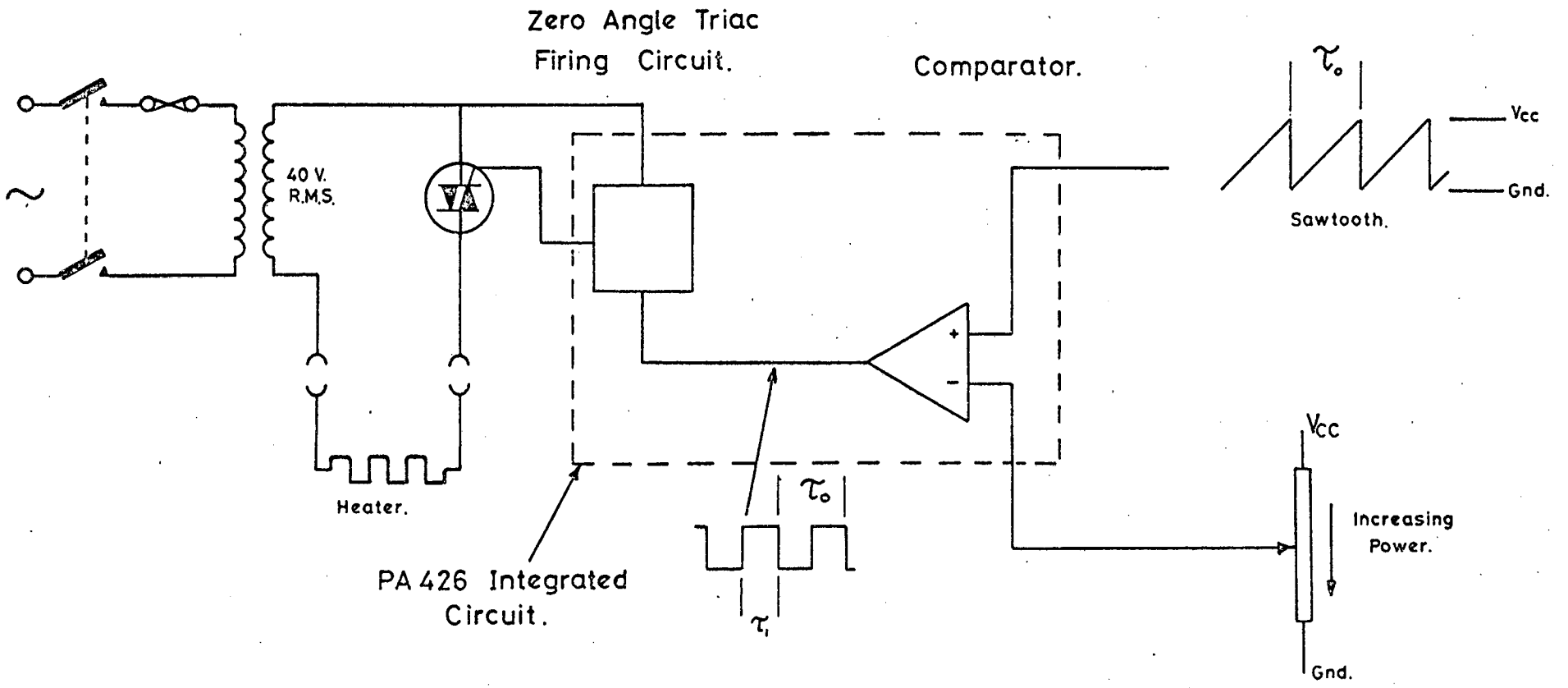

Fig. 38 Heater Power Supply Schematic Diagram.

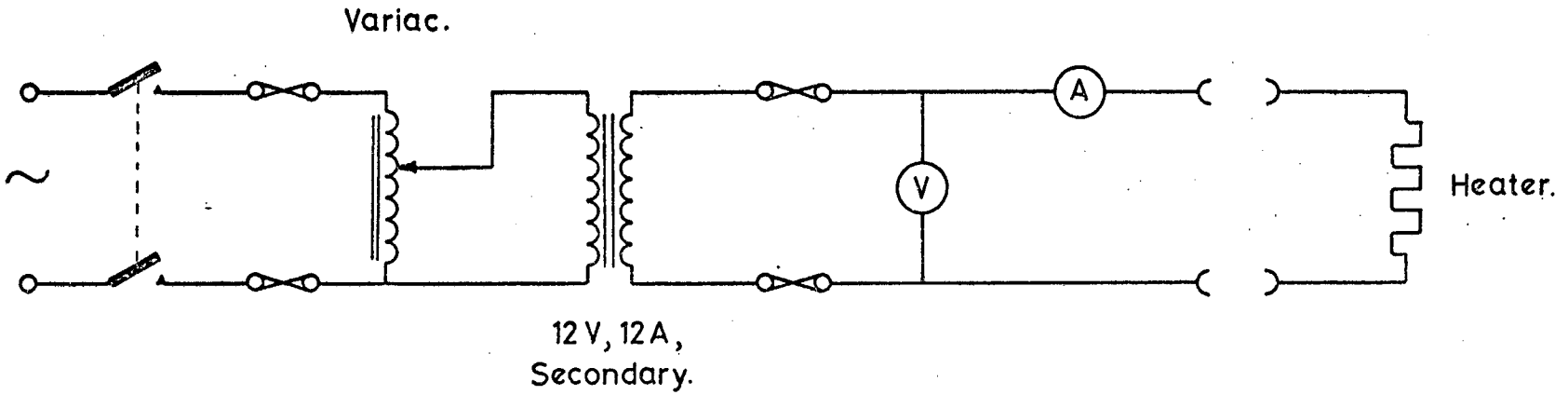

Fig. 39 Tungsten Heater Power Supply.

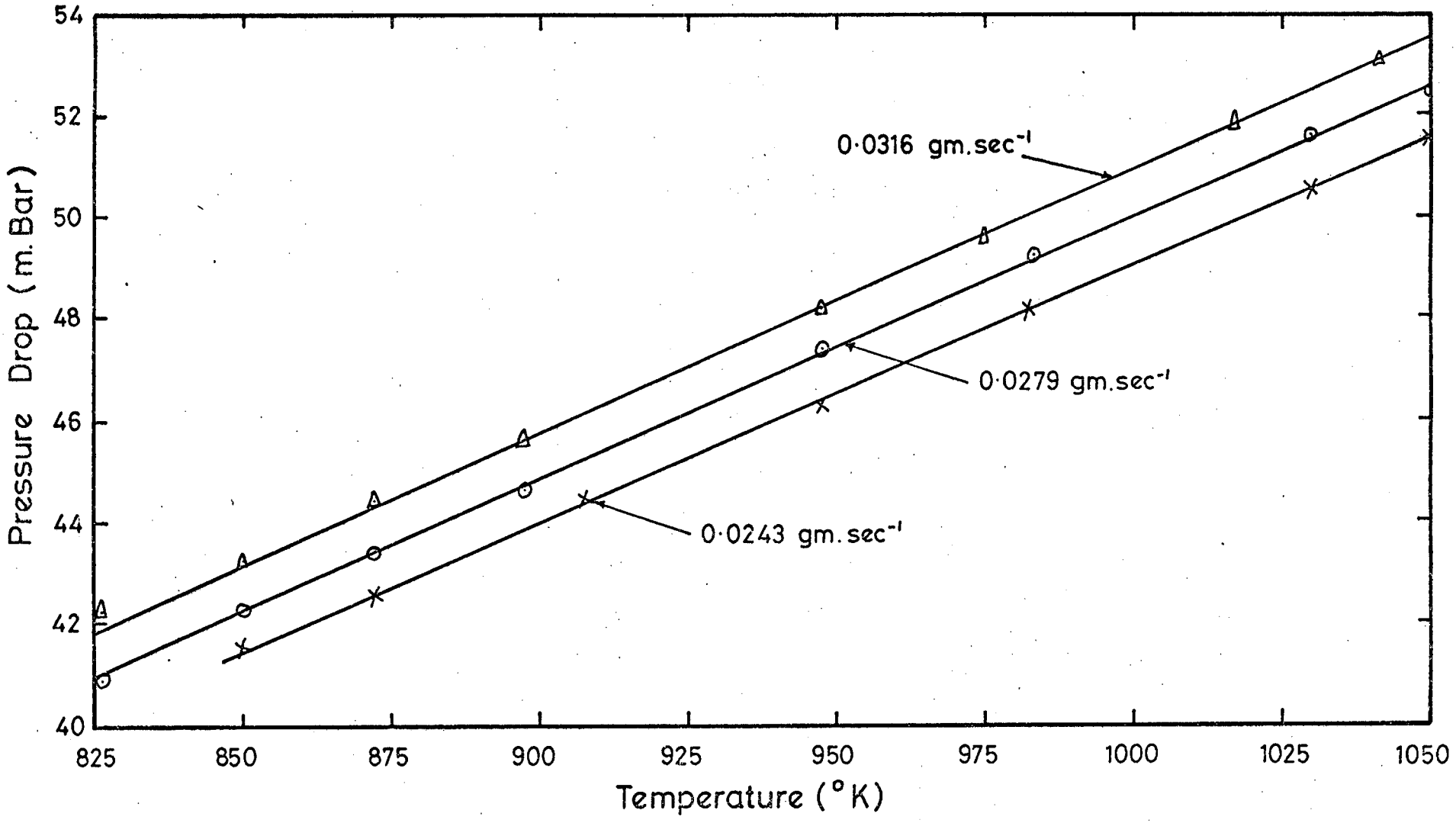

Fig. 40 Variation of Heater Pressure Drop with Temperature.

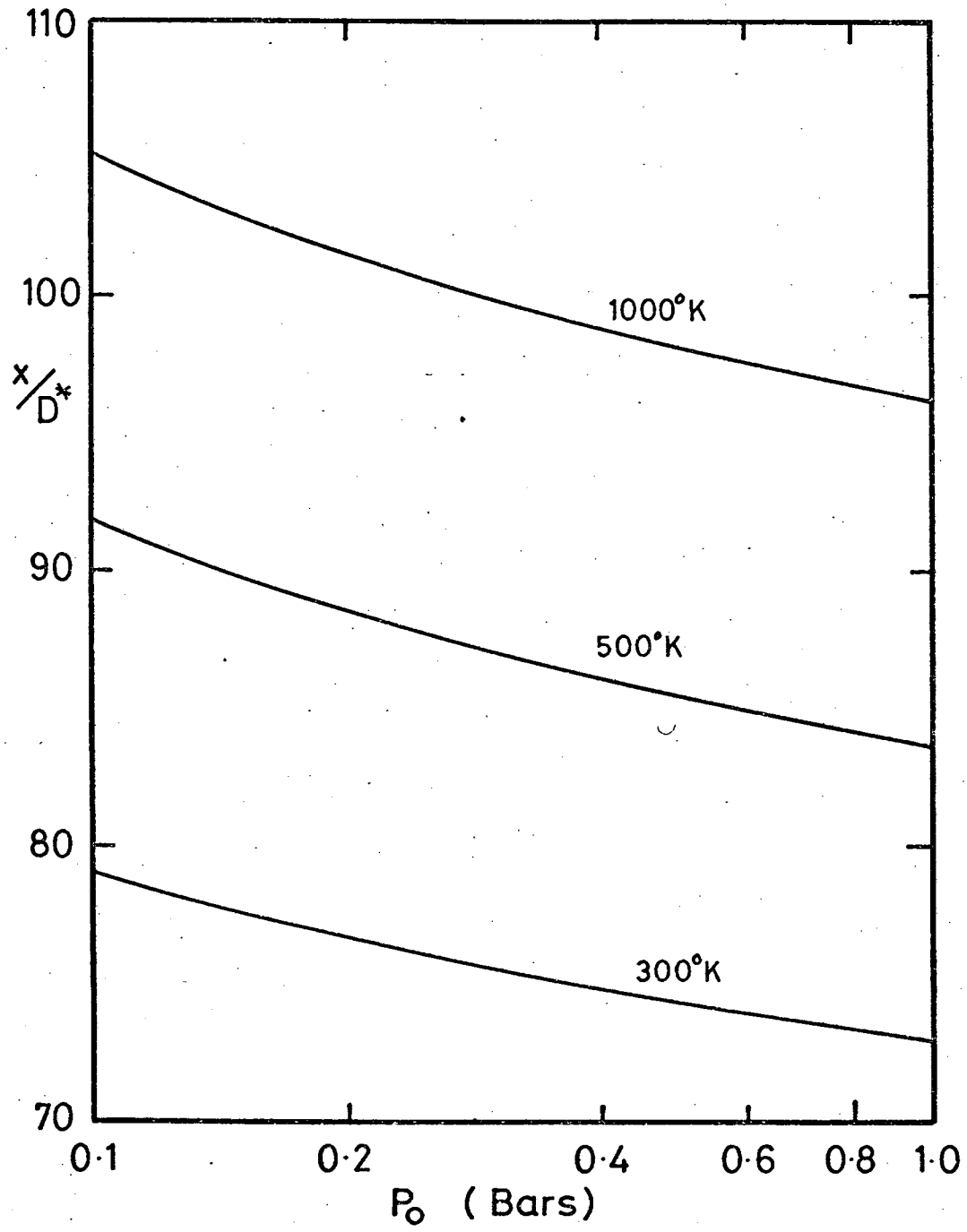

Fig. 41 Mach Disc Position with Changing Stagnation Pressure. (Nitrogen.)

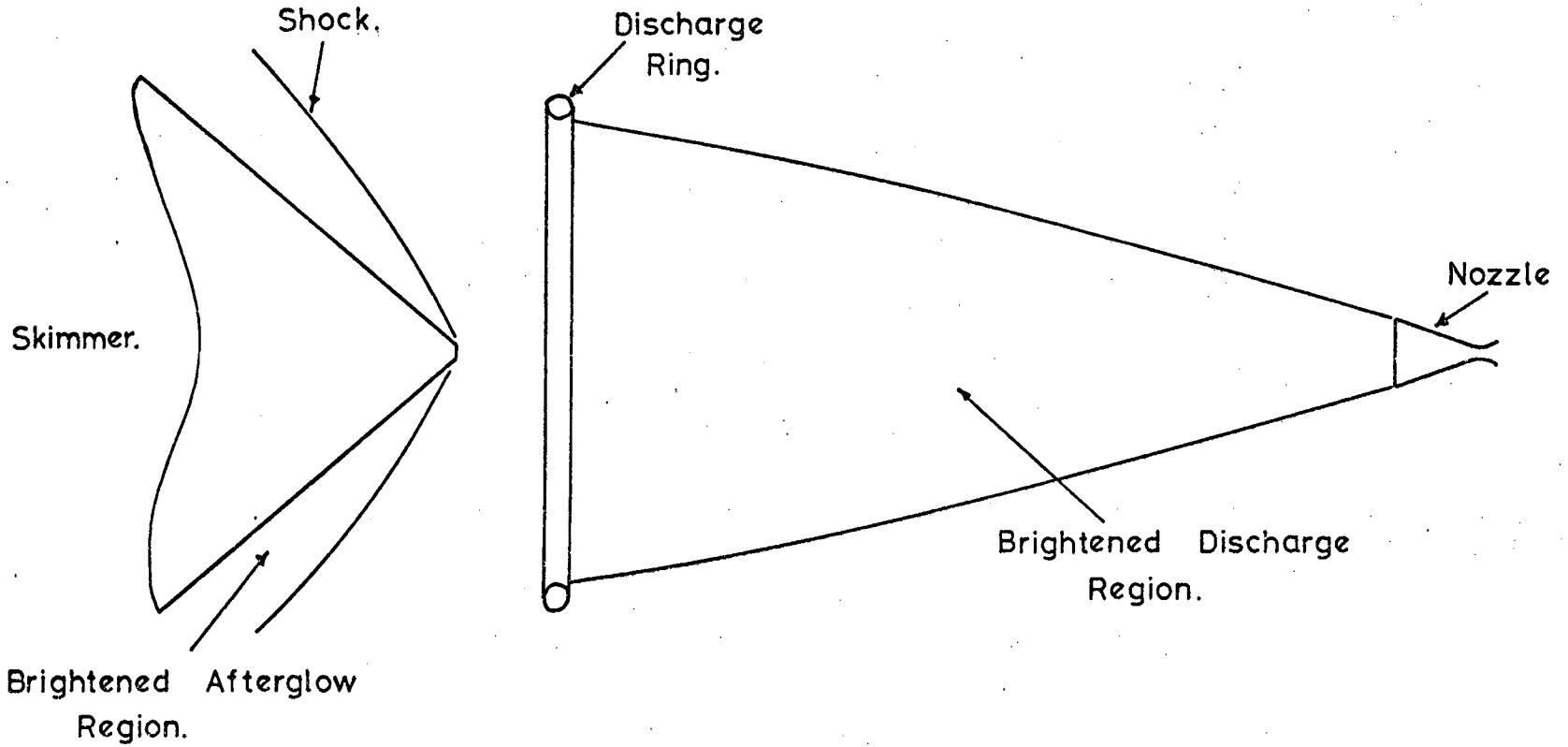

Fig. 42 Attached Shock at Skimmer Mouth.

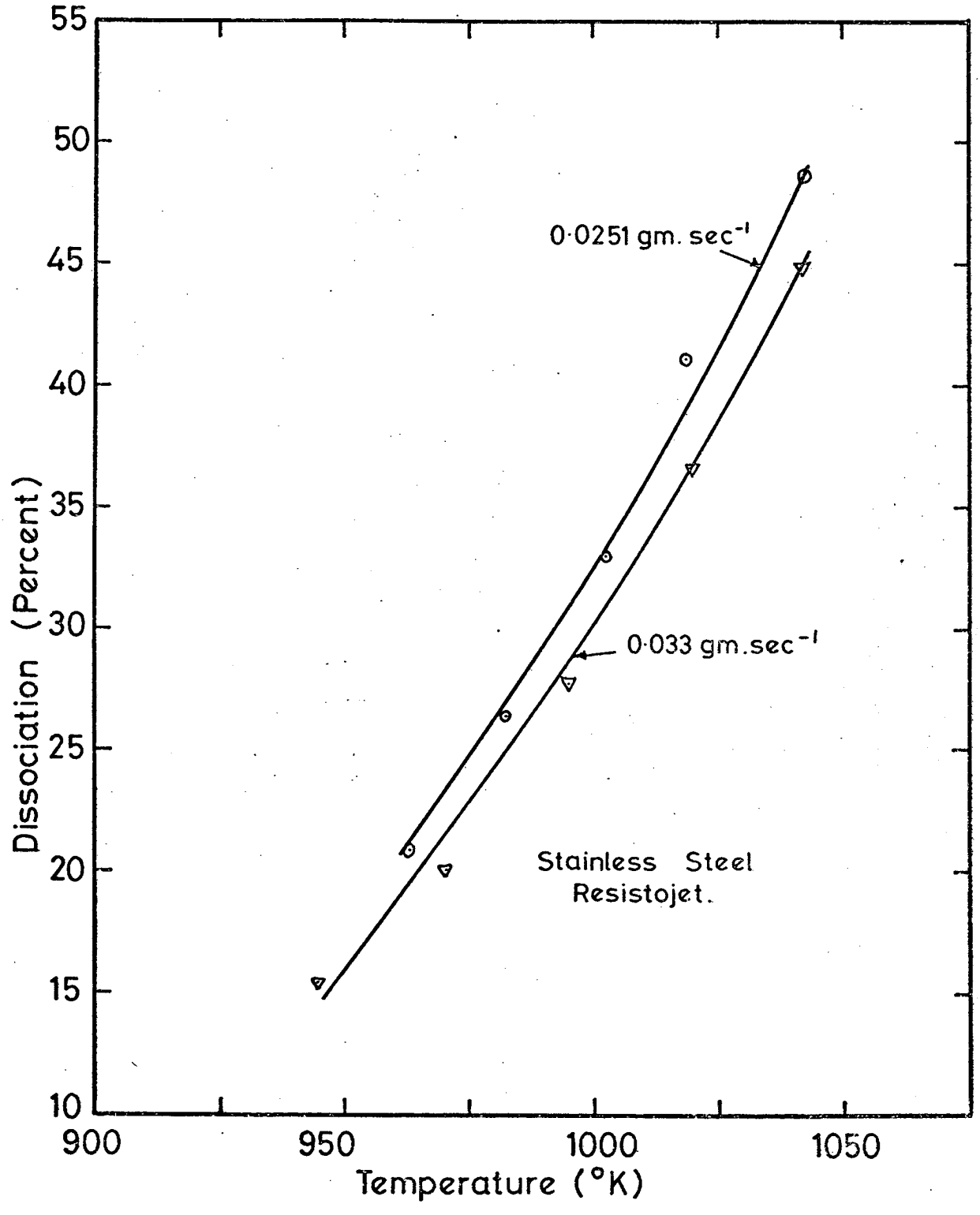

Fig. 43 Variation of Ammonia Dissociation with Temperature.

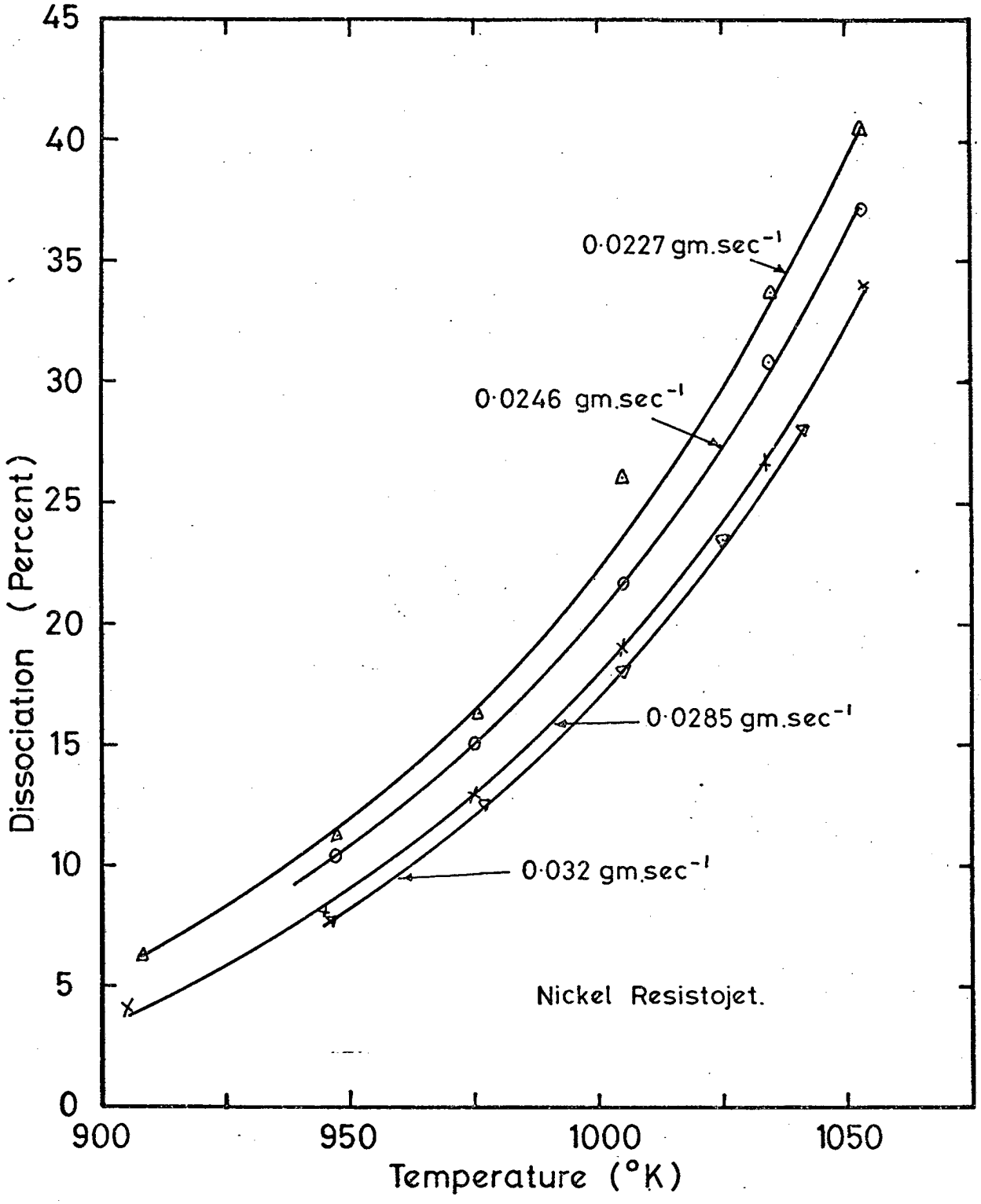

Fig. 44 Variation of Ammonia Dissociation with Temperature.

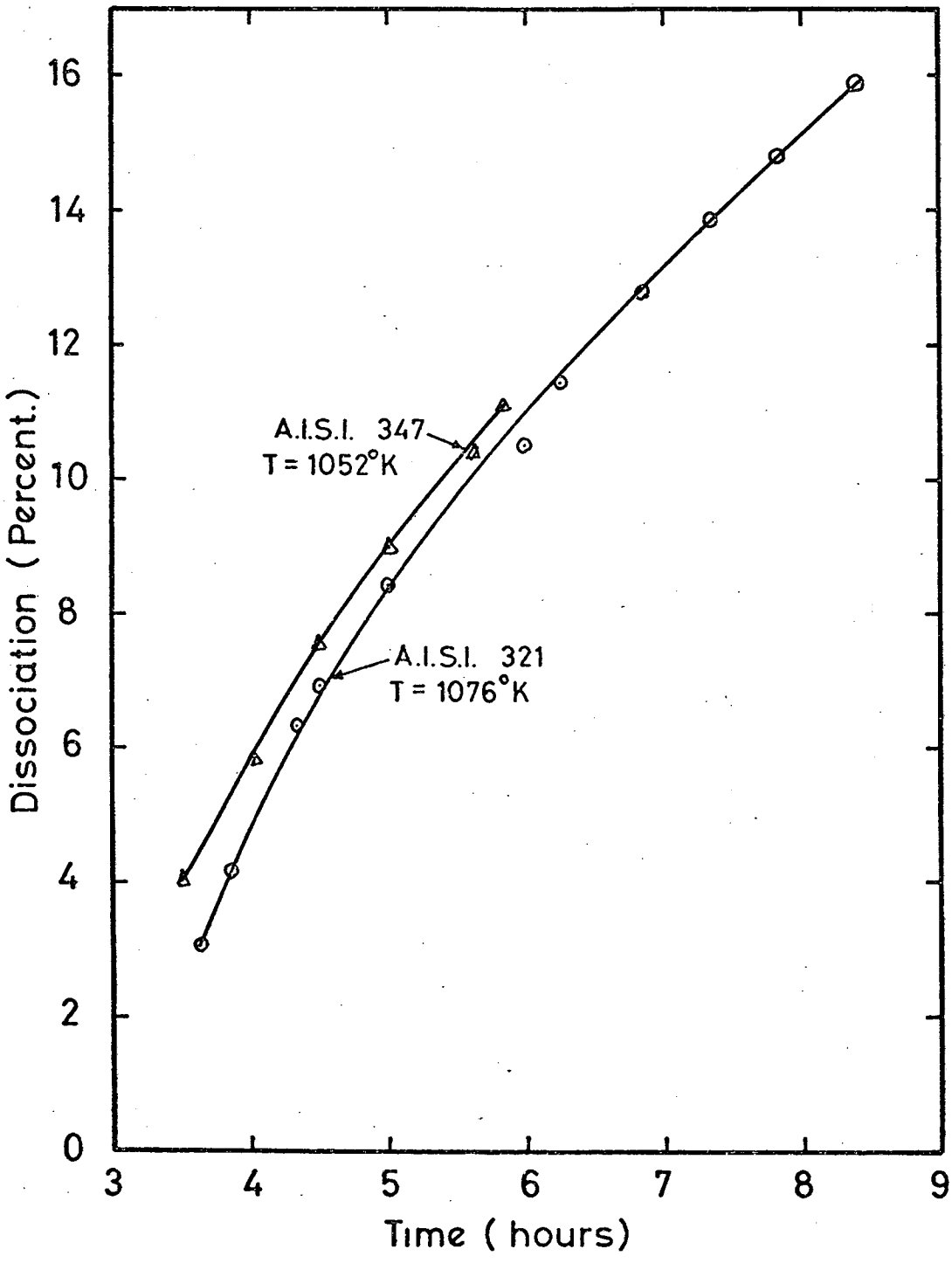

Fig. 45 Variation of Dissociation on Stainless Steel with Time.

Photograph of Surface

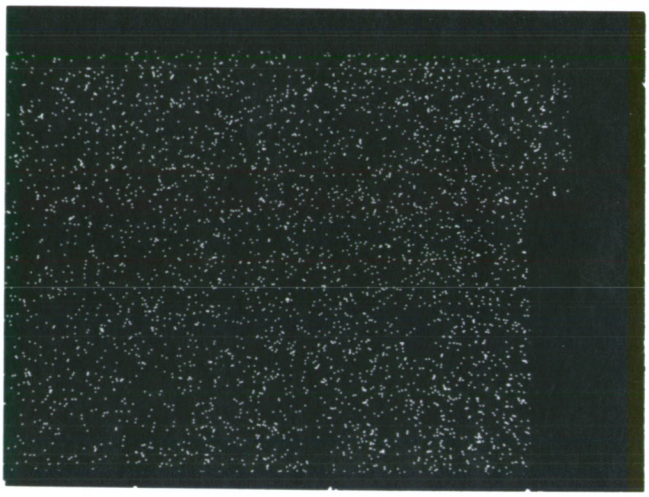

Nitrogen Concentration

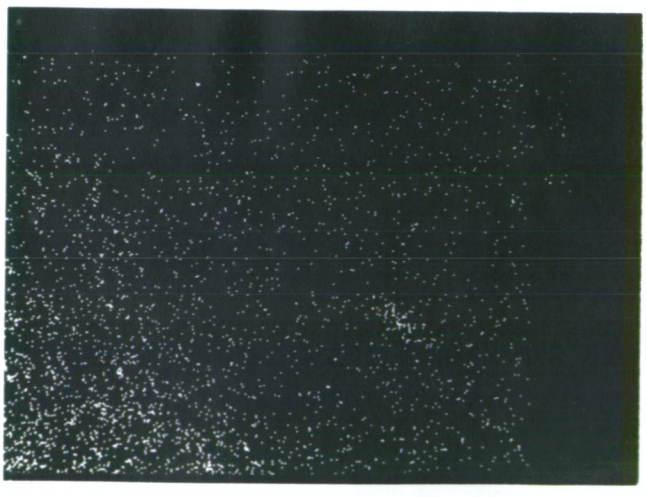

Iron Concentration

Fig. 46 Electron Beam Probe Results.

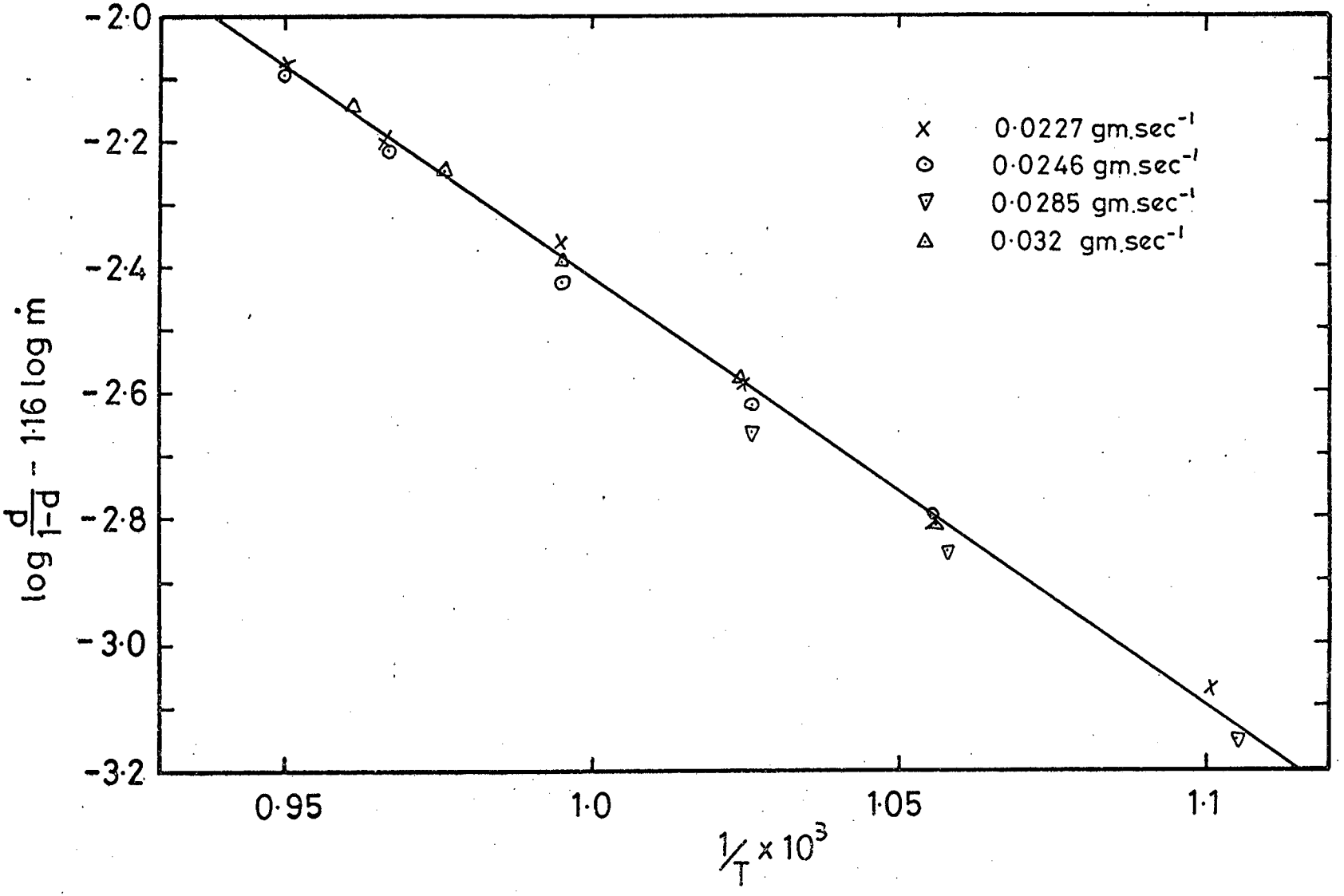

Fig. 47 Plot of Reduced Nickel Results.

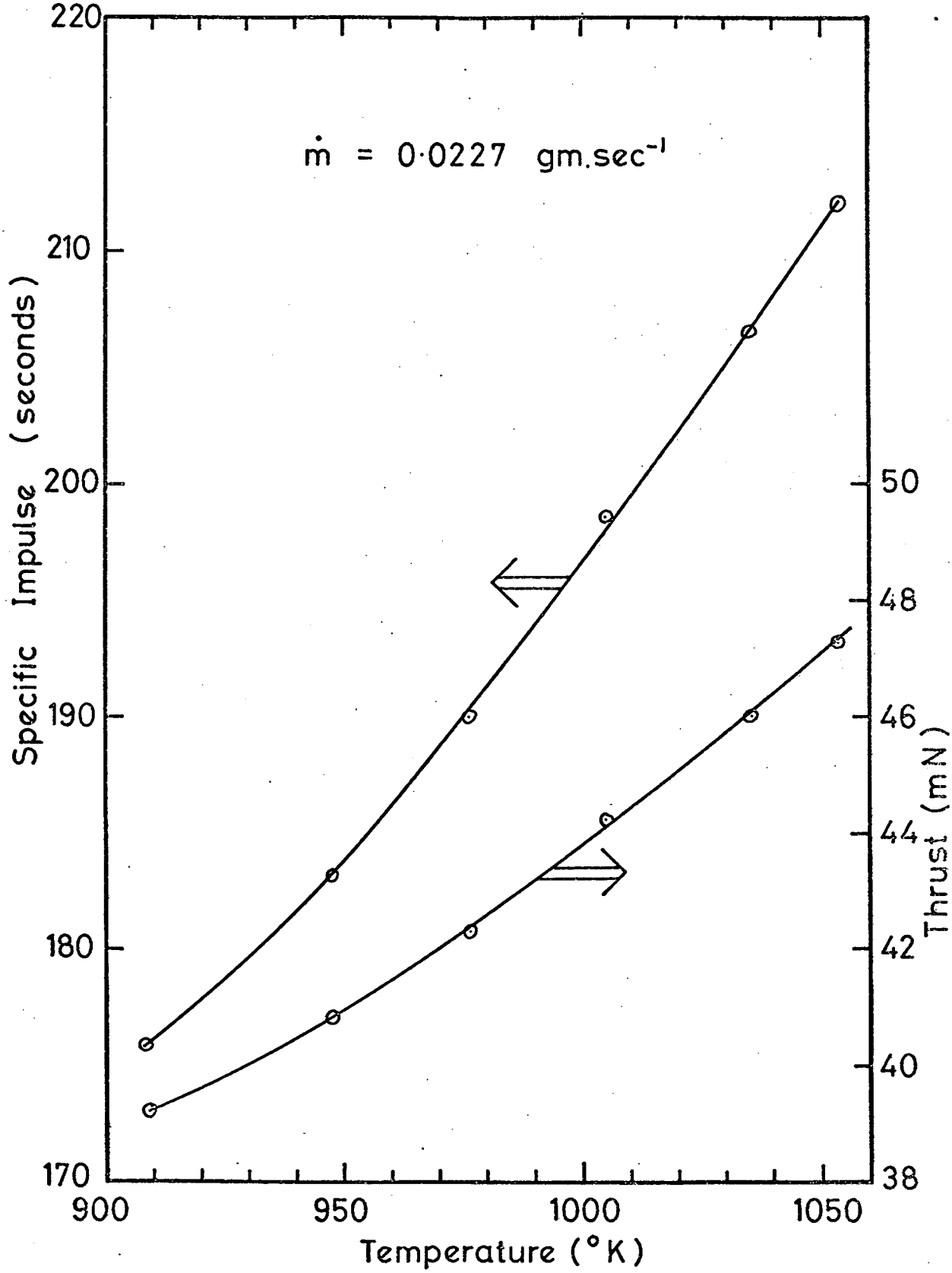

Fig. 48 Calculated Performance of Nickel Resistojet.

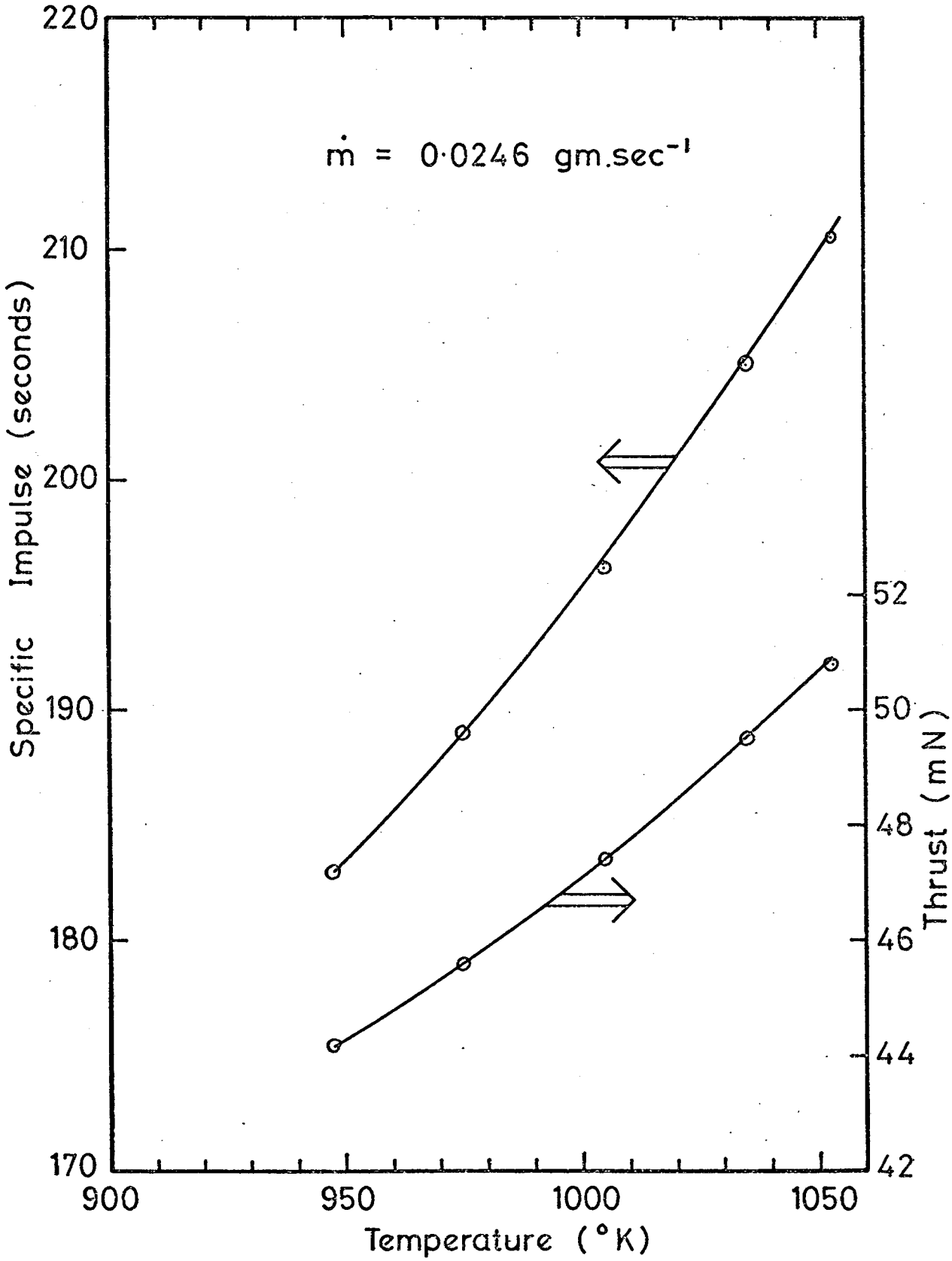

Fig. 49 Calculated Performance of Nickel Resistojet.

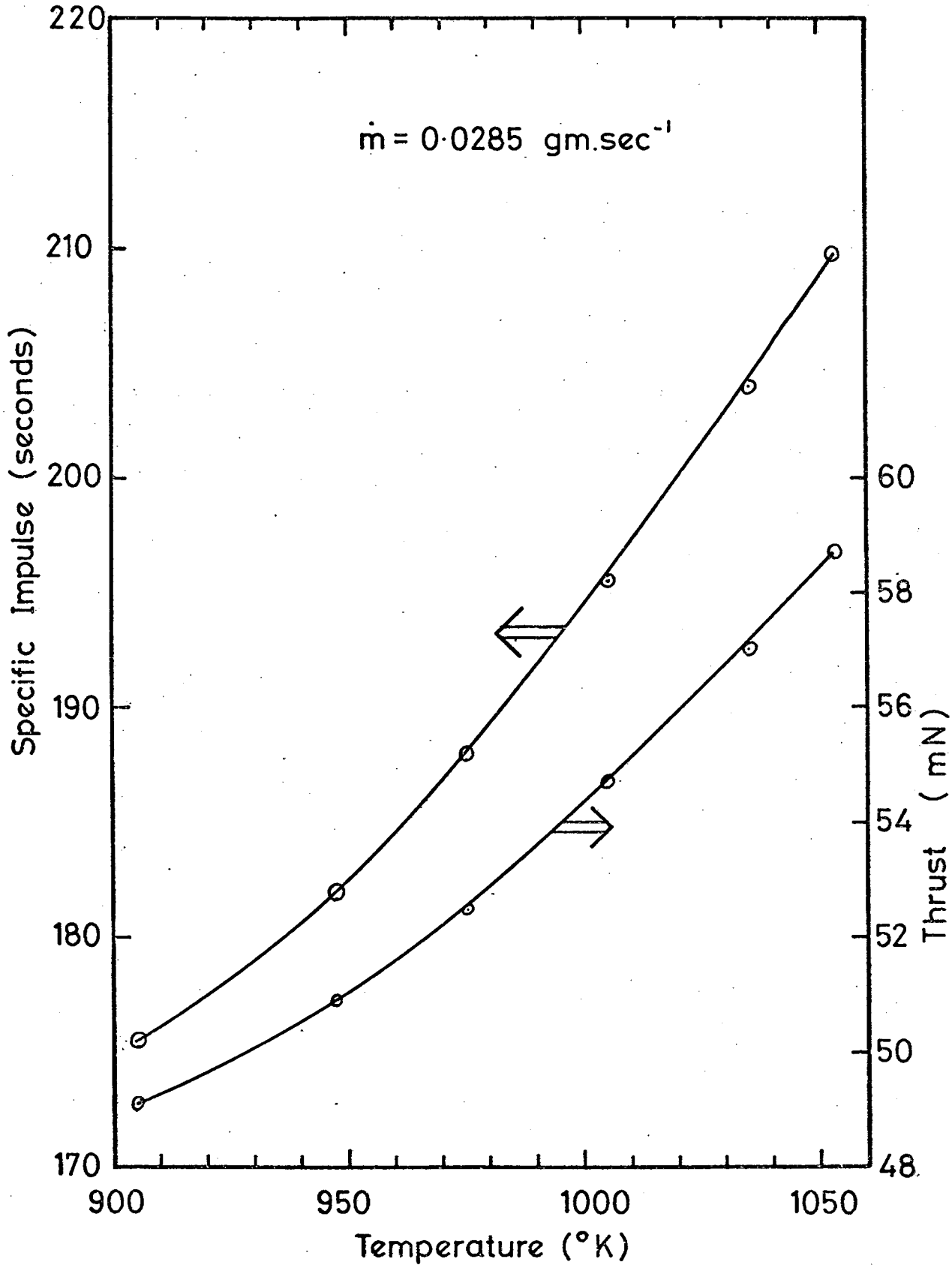

Fig. 50 Calculated Performance of Nickel Resistojet.

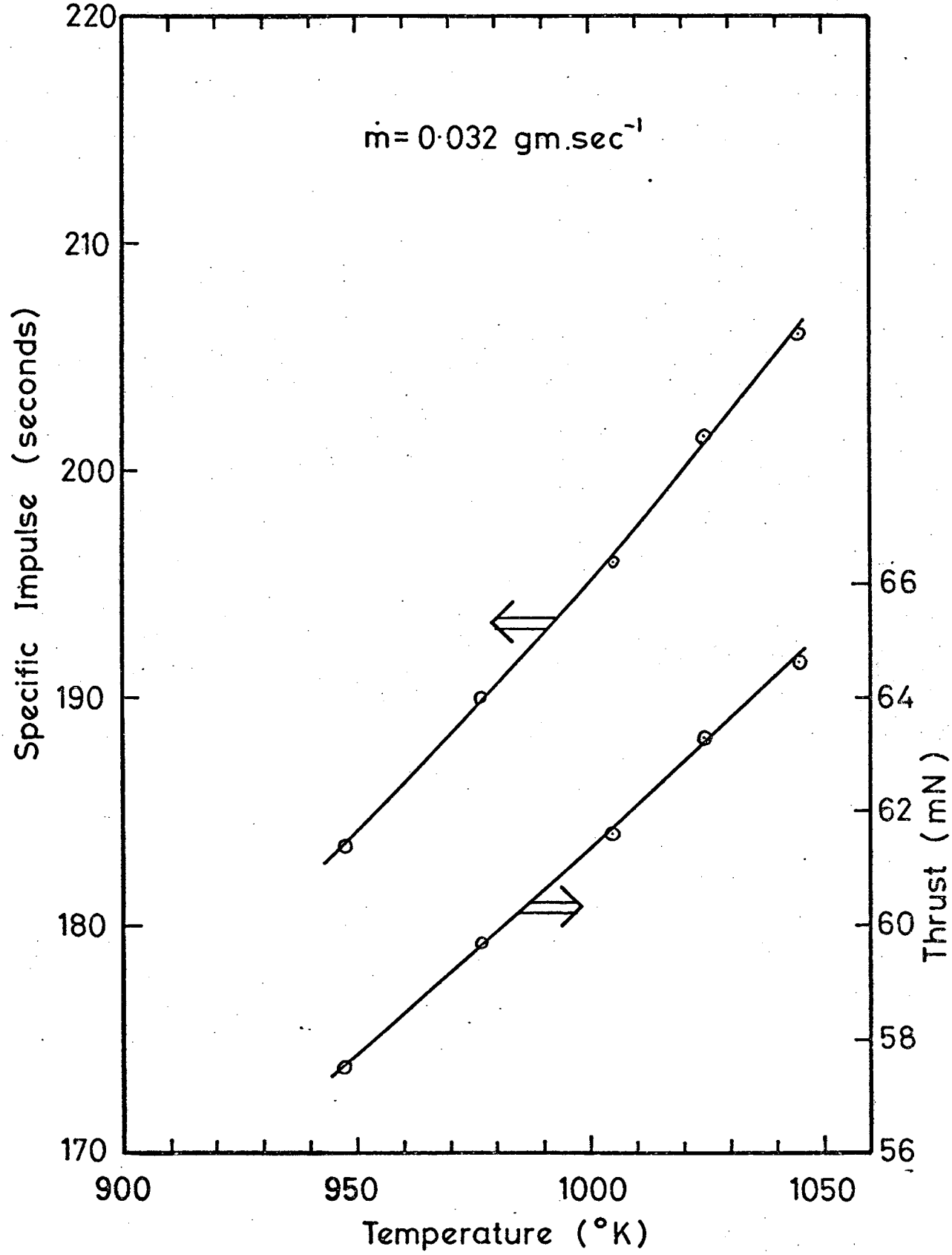

Fig. 51 Calculated Performance of Nickel Resistojet.

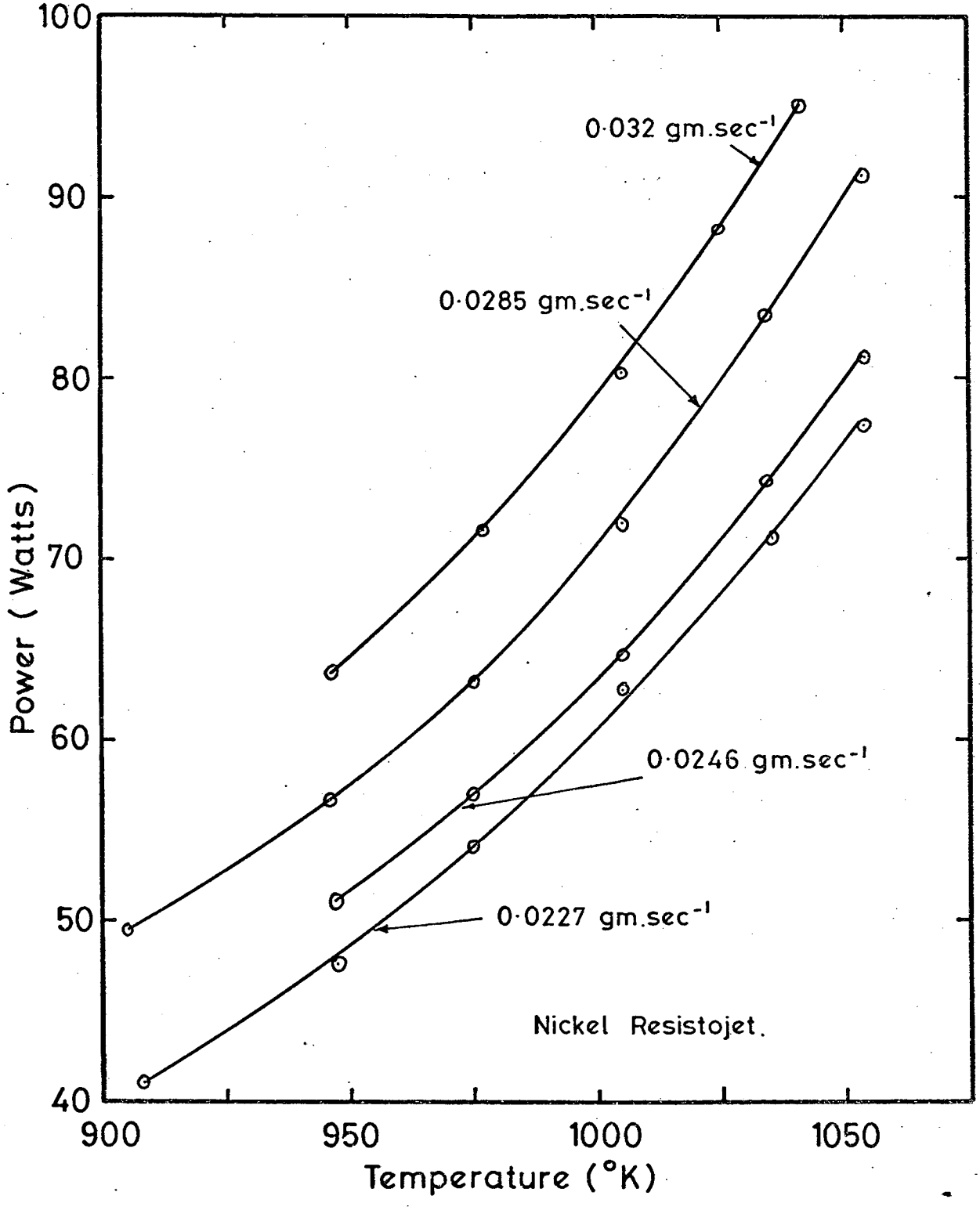

Fig. 52 Power to Gas with Changing Temperature.

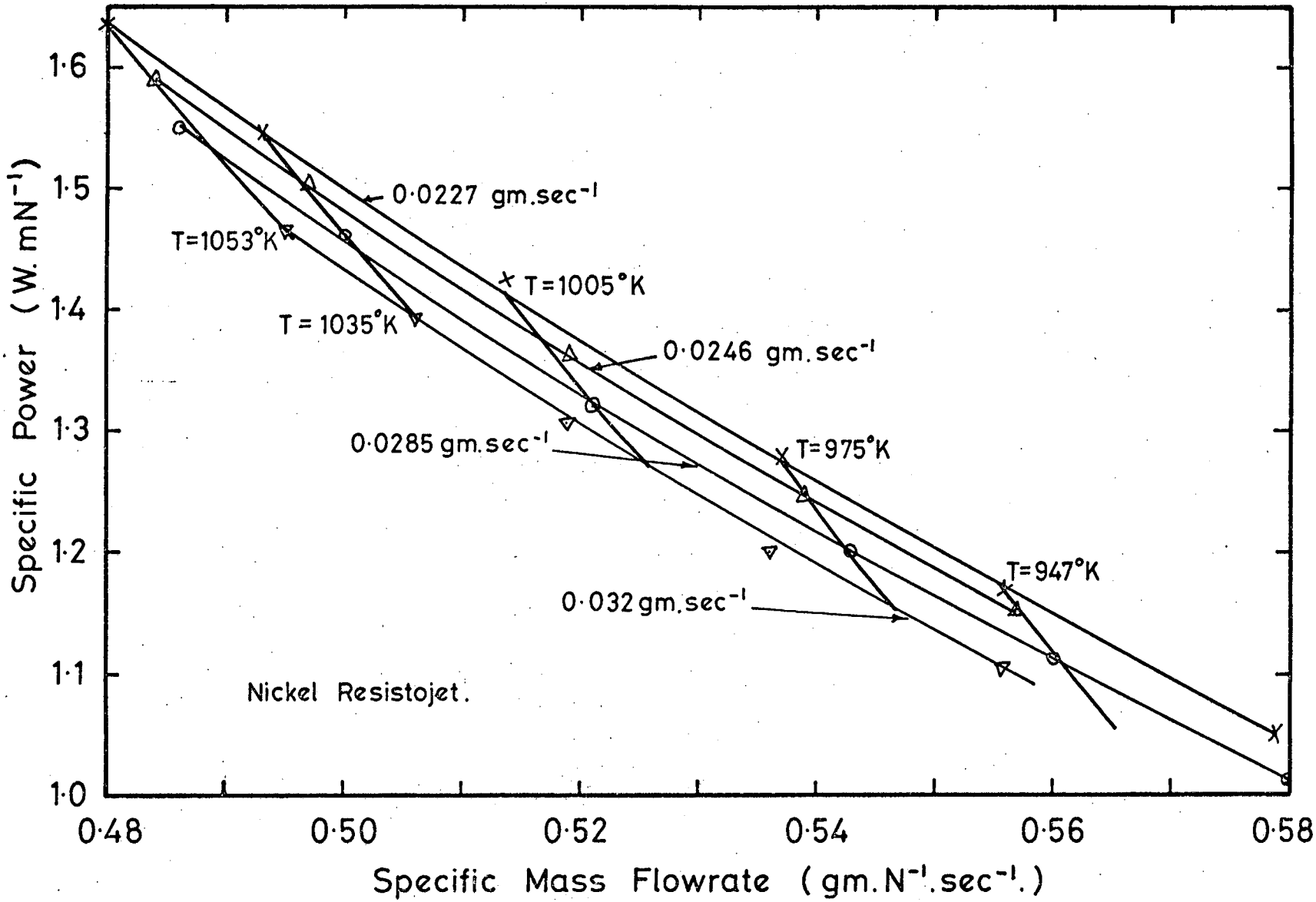

Fig. 53 Specific Power versus Specific Mass Flowrate.

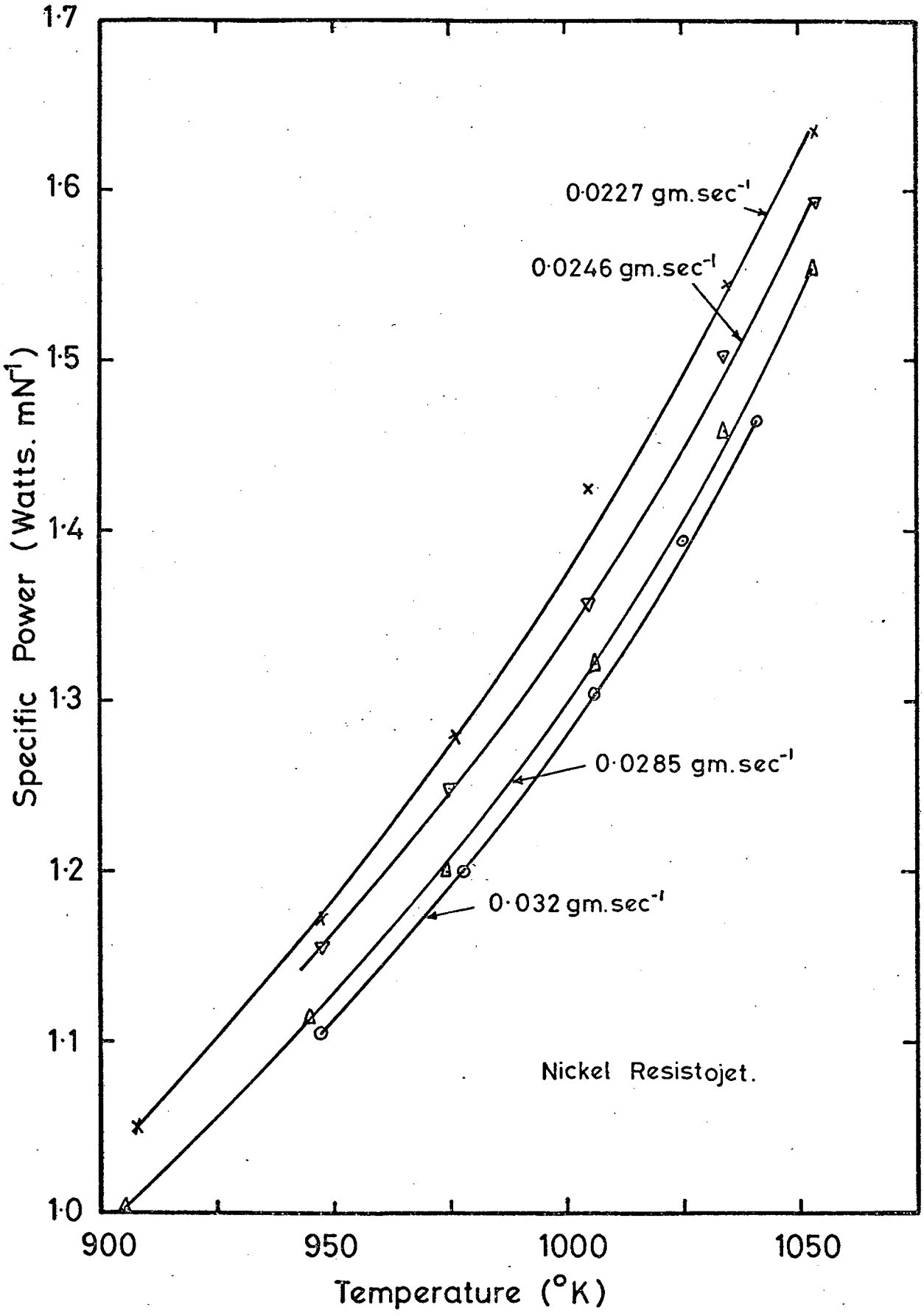

Fig. 54 Variation of Specific Power with Temperature.

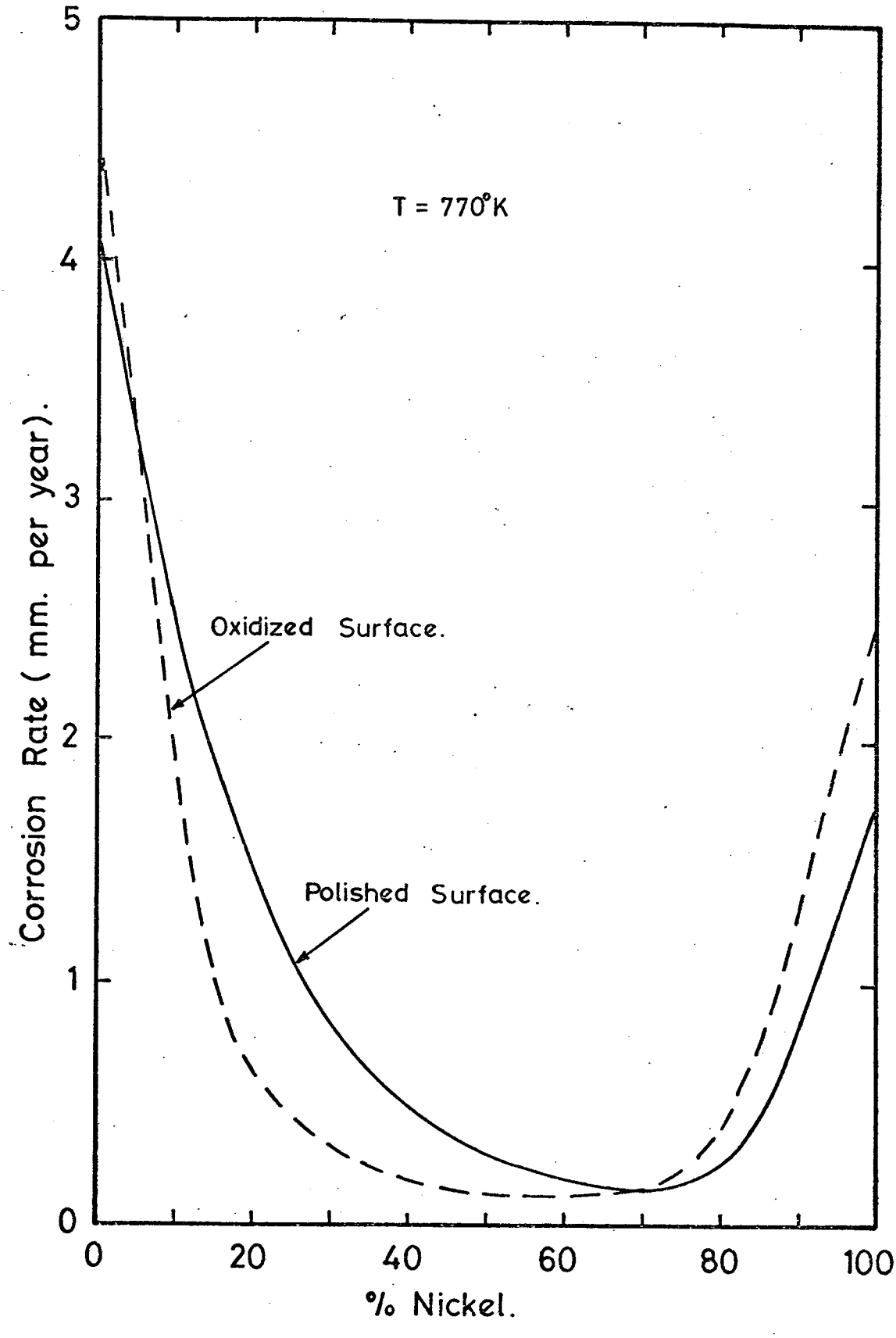

Fig. 55 Corrosion Behaviour of Nickel Alloys in Ammonia. (from Moran).

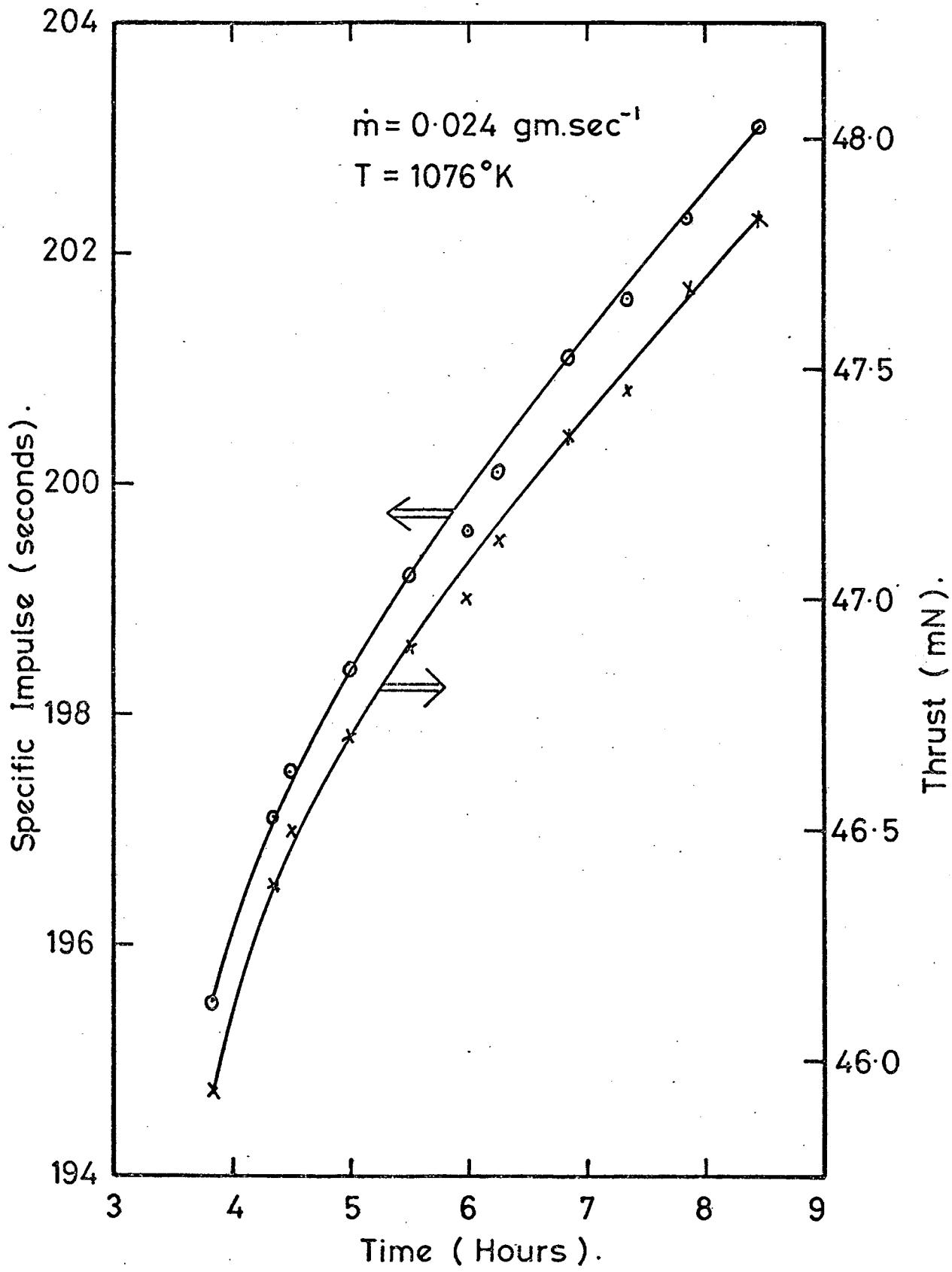

Fig. 56 Calculated Performance of Stainless Steel Resistojet.

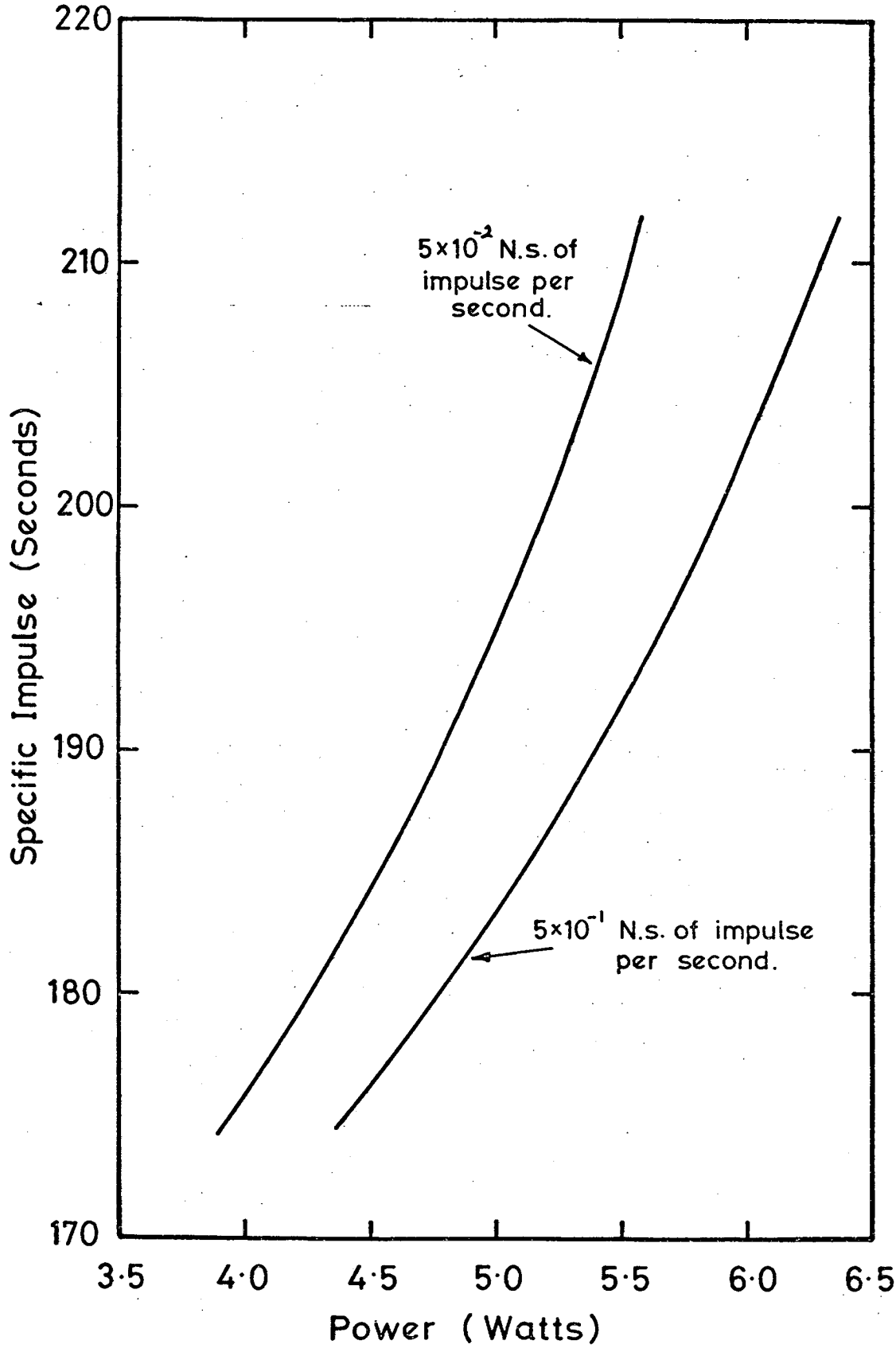

Fig. 57 Variation of Performance of Nickel Resistojet with Power Level.

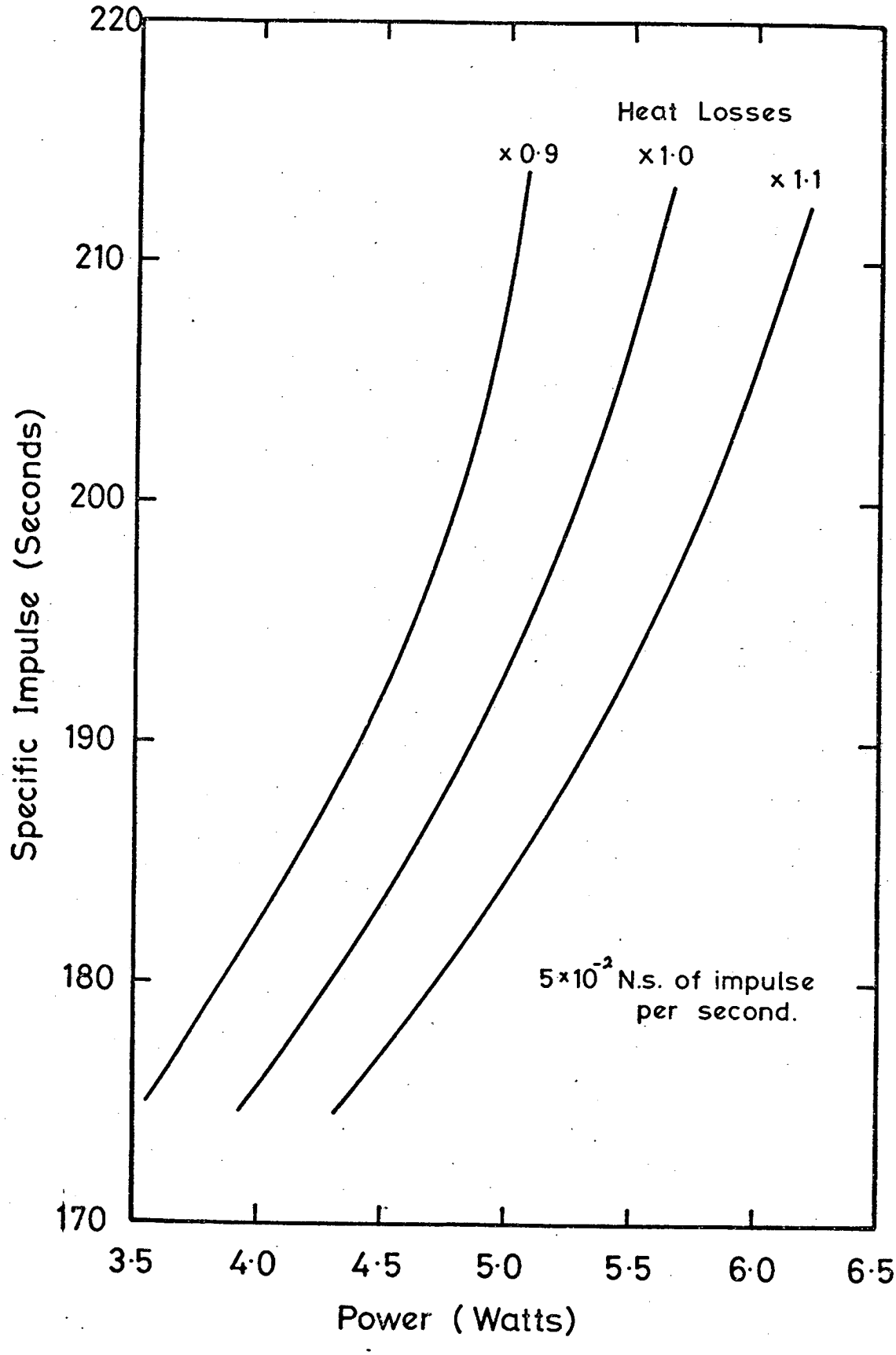

Fig. 58 Effect of Heat Losses on Performance of Nickel Resistojet.

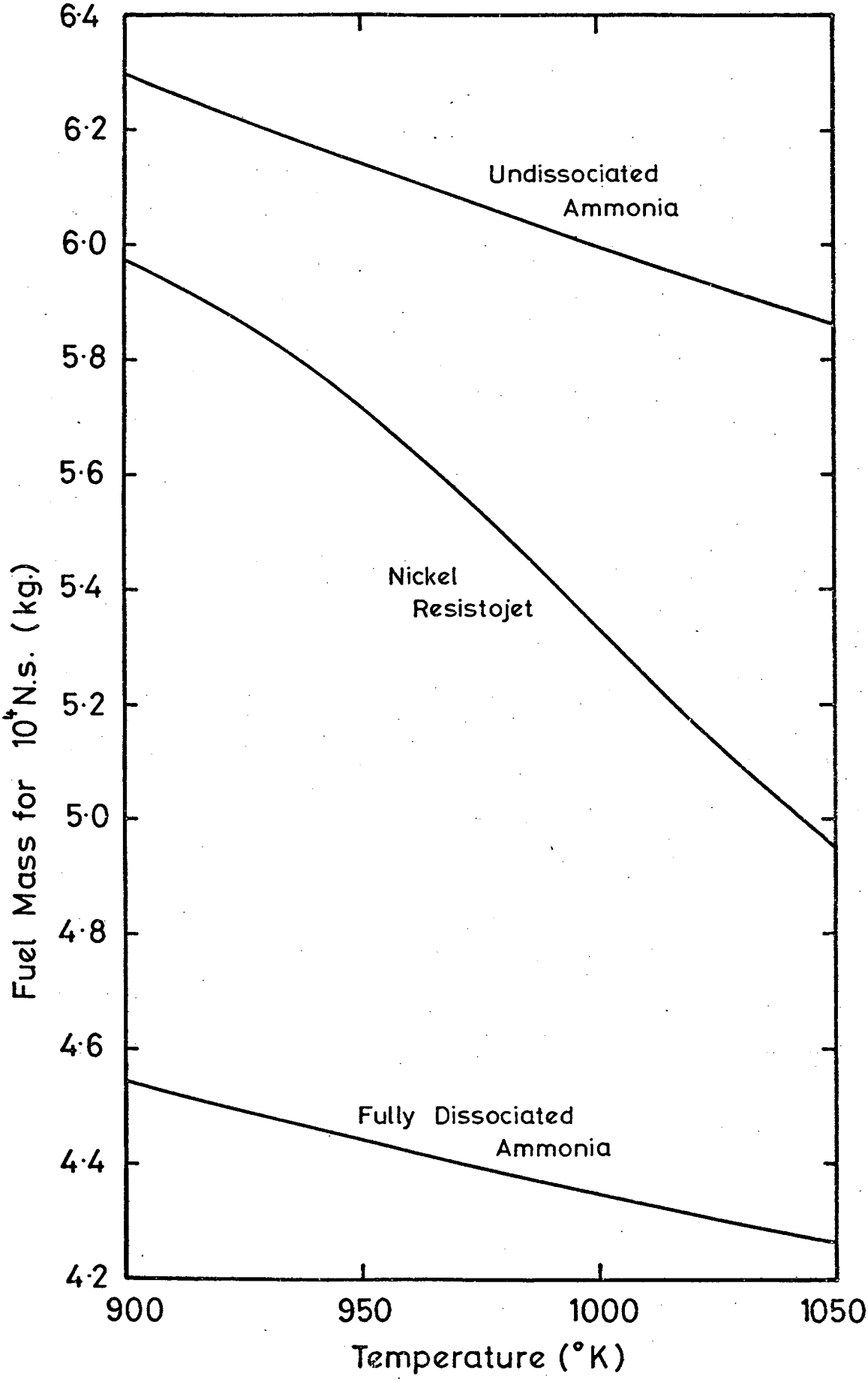

Fig. 59 Variation of Fuel Requirements with Temperature.

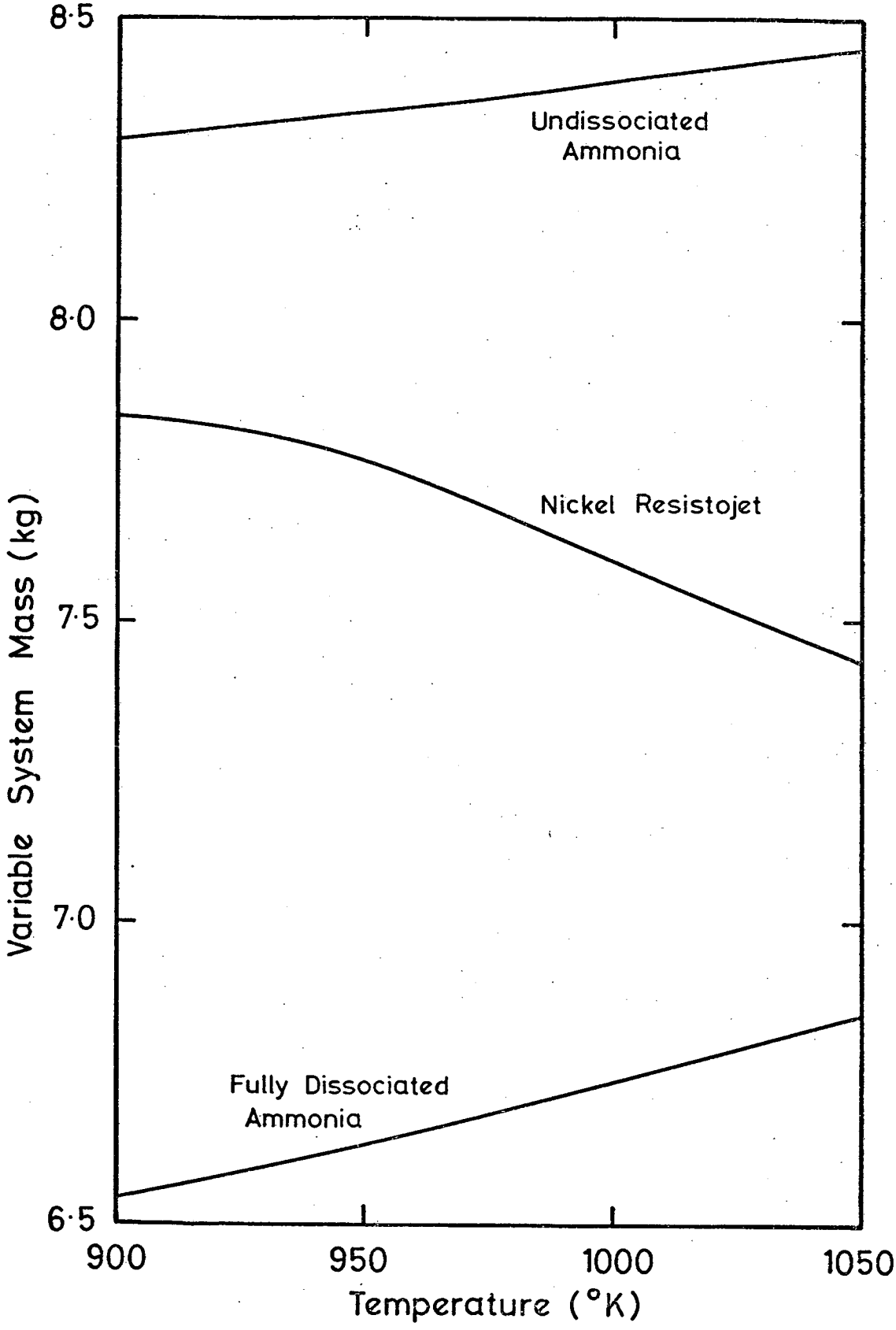

Fig. 60 Variable System Mass versus Temperature for 1 year of Operation.

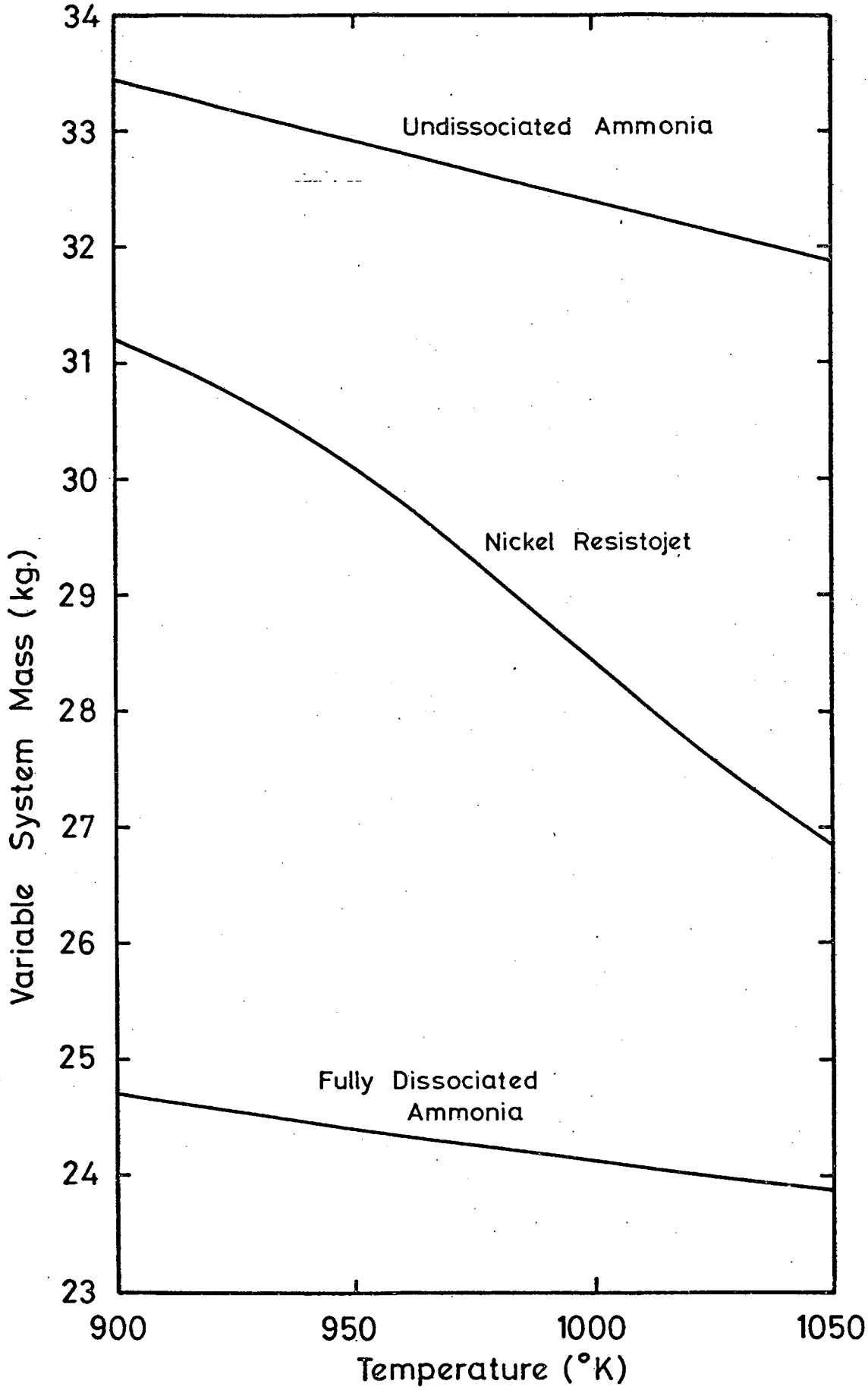

Fig. 61 Variable System Mass versus Temperature for 5 years of Operation

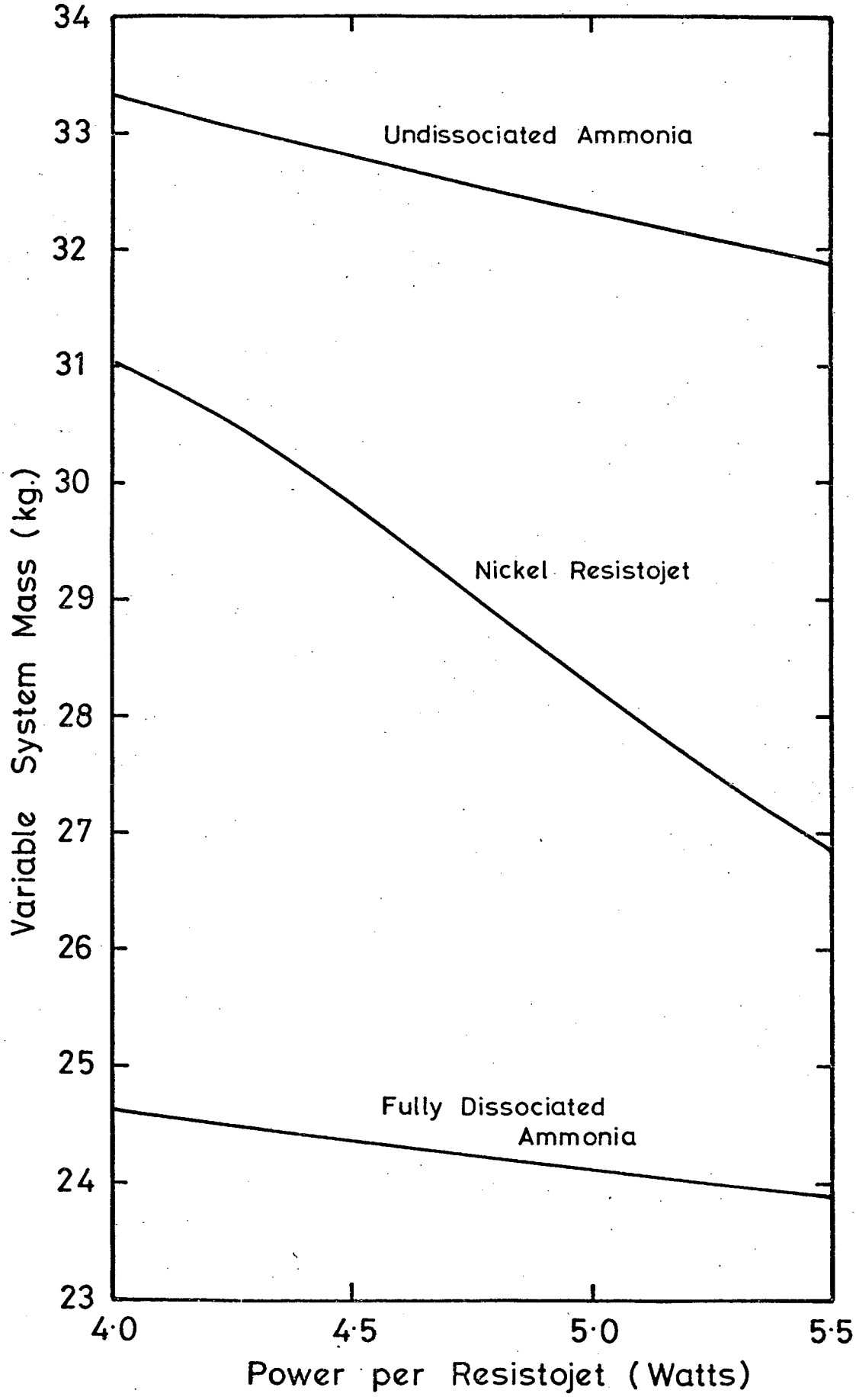

Fig. 62 Variable System Mass versus Power Level for 5 year Operation.

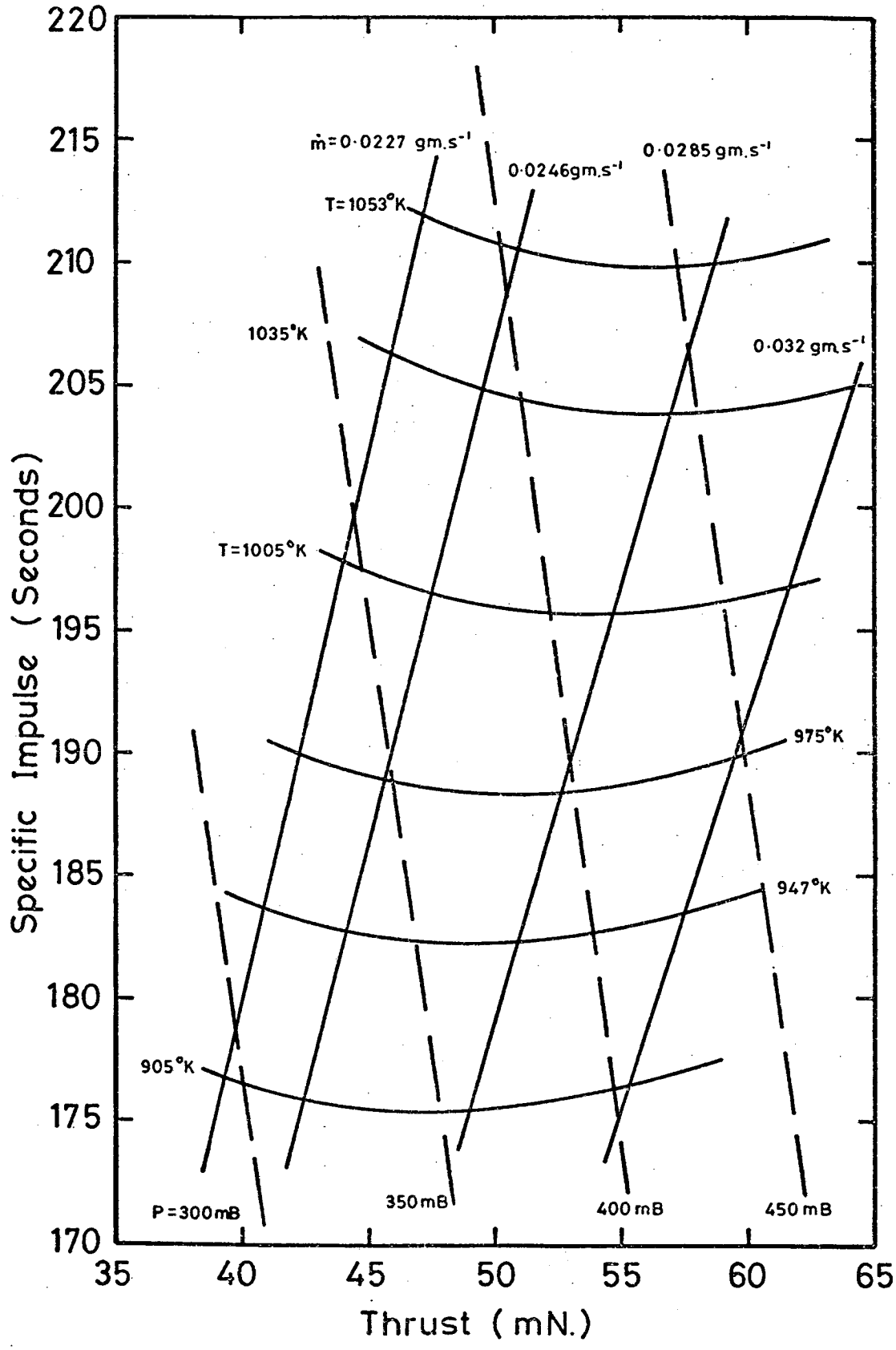

Fig. 63 Performance of Nickel Resistojet.